Development of Transition Metals based Electrolyser for Efficient Water Splitting

A dissertation submitted to the Department of Chemistry, Quaid-i-Azam University, Islamabad, as satisfying the partial fulfilment of requirements for the degree of

Masters of Philosophy

In

Physical Chemistry

By

Muhammad Ishaq

Reg. No. 02061613038

Department of Chemistry

Quaid-i-Azam University

Islamabad

Session

2016 - 2018

Hadith-e-Qudsi

1377. Ibn Mas`ud (May Allah be pleased with him) reported: The Prophet (PBUH) said, "Envy is permitted only in two cases: A man whom Allah gives wealth, and he disposes of it rightfully, and a man to whom Allah gives knowledge which he applies and teaches it."

(Al-Bukhari and Muslim)

DECLARATION

This is to certify that this dissertation submitted by ***Mr. Muhammad Ishaq*** is accepted in its present form by the Department of Chemistry, Quaid-i-Azam University, Islamabad, Pakistan, as satisfying the dissertation requirements for the degree of *Master of Philosophy* in *Physical Chemistry*.

Supervisor: _______________________

Dr. Afzal Shah
Assistant Professor
Department of Chemistry
Quaid-i-Azam University
Islamabad

Head of Section: _____________________

Dr. Hazrat Hussain
Department of Chemistry
Quaid-i-Azam University
Islamabad

External Examiner: _____________________

Chairman: _______________________

Prof Dr. Shahid Hameed
Department of Chemistry
Quaid-i-Azam University
Islamabad

PLAGIARISM CERTIFICATE

This is to certify that **Muhammad Ishaq (Reg. No. 02061613038)** has completed Master of Philosphy in Physical Chemistry, Quaid-i-Azam University Islamabad. The title of my research work is **“Development of transition metals based electrolyser for efficient water splitting”**. Similarity index of this thesis was checked on Turnitin and was found that its overall similarity index is 12 % .

Supervisor
Dr. Afzal Shah
Associate Professor
Department of Chemistry
Quaid-i-Azam University
Islamabad, Pakistan

AUTHOR'S DECLARATION

The research work presented in this thesis was carried out by me (Muhammad Ishaq) in the Physical Chemistry laboratory (Room No. 38), Department of Chemistry, Quaid-i-Azam University Islamabad. All the findings reported in this thesis are from my own investigations with the approval and membership of my supervisor **Dr. Afzal Shah**. No part of this work has been presented for any other degree.

Muhammad Ishaq

Dedication

<u>DEDICATED TO,</u>

<u>MY BELOVED PARENTS, BROTHERS AND SISTERS</u>

Table of Contents

Acknowledgements

First of all I pay my gratitude to Almighty Allah, the Lord and Creator of the heavens and earth. He is certainly the supreme patronage of my life. All respects for His last prophet Hazrat Muhammad (S.A.W) who bestowed us the perfect code of life.

I would first like to thank my advisor, Dr. Afzal shah for his guidance and encouragement over the years, and for always reminding me to consider a problem at its most basic, fundamental level. I am particularly grateful for his understanding and support of my involvement in activities outside of the lab, which allowed me to develop the nontechnical skills needed to advance my career. I would also like to extend a special thank you to professor Dr. Muhammad Shahid Hameed (chairman department of chemistry Q.A.U Islamabad, Dr. Hazrat Hussain (Head of physical section department of chemistry Q.A.U Islamabad) for their support and precious time. A special thank you to Dr. Faiza who took me under her wing and taught me how to be a great grad student while still living life to the fullest. I am honored to be your protégé. Thank you to Ali Akbar and Muhammad Assad and Dr. Saghir Abbas for sharing your vast knowledge and experience with me, which provided the foundation for this thesis project.

Thank you to all of my amazing labmates both past and present (Samina Seher, Anam Nawab, Sundus and M.Zulqarnain) for their support, guidance, and friendship among its members. I am thankful to all teaching faculty for their best deliverance of knowledge and all staff members of chemistry department for their best cooperation during the tenure of my studies. A huge thank you goes out to all of my friends specially Mr. Saifullah and Adnan Khalid, Hassam Arshad, Mahmoud Hussain, M. Kamran, Ziab Khalid, Nasir Abbas, M Safdar and M. Adeel Salfi both near and far. Because of you all, I have maintained my sanity through this long and strenuous process. I have enjoyed all over our conversations over the years, both technical and personal, and I hope our paths cross again in the future, Thank you to, for

being the classmates. Finely thanks to QAU for serving the nation by providing the best educational facilities.

Muhammad Ishaq

List of figures

List of tables

List of Abbreviations

CA	Chronoamperometry
CPE	Control potential electrolysis
CE	Counter electrode
CV	Cyclic voltammetry
DMFC	Direct methanol fuel cell
EDX	Energy dispersive R-ray spectroscopy
FTO	Fluorine doped Tin Oxide
HER	Hydrogen evolution reaction
OER	Oxygen evolution reaction
LSV	Linear sweep voltammetry
NHE	Normal hydrogen electrode
SHE	Standard hydrogen electrode
ORR	Oxygen reduction reaction
PEMFC	Proton exchange membrane fuel cell
RE	Reference electrode
RHE	Reversible hydrogen electrode
SCE	Saturated calomel electrode
SEM	Scanning electron microscopy

UV	Ultraviolet radiations
WE	Working electrode
XRD	R-ray diffraction spectroscopy
BSEI	Back scattered electron images

Abstract

The serious global energy crisis and environmental problems associated with the burning of hydrocarbons have compelled researchers to explore alternative sources of energy. However, generation of energy from renewable sources is a challenging task. In this context electrolysis of water is a smart approach of contributing in the energy generation domain because it stands out as a scalable technology, for which the only required inputs are water and potential. For realizing a zero carbon based economy, hydrogen must be efficiently and sustainably produced from water. However, in water splitting, oxygen evolution reaction (OER) is a sluggish half-cell reaction. Therefore, the development of efficient catalysts for speeding up OER is a key for boosting up the commercial viability of electrolysers. In this perspective researchers have employed several catalysts such as Au, Pt, Pd etc. for catalyzing OER, but their susceptibility to poisoning, high cost and limited availability have blocked the road for large scale commercialization of electrolysers. So in the search for an effective alternative, we have synthesized a novel tetra metallic electrocatalyst (Fe-Ni-Zn-Co) by a facile and low cost method compared to traditional precious noble-metal-based electrocatalysts, such as RuO_2 and IrO_2. The electrodeposited of the catalyst over the surface of FTO was confirmed through XRD, SEM and EDX and investigation of its catalytic activity was carried out through electrochemical techniques. The catalyst was found to accelerate OER with a very low overpotential and high current density. Linear scan voltametric results revealed that a current density of 1 mA/cm^2 demanded an overpotential of just 52.6 mV in alkaline medium, thus, proving high OER efficiency of the modified FTO electrode. Furthermore, oxygen bubbles at the surface of the modified electrode offered naked eye evidence of the catalytic activity of the prepared tetra-metallic electrocatalyst during water oxidation. The aforementioned advantages of the electrochemically synthesized OER catalyst indicate that tetra metallic electrocatalysts hold great promise for contributing in clean energy production.

Chapter # 01

Introduction

With the worldwide increase in population and adopting high standard of life, energy needs are increasing with a rapid pace [1]. Consequently, the average global energy demands are predicted to be roughly 30 and 46 TW in 2050 and 2100 respectively [2]. Continuous increase of energy requirements limits the use of fossil fuels because of their non-renewability and environmental problems, thus, suggesting search for new power systems which could be free from the issues of perishability and release of ozone damaging gases. The current focus of researchers is on sustainable and efficient energy generation systems [3, 4]. Solar and wind energy are excellent sources but their unscheduled supply frequently does not run parallel with the grid power requirements. So development of a technology based on electrocatalyst holds great promise in indirect storage and conversion of energy from one form to another i.e. electrical to chemical [5, 6]. Water electrolysis using renewable energy as electricity source produces H_2 and O_2. The generated gases can be either stored and utilized for industrial purposes or used for power generation (via fuel cells) with no environmental hazards [7].

1.1 Energy Source

Resolving issues related with consuming non-renewable energy sources by making use of an alternate energy supply with low carbon and renewable source is primarily significant for sustainable sector [8, 9]. Hydrogen as a fuel is a useful option owing to its high energy density (144 MJ/kg) amongst all fuels with the additional advantages in the form of its production from water and its combustion into a zero carbon product i.e. water, thus suitable for realizing the dream of a carbon free energy economy [10, 11]. **Figure 1.1** shows energy consumption with every passing year [12]. This requires an attention to develop a well-planned scheme for sustained energy production technologies. As earth`s atmosphere can provide abundant feedstock of H_2O, CO_2 and N_2 that can potentially be utilized into useful products via electrochemical processes. So until now a number of electrocatalysts have been made to overcome energy crises and environmental problems. **Table 1.1** summarizes merits and demerits of a variety of fuels.

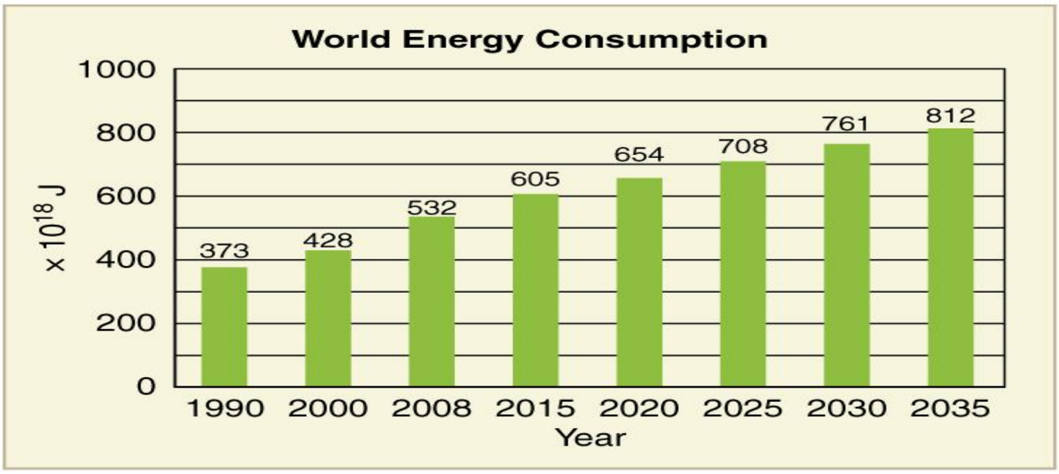

Figure 1.1 expected global energy consumption chart.

Table 1.1 Comparison of currently employed fuels for energy generation

Fuel type	**CO_2 emission per KWh**	**Power supply**	**Ongoing fuel costs**	**Other issues**
Coal	200 pounds	Throughout the year	Yes	Ground water, Non-renewable and causes pollution
Natural gas	130 pounds	Throughout the year	Yes	Non renewable
Nuclear	Zero	Throughout the year	Yes	Extremely dangerous
Wind	Zero	Totally depends on wind speed	No	Potential bird kill, noise pollution
Solar	Zero	Daytime only	No	Unscheduled
Hydro-electric	**Zero**	**Throughout the year**	**No**	**---**

1.2 Energy driven electrolysis of water

From thermodynamic aspects, water splitting reaction is difficult to proceed in spontaneous way without using any external source because reverse reaction occurs easily. As **Figure 1.2** shows that there are different routes for water splitting including thermal, electrical, photonic and biochemical energy through thermolysis (e.g. thermochemical cycles), electrolysis (e.g. electrocatalysis) [13, 14], photolysis (e.g. photocatalysis) [15], and biolysis (e.g. dark fermentation), respectively. Photocatalytic water splitting process was considered over long time because one can use solar energy directly in this process. However, this process has low power conversion efficiency. In contrast electrocatalysis has attracted more attention because in electrocatalytic water splitting process water produces hydrogen in adaptively method using electrical energy source. Water electrocatalysis was initially stated in 1789 with certain features like high efficiency, flexibility and (100 percent) pure hydrogen production. Hydrogen is a perfect energy transporter with ultrahigh energy density, which is for quite some time accepted to be a promising possibility for the substitution of petroleum products later on [16]. Notwithstanding, the hydrogen development response (HER) is entirely compelled by the slow reaction kinetics for the multi-step reaction and should have been quickened by cutting edge synergist metals, for example, Pt which can bring down the energy boundary and enhance energy productivity. Supplanting of Pt-family metals with earth-plenteous materials is exceedingly alluring to encourage the worldwide versatility of practical hydrogen generation. In such a manner, gigantic endeavors have been committed to growing elite and minimal effort honorable without metal HER electrocatalysts for down to practical purposes, however it stays testing. The principal push change metal nickel and its composites such as chalcogenides, phosphides, borides and combinations, have as of late pulled in significant consideration as the most encouraging Pt elective HER electrocatalysts

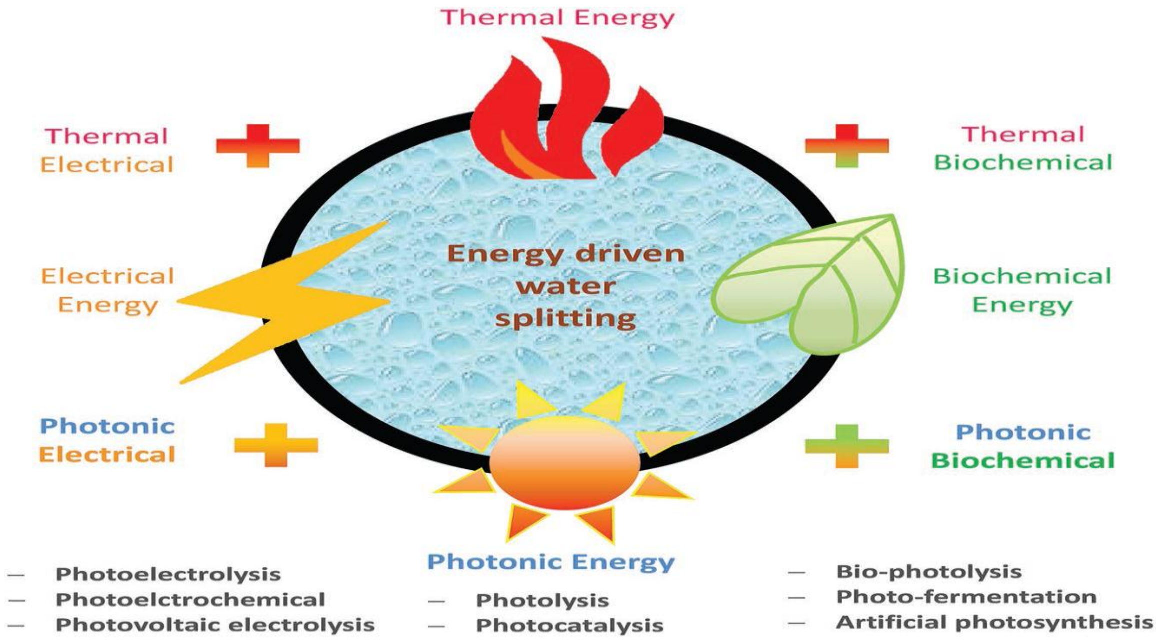

Figure 1.2 Water splitting process driven by various energy forms.

.

1.3 Fundamentals of water electrolysis

Electrocatalytic or photocatalytic water splitting is a pollution free, affordable and high purity rout of obtaining oxygen and hydrogen [17, 18]. In both of pathways during water electrolysis Hydrogen gas is evolved at cathode called HER and Oxygen is at anode called OER. OER and HER stands for oxygen evolution reaction and hydrogen evolution reaction respectively [19]. Theoretically cell potential for overall reaction is accepted 1.23 V which is considered as thermodynamically equilibrium potential. Experimentally more voltage is required then above given value. In case of HER, electrochemical adsorption of H ion takes place and electrochemically/chemically a single H_2 molecule is liberated. While OER involves the four electrons transfer mechanism comprises of O-H bond breakage and O-O bond formation; therefore, to overcome this high kinetic energy barrier more potential is needed in case of OER. However relative to OER, HER catalysis is easier liberating H_2 at 0 V. The thermodynamically equilibrium voltage value 1.23 V, which is equal to $\Delta G^0 = 2FE = 237.2$ KJ/mole at room temperature. Water electrolysis occurs at an electrical energy of $\Delta H^0 = 285.8$ KJ/mole that is equal to 1.48 under isothermal conditions as shown in **Figure 1.3.** This value is independent of the pH of the electrolyte but alters with change of temperature and pressure of the gas [20].

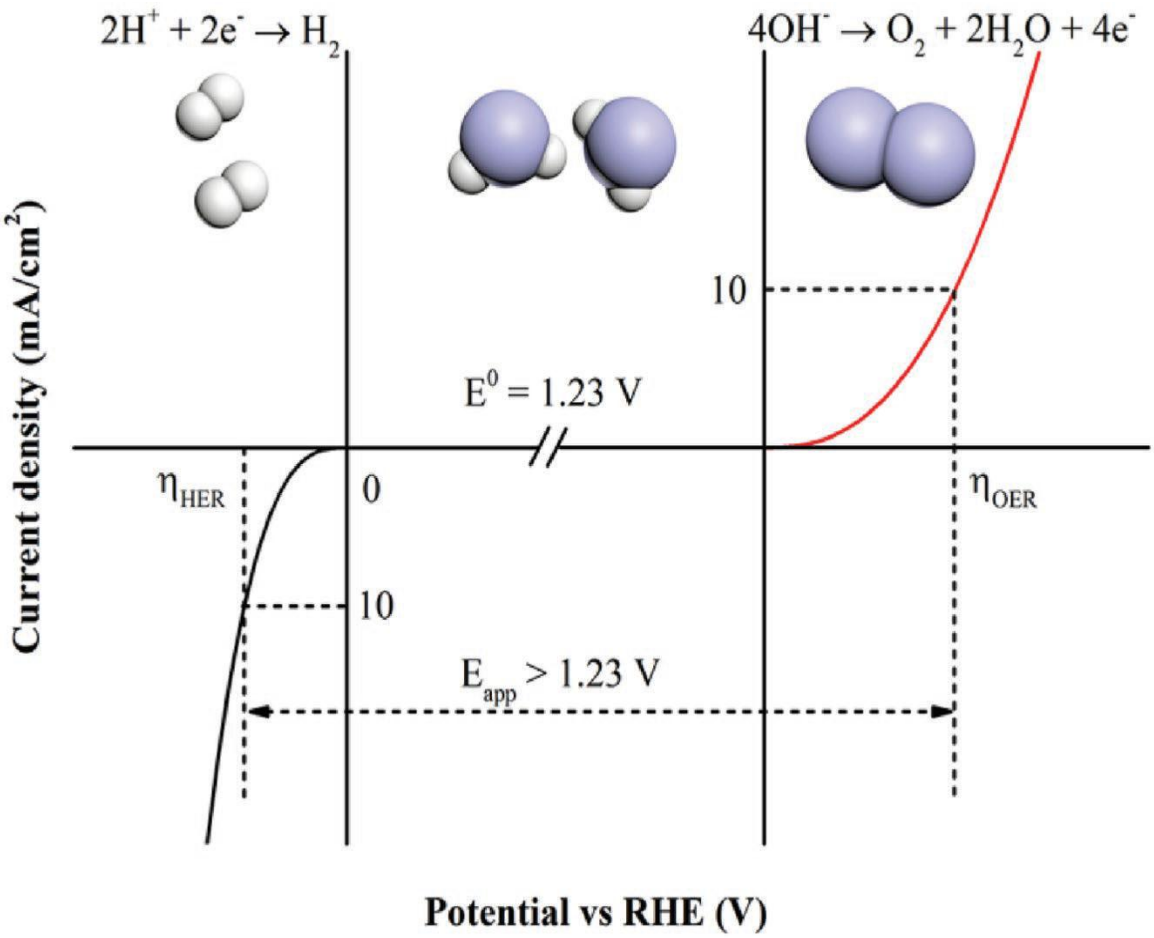

Figure 1.3 Polarization lines for HER and OER.

The thermodynamic equilibrium potential at which water gets start splitting is 1.23 V, but the practical applied potential is far greater than 1.23 V to attain the water-splitting at current density (*j*) of 10 mA cm^{-2}. The η HER and η OER correspond to the cathodic and anodic overpotential for water splitting at the given current, respectively.

At anode (Oxygen Evolution Reaction)

$2H_2O \leftrightarrow O_2 + 4e^- + 4H^+ \quad E^0_a = 1.23V$ vs. SHE (1.1)

At cathode (Hydrogen Evolution Reaction)

$4e^- + 4H^+ \leftrightarrow 2H_2 \quad E^0_c = 0.00V$ vs. SHE (1.2)

Overall reaction

$2H_2O \quad \leftrightarrow \quad O_2 + 2H_2 \qquad E = 1.23V \text{ vs. SHE} \qquad (1.3)$

Where E^0_c and E^0_a are equilibrium half-cell potentials at STP condition (1 atm and 25^oC) [21].

Basic media (pH = 14)

$4H_2O + 4e^- \rightarrow 2H_2 + 4OH^- \qquad E^0_c = -0.826 \text{ V vs. SHE} \qquad (1.4)$

$4OH^- \rightarrow O_2 + 2H_2O + 4e^- \qquad E^0_a = 0.404 \text{ V vs. SHE} \qquad (1.5)$

Neutral conditions (pH = 07)

$4H_2O + 4e^- \rightarrow 2H_2 + 4OH^- \qquad E^0_c = -0.413 \text{ V vs. SHE} \qquad (1.6)$

$2H_2O \rightarrow O_2 + 4H^+ + 4e^- \qquad E^0_a = 0.817 \text{ V vs. SHE} \qquad (1.7)$

Acidic media (pH = 0)

$4e^- + 4H^+ \leftrightarrow 2H_2 \qquad E^0_a = 0.000 \text{ V vs. SHE} \qquad (1.8)$

$2H_2O \leftrightarrow O_2 + 4e^- + 4H^+ \qquad E^0_c = 1.230 \text{ V vs. SHE} \qquad (1.9)$

1.4 OER Catalysts

In the past several decades the scientist are making a great effort to achieve a good target in developing electrocatalysts for OER that can work under different electrolytic environments. For example, RuO_2 demonstrates brilliance OER movement in both acidic and basic environment [22, 23]. However, $Ru0_2$ is unable to show best OER activity in both media under high anodic potential because it oxidizes to form RuO_4 and become soluble in solution [24]. IrO_2 is another important example of typical OER catalyst with some advantages and disadvantages. Advantages of IrO_2 are that it shows good catalytic activity, more stable and it can withstand high anodic potential in acidic and basic media. Disadvantages related to IrO_2 are similar to that of RuO_2. However, both are made of precious metals pushing back the cost effective aspects of a catalyst.

Catalysts that have been extensively investigated are

(A) Metals [25, 26]

(B) Metals oxide families

(i) Pervoskite (ABO_3; A = alkaline and/or rare-earth metals, B = transition metals) [27]

(J) Spinals (AB_2O_4; A = alkaline-earth and/or transition metals B = group 13 elements and/or transition metals)

(k) Layer-structure type family (M $(OH)_2$, MOOH and $LiMO_2$; M = Mn, Fe, Co and Ni) [28, 29]

Transition metals-based oxides have following characteristics properties with respect to OER

(a) Low cast

(b) Easily synthesized

(c) Environmental friendly

(d) Stable in alkaline solution

(e) Show moderate conductivities

(f) Transition metals have different oxidation states (i.e. tetrahedral and octahedral sites) so, they can possess rich combinations of transition metals structures.

(g) Layer-structure family shows high catalytic activity

Doping is considered to be effective way to enhance catalytic performance

Other metals oxides also show better catalytic activity, [30, 31] and some of them are prepared in situ and offers good catalytic performance in neutral electrolyte [32].

After a tremendous effort it has been investigate the non-oxide catalysts like metal chalcogenides TC, TC_2, T_9S_8, Ni_3C_2, T_3S_4 (T = Co and Ni, C = S, Se and Te) [33], Metals pnictide Co_2N, Co_3N, Co_4N, NiN, TP and T_2P [34] and organometallic (metals-coordination complexes) [35, 36] as strong candidate for OER and/or HER. Organometallic have been investigated, these compounds are made suitable for OER by tuning their molecular/electronic structure to achieve the specific effect toward OER. However, they show little catalytic activity. By dispersing organometallic on suitable substrate (graphene or reduced grapheme oxide) a remarkable enhancement in their catalytic performance have been observed [37].

Some non-metallic carbon based materials have additionally been examined for OER [38]. An upgraded and advanced methods and techniques played a key role in achieving good OER activity by altering their intrinsic properties [39, 40]. In case of nanotechnology, size and morphology are primary factors responsible for the remarkable change in their activity towards OER. Active sites on the material can be expanded by decorating multiple sheets into single sheet or rearranging single sheet with another material (grapheme) to form an alternatively stacked pattern [41]. This approach can also alter their intrinsic properties like that electrical conductivity, binding energy of OER intermediates. Recently, there are many cutting-edge instruments that help us to monitor the OER in situ to confirm the actual active intermediates and electrochemical response during OER [42, 43].

First row transition elements and their oxides are extensively studied for their enhanced catalytic activities. Co and Ni demonstrate efficient catalytic activity towards OER however, their oxides serve as the source for corrosion, and therefore their use is limited. Oxide based complexes of Fe, Ni and Co have also been well-thought-out to augment the catalytic activity and stability toward OER in alkaline media [44].

Nickel and Nickel based alloys are highly stable to corrosion activity in hot alkaline medium but at the same time their electrocatalytic activity is not very good. Moreover, low resistance to intermittent electrolysis limits the use of Ni alone. Thus, nickel must be alloyed with other metals (e.g. Fe, Co, Cu, W, Mo) [45, 46]. Arul et al., reported few ternary alloys of Ni and established the catalytic order (NiMoFe > NiMoCu > NiMoZn >NiMoCo ~ NiMoW >NiMoCr > Ni-plated steel) [47, 48]. Iron based catalysts are also reported to be efficient towards OER in alkaline medium. Iron normally possesses enhanced surface area and thus improved number of active sites which increases the catalytic efficiency of Iron. However corrosion still is an issue when Iron is attempted to use alone for OER. To enhance the corrosion resistivity of iron, it must be alloyed with other metals (e.g. Co, Ni, Mo, Cu, and Zn). Renato et al., reported that Ni-Fe-Mo ternary alloy showed enhanced catalytic activity toward HER/OER [49]. Similarly, Jafarian et al. reported that nanocrystalline Co-Ni-Fe showed improved catalytic activity then Ni alone [50]. Nocera et al., reported that the Co-phosphate catalysts which were electrodeposited in Cobalt Nitrate/phosphate buffer solutions exhibited admirable activity towards oxidation of water in neutral and mild alkaline medium [51].

1.5 Fundamentals of OER (oxygen evolution reaction) catalysis

1.5.1 Electrocatalytic kinetics

An electrocatalysts is utilized to facilitate electrochemical reaction. It can either be modified on the surface of electrode or act as electrocatalysts itself. The primary role of an electrocatalyst is adsorbing active intermediates on the surface and facilitates charge transfer between the electrode and specie. There are many peculiar parameters such as over potential (η), current density ($\boldsymbol{i}$o) and tafel slope ($\boldsymbol{b}$) that decide the performance of an electrocatalysts and also provide the information about mechanism of working of electrocatalysts

$$O + ne^{-} \leftrightarrow R \qquad (1.10)$$

1.5.1.1 Overpotential (η)

Over potential is one of the critical parameter to decide the performance of an electrocatalysts under study. Ideally, applied voltage to derive a reaction should have the same value as that of equilibrium potential. Practically it is not the case that the applied voltage is much higher than that at equilibrium in order to overcome the electrode kinetics barrier of the reaction. According to the Nernst equation in term of applied voltage can be written as,

$$E = E^{o} + \frac{RT}{nF} ln\frac{Co}{C_R} \qquad (1.11)$$

$E =$ Applied potential, $E^{o} =$ formal voltage of overall reaction, T = Absolute temperature, F = Faraday constant, n = no. of exchange electrons, C_0 and C_R are concentrations of species getting oxidized and reduced respectively.

$$\eta = E - E_{eq} \qquad (1.12)$$

E = applied voltage, E_{eq} = equilibrium voltage

1.5.1.2 Exchange current density (i_0)

Exchange current density (i_0) is another valuable parameter. Overall current ($\boldsymbol{j}$) is equal to the sum of contribution of anodic (j_a) and cathodic current (j_c) [52].

$$\boldsymbol{j} = j_a + j_c \tag{1.13}$$

$$j_a = nFk_a[C_R]\exp(\frac{\alpha_a nFE}{RT}) \tag{1.14}$$

$$j_c = nFk_a[C_o]\exp(\frac{\alpha_c nFE}{RT}) \tag{1.15}$$

K_a and $\propto_a$ referred to rate constant and transfer coefficient for anodic half reaction and $\propto_c$, K_c stand for same meaning for cathodic half reaction.

When η is zero then E will be equal to E_{eq} and net current will be zero. Intercept at $\eta = 0$, referred to j_0 value.

$$\mathbf{j_0}/A = i_0 \tag{1.16}$$

i_0 Provide information about intrinsic bonding and charge transferring interactions between electrocatalysts and reactant. High current density is a right signal for high performance electrocatalysts.

1.5.1.3 Tafel equation and Tafel slope (*b*)

Butler – Volmer equation;

$$\boldsymbol{i} = i_0 \, [\exp(\frac{\alpha_a nFE}{RT}) + \exp(\frac{\alpha_c nFE}{RT})] \tag{1.17}$$

From practical point of view over potential and exchange current density has direct relationship. Minimum over potential value with high current density is required. In this equation net current is contributed by anodic reaction while cathodic part is negligible above equation is can be written as

$$\boldsymbol{i} \approx io \exp(\frac{\alpha_a nFE}{RT})) \tag{1.18}$$

In logarithm function form Butler-Volmer equation can be expressed in the form of eq. we can understand the response of current density (i_0) against over potential (η) and its value is dependent on transfer coefficient (∝).

$$\log(\boldsymbol{i}) = \log(i_0) + \frac{\eta}{b} \tag{1.19}$$

$$b = \frac{\partial\eta}{\partial\log(i)} = \frac{2.303RT}{\propto F} \tag{1.20}$$

Current density increases with faster rate with smaller over potential change (η) when value of Tafel slope ($\boldsymbol{b}$) will be small, Tafel slope ($\boldsymbol{b}$) expressed information about mechanism of the reaction, especially for rate determining step.

1.5.2 Electron transfer reaction and mechanism of OER

There are two possible route from which O_2 can be produced one is explain in eq (1.25) and second one is stated in eq (1.27) The most probable mechanism is second one because kinetic energy barrier for first one is too large.

Overall electrolysis reaction

$$2H_2O_{(l)} \rightarrow 2H_2 + O_{2(g)} \tag{1.21}$$

(a) In acidic media

Cathode process

$$4H^+ + 4e^- \rightarrow 2H_2 \qquad E_c^o = 0\ V \tag{1.22}$$

Anode process

$$2H_2O_{(l)} \rightarrow O_{2(g)} + 4H^+ + 4e^- \qquad E_a^o = 1.23\ V \tag{1.23}$$

Proposed scheme for anode process in acidic media

$$M + H_2O_{(l)} \rightarrow MOH + H^+ + e^- \tag{1.24}$$

$$2MO \rightarrow 2M + O_{2(g)} \tag{1.25}$$

$$MO + H_2O_{(l)} \rightarrow MOOH + H^+ + e^- \tag{1.26}$$

$$MOOH + H_2O_{(l)} \rightarrow M + O_{2(g)} + H^+ + e^- \qquad (1.27)$$

(b) In alkaline media

Cathode process

$$4H_2O \ + 4e^- \rightarrow 2H_2 + 4OH^- \qquad E_c^o = -0.83\ V \qquad (1.28)$$

Anode process

$$4OH^- \rightarrow 2H_2 + 2H_2O_{(l)} + 4e^- \qquad E_a^o = 0.40\ V \qquad (1.29)$$

Proposed mechanism for anode process in alkaline media

$$M + OH^- \rightarrow MOH \qquad (1.30)$$

$$MOH + OH^- \rightarrow MO + H_2O_{(l)} \qquad (1.31)$$

$$2MO \rightarrow 2M + O_{2(g)} \qquad (1.32)$$

$$MO + OH^- \rightarrow MOOH + e^- \qquad (1.33)$$

$$MOOH + OH^- \rightarrow M + O_{2(g)} + H_2O_{(l)} \qquad (1.34)$$

1.5.3 Standard methods for evaluation of catalysts

Many research groups take catalytic measurements under different conditions so sometime their result does not match with each other's. That's why there is strong need to establish a standard catalyst evaluation protocol. McCrory et al, [53] proposed a standard flow chart. With the help of this chart we can evaluate many peculiar properties of catalysts like elemental composition, surface area, Faradic efficiency, catalytic activity and stability. Some important suggestions were made like1 M H_2SO_4 and 1 M NaOH as acidic and basic environment respectively, determine the over potential when current density reach to the10 mA/cm^2.

Electrochemically dynamic surface zone (ECSA) and Faradaic effectiveness (FE) measurements are two estimations which need a worth discussion. In the electrocatalysis of OER, numerous examinations report the estimation of Overpotential just for electrocatalysts at a fixed value of current density i.e. 10 mA cm^{-2}, and Faradaic efficiency was supposed to be 100%. However, current density does not explain the catalytic performance of OER catalyst and it leads to overestimation of catalytic efficiency of OER electrocatalysts. This point could be extremely significant particularly in a high anodic potential value potential circumstance while the electrocatalysts or substrates (carbon-based materials) experienced stage change or decay. In this manner, it is essential to do the estimations of Faradaic effectiveness either from H_2 and O_2 test as McCrory et al. proposed or utilizing GC estimations to distinguish the created O_2 gas and figure the Faradaic.

1.6 Thermodynamics of OER

Under standard conditions the thermodynamic potential for electrolysis with respect to OER is 1.23 V, however for practical purpose an extra potential is required. Value of extra potential is expressed as overpotential. It is discovered that other than IrO_2, the basic mechanism of the OER explains the adsorption of O and OH species on the substrate material for all OER catalysts [54].The accompanying protocol is exhibited under basic environment, which is similar to that in acidic medium:

$$OH + * \rightarrow OH_{ads} + e^- \qquad (1.35)$$

$$OH_{ads} + OH^- \rightarrow O_{ads} + H_2O + e^- \qquad (1.36)$$

Where, $*$ eludes the dynamic site of the stimulus surface, and "ads" addresses the adsorption on the impetus surface. The liberation of O_2 may be through two discretionary pathways. The first is the prompt coupling of two O_{ads} intermediates

$$O_{ads} + O_{ads} \rightarrow O_2 \qquad (1.37)$$

While second mechanism explains the combination of O_{ads} of with $OH^-$to form OOH_{ads} which further join with OH^- to liberate O_2. The second proposed mechanism for OER is more acceptable because thermodynamic barrier is less here.

$$O_{ads} + OH^- \rightarrow OOH_{ads} + e^- \qquad (1.38)$$

$$OOH_{ads} + OH^- \rightarrow O_2 + H_2O + e^- \tag{1.39}$$

$$2H_2O + * \rightarrow H^+ + e^- + OH_{ads} + H_2O \tag{1.40}$$

$$OH_{ads} + H_2O + * \rightarrow H^+ + e^- + O_{ads} + H_2O \tag{1.41}$$

$$H_2O + O_{ads} \rightarrow H^+ + e^- + OOH_{ads} \tag{1.42}$$

$$OOH_{ads} \rightarrow H^+ + e^- + O_2 \tag{1.43}$$

The Gibbs free energy for above mention steps can be written as,

$$\Delta G_1 = \Delta G_{OH} - eU + \Delta G_{H^+}(pH) \tag{1.44}$$

$$\Delta G_2 = \Delta G_O - \Delta G_{OH} - eU + \Delta G_{H^+}(pH) \tag{1.45}$$

$$\Delta G_2 = \Delta G_O - \Delta G_{OH} - eU + \Delta G_{H^+}(pH) \tag{1.46}$$

$$\Delta G_3 = \Delta G_{OOH} - \Delta G_O - eU + \Delta G_{H^+}(pH) \tag{1.47}$$

$$\Delta G_4 = 4.92[eV] - \Delta G_{OOH} - eU + \Delta G_{H^+}(pH) \tag{1.48}$$

Where U is the consider potential referenced to NHE in standard conditions, and the Gibbs energy change of the proton is processed using the Nernst condition as $\Delta G_{H+}[P] = -K_B T ln(10) \times pH$.. The Gibbs free energies of eq (1.49) identified with the adsorption energies of O_{ads}, OH_{ads} and OOH_{ads}. In a perfect circumstance, each elementary step is equal to 1.23 eV, which shows that there is no Overpotential gotten from thermodynamic boundary. Here, this doubt disregards the effect of dynamic impediments. Indeed as exhibited by Rossmeisl et al [55]. For the catalyst like RuO_2, the third step where the second water atom was expended requires a huge free energy gap of 1.6 eV. These results demonstrated that at possibilities more than 1.60 V, all elementary steps of the OER catalysis (over RuO_2) are exothermic. Koper et al. in like manner suggested that the excited association between OH_{ads} and OOH_{ads}. It tends to be the risky one in achieving an immaculate condition. Like the HER, the Overpotential of the OER is normally thought to be picked by the highest activation barrier of the individual reaction steps. Figuratively speaking, the Overpotential is controlled by the huge difference in the Gibbs free chemisorption energy of two coming about adsorbed intermediates. In this way, the speculative Overpotential can be obviously portrayed as,

$$\eta = \max[\Delta G_1, \Delta G_2, \Delta G_3, \Delta G_4]\,/e - 1.23[V] \qquad (1.49)$$

$$E_{OER} = E^0_{(\frac{O_2}{H_2O})} - \frac{RT}{4F} \times \ln(\frac{a_{H^+P(O_2)}\frac{}{P^0}}{a_{H_2O}}) \qquad (1.50)$$

Based on experimental results, the overpotential is related to logarithmical current density and thus, the linear portion of Tafel plot can be expressed as the Tafel equation.

$$\eta = \alpha + b\ logj \qquad (1.51)$$

1.7 Role of Co, Ni, Fe, Zn towards OER/HER

It is accounted for that after joining of other metal particles, the performance of individual Ni or Co metal oxide can be improved. Specifically, Ni– Fe oxides sharing hands with third metal (e.g., Ni– Al– Fe, Ni– Ga– Fe, and Ni– Cr– Fe) were ended up being exceedingly successful catalysts. Co metal is a promising candidate for the OER catalysis. Be that as it may, despite the fact that a few efforts have been taken to fabricate more stable Co metal nanoparticles metallic Co is as yet not stable at high anodic potentials [56]. Keeping in mind the end goal to exceedingly proficient option OER electrocatalysts, various Co based impetuses, for example, metal oxides [57], hydro(oxy) oxides [58, 59], Pervoskite [60], sulfides [61], nitride [62] and phosphates [64] have been contemplated. CoSx, CoNx and CoPx materials have displayed prevalent HER electrocatalytic performance [62], yet they have additionally pulled in colossal consideration for OER catalysis on account of their remarkable 3d electronic configuration. Li et al. [63] exhibited great HER and OER activity of hollow polyhedral CoP in both acidic and basic conditions. Liu et al. [64] investigated that Ti work upheld CoS_2 nano sheets showed a high current density of 300 $mA\ cm^{-2}$ at an applied voltage of 1.7 V versus RHE.

Ni-based electrocatalysts are a standout amongst the most encouraging other options to catalyze the OER inferable from their points of interest of minimal cost and rich stores. Oxides and hydroxides are suggested as the most productive nickel-based electrocatalysts for the OER. Currently Nickel Phosphides, [65] Sulfides [66] and Selenides [67] likewise pulled in impressive consideration since some fascinating outcomes were provided by these species. As examined above, Nickel Sulfides are productive HER catalysts with low overpotential, however their current densities were not attractive. Du et al. [67] right off the bat considered the electrocatalytic action of Ni_2P nanowires for the OER, and found that with CV persistent scanning, the current density was enhanced while the overpotential potential was lessened and showing that Ni_2P nanowires were the catalytic forerunner and the electroactive species were framed consequently. Matranga and associate [68] fabricated an organometallic $Ni_6(PET)_{12}$ (PET ¼ phenylethyl thiol) complex with crystal structure, and affirmed countless available active site by turnover frequency assurance ($70S^{-1}$ @2 V versus RHE). In view of DFT estimations, it was discovered that the little change in the adsorbate binding structure can change the deciding step amid the OER procedure and the onset potential.

Fabrication of the upgraded electrocatalysts in view of Mo with iron family or Fe alone is one of the fascinating fields of research. The fundamental purpose behind the high rate hydrogen evolution of Fee Mo alloys can be linked with impressive genuine surface region of these alloys [69]. The investigations on electrodeposited Fee Mo compounds expressed an overvoltage drop of 0.15 – 0.3 V for HER when contrasted with mild steel in a reproduced commercial electrolyte for chlorate generation Elezovic et al. [70] revealed that amid the electrodepositing of Fee Mo alloy, with an enhancement of current thickness, the substance of Mo expanded while the substance of Fe decreased. They additionally found the most minimal hydrogen overvoltage and the most astounding trade current thickness ($i = 2 \times 10^{-5}$) for the anode containing 40.7 at % Fe and 59.3 at % Mo.

1.8 References:

[1] S. Chu, A. Majumdar, Opportunities and challenges for a sustainable energy future, *Nat*, 488 (2012) 294.

[2] A.K. Hussein, Applications of nanotechnology in renewable energies, a comprehensive overview and understanding, *Renew. Sust. Energ. Rev*, 42 (2015) 460-476.

[3] J. Chen, D. Yang, D. Song, J. Jiang, A. Ma, M.Z. Hu, C. Ni, Recent progress in enhancing solar-to-hydrogen efficiency, *J. Power Sources*, 280 (2015) 649-666.

[4] K. Mazloomi, C. Gomes, Hydrogen as an energy carrier: prospects and challenges, *Renew. Sust. Energ. Rev*, 16 (2012) 3024-3033.

[5] H. Ibrahim, A. Ilinca, J. Perron, Energy storage systems—characteristics and comparisons, *Renew. Sust. Energ. Rev*, 12 (2008) 1221-1250.

[6] D.A. Rand, A journey on the electrochemical road to sustainability, *J. Solid State. Electrochem*, 15 (2011) 1579-1622.

[7] A. Veziroglu, R. Macario, Fuel cell vehicles: State of the art with economic and environmental concerns, *Int. J. Hydrogen Energy*, 36 (2011) 25-43.

[8] B.M. Hunter, H.B. Gray, A.M. Muller, Earth-abundant heterogeneous water oxidation catalysts, *Chem. Rev*, 116 (2016) 14120-14136.

[9] X. Yu, Z. Tang, D. Sun, L. Ouyang, M. Zhu, Recent advances and remaining challenges of nanostructured materials for hydrogen storage applications, *Prog. Mater. Sci*, 88 (2017) 1-48.

[10] C.G. Morales-Guio, L-A. Stern, X. Hu, Nanostructured hydrotreating catalysts for electrochemical hydrogen evolution, *Chem. Soc. Rev*, 43 (2014) 6555-6569.

[11] N.Z. Muradov, T.N. Veziroğlu, “Green” path from fossil-based to hydrogen economy: an overview of carbon-neutral technologies, *Int. J. Hydrogen Energy*, 33 (2008) 6804-6839.

[12] K. Maeda, K. Domen, Photocatalytic water splitting: recent progress and future challenges, *J. Phys. Chem. Lett*, 1 (2010) 2655-2661.

[13] B. Rausch, M.D. Symes, G. Chisholm, L. Cronin, Decoupled catalytic hydrogen evolution from a molecular metal oxide redox mediator in water splitting, *Science*, 345 (2014) 1326-1330.

[14] G. Valenti, A. Boni, M. Melchionna, M. Cargnello, L. Nasi, G. Bertoni, R.J. Gorte, M. Marcaccio, S. Rapino, M. Bonchio, Co-axial heterostructures integrating palladium/titanium dioxide with carbon nanotubes for efficient electrocatalytic hydrogen evolution, *Nat. Commun* , 7 (2016) 13549.

[15] R. Navarro, F. Del Valle, J.V. De La Mano, M. Álvarez-Galván, J. Fierro, Photocatalytic water splitting under visible light: Concept and catalysts development, *Adv. Chem*, 36 (2009) 111-143.

[16] C. Acar, I. Dincer, Comparative assessment of hydrogen production methods from renewable and non-renewable sources, *Int. J. Hydrogen Energy*, 39 (2014) 1-12.

[17] B. Lim, M. Jiang, P.H. Camargo, E.C. Cho, J. Tao, X. Lu, Y. Zhu, Y. Xia, Pd-Pt bimetallic nanodendrites with high activity for oxygen reduction, *Science*, 324 (2009) 1302-1305.

[18] J. Luo, J. Im, MT mayer, M. Schreier, MK Nazeeruddin, N. Park, D. Tilley, HJ Fan and M. Grätzel, *Science*, 345 (2014) 1593.

[19] M. Kuang, G. Zheng, Nanostructured bifunctional redox electrocatalysts, *Small,* 12 (2016) 5656-5675.

[20] B. Winther-Jensen, O. Winther-Jensen, M. Forsyth, D.R. MacFarlane, High rates of oxygen reduction over a vapor phase–polymerized PEDOT electrode, *Science*, 321 (2008) 671-674.

[21] M.W. Kanan, D.G. Nocera, In situ formation of an oxygen-evolving catalyst in neutral water containing phosphate and Co^{2+}, *Science*, 321 (2008) 1072-1075.

[22] R. Frydendal, E.A. Paoli, B.P. Knudsen, B. Wickman, P. Malacrida, I.E. Stephens, I. Chorkendorff, Benchmarking the stability of oxygen evolution reaction catalysts: the importance of monitoring mass losses, *ChemElectroChem*, 1 (2014) 2075-2081.

[23] T. Reier, M. Oezaslan, P. Strasser, Electrocatalytic oxygen evolution reaction (OER) on Ru, Ir, and Pt catalysts: a comparative study of nanoparticles and bulk materials, *ACS. Catal*, 2 (2012) 1765-1772.

[24] R. Kötz, H. Lewerenz, S. Stucki, XPS studies of oxygen evolution on Ru and RuO_2 anodes, *J. Electrochem. Soc*, 130 (1983) 825-829.

[25] J. Suntivich, K.J. May, H.A. Gasteiger, J.B. Goodenough, Y. Shao-Horn, A perovskite oxide optimized for oxygen evolution catalysis from molecular orbital principles, *Science*, 334 (2011) 1383-1385.

[26] R. Subbaraman, D. Tripkovic, K-C. Chang, D. Strmcnik, A.P. Paulikas, P. Hirunsit, M. Chan, J. Greeley, V. Stamenkovic, N.M. Markovic, Trends in activity for the water electrolyser reactions on 3d M (Ni, Co, Fe, Mn) hydr (oxy) oxide catalysts, *Nat. Mate* , 11 (2012) 550.

[27] A. Vojvodic, J.K. Nørskov, Optimizing perovskites for the water-splitting reaction, *Science*, 334 (2011) 1355-1356.

[28] H. Liang, F. Meng, M. Cabán-Acevedo, L. Li, A. Forticaux, L. Xiu, Z. Wang, S. Jin, Hydrothermal continuous flow synthesis and exfoliation of NiCo layered double hydroxide nanosheets for enhanced oxygen evolution catalysis, *Nano. Lett* , 15 (2015) 1421-1427.

[29] Z. Lu, H. Wang, D. Kong, K. Yan, P.-C. Hsu, G. Zheng, H. Yao, Z. Liang, X. Sun, Y. Cui, Electrochemical tuning of layered lithium transition metal oxides for improvement of oxygen evolution reaction, *Nat. Commun*, 5 (2014) 4345.

[30] D. Jeong, K. Jin, S.E. Jerng, H. Seo, D. Kim, S.H. Nahm, S.H. Kim, K.T. Nam, Mn_5O_8 nanoparticles as efficient water oxidation catalysts at neutral pH, *ACS. Catal*, 5 (2015) 4624-4628.

[31] Z-P. Nie, D-K. Ma, G-Y. Fang, W. Chen, S-M. Huang, Concave Bi_2WO_6 nanoplates with oxygen vacancies achieving enhanced electrocatalytic oxygen evolution in near-neutral water, *J. Mater. Chem*, 4 (2016) 2438-2444.

[32] M. Huynh, D.K. Bediako, D.G. Nocera, A functionally stable manganese oxide oxygen evolution catalyst in acid, *J. Am. Chem. Soc* , 136 (2014) 6002-6010.

[33] M. Liao, G. Zeng, T. Luo, Z. Jin, Y. Wang, X. Kou, D. Xiao, Three-dimensional coral-like cobalt selenide as an advanced electrocatalyst for highly efficient oxygen evolution reaction, *Electrochim. Acta*, 194 (2016) 59-66.

[34] L. Jiao, Y-X. Zhou, H-L. Jiang, Metal–organic framework-based CoP/reduced graphene oxide: high-performance bifunctional electrocatalyst for overall water splitting, *Chem. Sci*, 7 (2016) 1690-1695.

[35] H. Lei, C. Liu, Z. Wang, Z. Zhang, M. Zhang, X. Chang, W. Zhang, R. Cao, Noncovalent immobilization of a pyrene-modified cobalt corrole on carbon supports for enhanced electrocatalytic oxygen reduction and oxygen evolution in aqueous solutions, *ACS. Catal*, 6 (2016) 6429-6437.

[36] B. Wurster, D. Grumelli, D. Hötger, R. Gutzler, K. Kern, Driving the oxygen evolution reaction by nonlinear cooperativity in bimetallic coordination catalysts, *J. Am. Chem. Soc*, 138 (2016) 3623-3626.

[37] N. Zhang, M-Q. Yang S. Liu Y. Sun, Y-J. Xu, Waltzing with the versatile platform of graphene to synthesize composite photocatalysts, *Chem. Rev*, 115 (2015) 10307-10377.

[38] Y. Cheng, C. Xu, L. Jia, J.D. Gale, L. Zhang, C. Liu, P.K. Shen, S.P. Jiang, Pristine carbon nanotubes as non-metal electrocatalysts for oxygen evolution reaction of water splitting, *Appl. Catal. B*, 163 (2015) 96-104.

[39] B.J. Trześniewski, O. Diaz-Morales, D.A. Vermaas, A. Longo, W. Bras, M.T. Koper, W.A. Smith, In situ observation of active oxygen species in Fe-containing Ni-based oxygen evolution catalysts: the effect of pH on electrochemical activity, *J. Am. Chem. Soc*, 137 (2015) 15112-15121.

[40] H.S. Ahn, A.J. Bard, Surface interrogation scanning electrochemical microscopy of $Ni_{1-x}Fe_xOOH$ ($0< x< 0.27$) oxygen evolving catalyst: kinetics of the “fast” iron sites, *J. Am. Chem. Soc*, 138 (2015) 313-318.

[41] W. Ma, R. Ma, C. Wang, J. Liang, X. Liu, K. Zhou, T. Sasaki, A superlattice of alternately stacked Ni–Fe hydroxide nanosheets and graphene for efficient splitting of water, *ACS. Nano*, 9 (2015) 1977-1984.

[42] C-W. Tung, Y-Y. Hsu, Y-P. Shen, Y. Zheng, T-S. Chan, H-S. Sheu, Y-C. Cheng, H.M. Chen, Reversible adapting layer produces robust single-crystal electrocatalyst for oxygen evolution, *Nat. Commun*, 6 (2015) 8106.

[43] D.F. Abbott, D. Lebedev, K. Waltar, M. Povia, M. Nachtegaal, E. Fabbri, C. Copéret, T.J. Schmidt, Iridium oxide for the oxygen evolution reaction: correlation between particle size, morphology, and the surface hydroxo layer from operando XAS, *Chem. Mater*, 28 (2016) 6591-6604.

[44] I. Katsounaros, S. Cherevko, A.R. Zeradjanin, K.J. Mayrhofer, Oxygen electrochemistry as a cornerstone for sustainable energy conversion, *Angew. Chem. Int. Ed*, 53 (2014) 102-121.

[45] R. Solmaz, A. Döner, G. Kardaş, The stability of hydrogen evolution activity and corrosion behavior of NiCu coatings with long-term electrolysis in alkaline solution, *Int. J. Hydrogen Energy*, 34 (2009) 2089-2094.

[46] R. Solmaz, G. Kardaş, Electrochemical deposition and characterization of NiFe coatings as electrocatalytic materials for alkaline water electrolysis, *Electrochim. Acta*, 54 (2009) 3726-3734.

[47] F. Safizadeh, E. Ghali, G. Houlachi, Electrocatalysis developments for hydrogen evolution reaction in alkaline solutions–a review, *Int. J. Hydrogen Energy*, 40 (2015) 256-274.

[48] I.A. Raj, K. Vasu, Transition metal-based cathodes for hydrogen evolution in alkaline solution: electrocatalysis on nickel-based ternary electrolytic codeposits, *J. Appl. Electrochem*, 22 (1992) 471-477.

[49] R.A. Santana, S. Prasad, E.S. Moura, A.R. Campos, G.P. Silva, P. Lima-Neto, Studies on electrodeposition of corrosion resistant Ni–Fe–Mo alloy, *J. Mater. Sci*, 42 (2007) 2290-2296.

[50] M. Jafarian, O. Azizi, F. Gobal, M. Mahjani, Kinetics and electrocatalytic behavior of nanocrystalline CoNiFe alloy in hydrogen evolution reaction, *Int. J. Hydrogen Energy*, 32 (2007) 1686-1693.

[51] K. Macounová, J. Jirkovský, M.V. Makarova, J. Franc, P. Krtil, Oxygen evolution on $Ru_{1-x}NixO_{2-y}$ nanocrystalline electrodes, *J. Solid State. Electrochem*, 13 (2009) 959-965.

[52] A.J. Bard, L.R. Faulkner, J. Leddy, C.G. Zoski, Electrochemical methods: fundamentals and applications, Wiley New York 1980.

[53] C.C. McCrory, S. Jung, I.M. Ferrer, S.M. Chatman, J.C. Peters, T.F. Jaramillo, Benchmarking hydrogen evolving reaction and oxygen evolving reaction electrocatalysts for solar water splitting devices, *J. Am. Chem. Soc*, 137 (2015) 4347-4357.

[54] M. Bajdich, M. García-Mota, A. Vojvodic, J.K. Nørskov, A.T. Bell, Theoretical investigation of the activity of cobalt oxides for the electrochemical oxidation of water, *J. Am. Chem. Soc*, 135 (2013) 13521-13530.

[55] J. Rossmeisl, Z-W. Qu, H. Zhu, G-J. Kroes, J.K. Nørskov, Electrolysis of water on oxide surfaces, *J. Electroanal. Chem*, 607 (2007) 83-89.

[56] L. Wu, Q. Li, C.H. Wu, H. Zhu, A. Mendoza-Garcia, B. Shen, J. Guo, S. Sun, Stable cobalt nanoparticles and their monolayer array as an efficient electrocatalyst for oxygen evolution reaction, *J. Am. Chem. Soc*, 137 (2015) 7071-7074.

[57] Y-C. Liu, J.A. Koza, J.A. Switzer, Conversion of electrodeposited $Co(OH)_2$ to CoOOH and Co_3O_4, and comparison of their catalytic activity for the oxygen evolution reaction, *Electrochim. Acta*, 140 (2014) 359-365.

[58] Y. Zhan, G. Du, S. Yang, C. Xu, M. Lu, Z. Liu, J.Y. Lee, Development of cobalt hydroxide as a bifunctional catalyst for oxygen electrocatalysis in alkaline solution, *ACS. Appl. Mater. Interfaces*, 7 (2015) 12930-12936.

[59] M.A. Sayeed, T. Herd, A.P. O'Mullane, Direct electrochemical formation of nanostructured amorphous $Co(OH)_2$ on gold electrodes with enhanced activity for the oxygen evolution reaction, *J. Mater. Chem. A*, 4 (2016) 991-999.

[60] M. Xing, L-B. Kong, M-C. Liu, L-Y. Liu, L. Kang, Y-C. Luo, Cobalt vanadate as highly active, stable, noble metal-free oxygen evolution electrocatalyst, *J. Mater. Chem. A*, 2 (2014) 18435-18443.

[61] H. Wang, Z. Li, G. Li, F. Peng, H. Yu, Co_3S_4/NCNTs: A catalyst for oxygen evolution reaction, *Catal. Today*, 245 (2015) 74-78.

[62] P. Chen, K. Xu, Y. Tong, X. Li, S. Tao, Z. Fang, W. Chu, X. Wu, C. Wu, Cobalt nitrides as a class of metallic electrocatalysts for the oxygen evolution reaction, *Inorg. Chem. Front*, 3 (2016) 236-242.

[63] J. Suntivich, H.A. Gasteiger, N. Yabuuchi, H. Nakanishi, J.B. Goodenough, Y. Shao-Horn, Design principles for oxygen-reduction activity on perovskite oxide catalysts for fuel cells and metal–air batteries, *Nat. Chem*, 3 (2011) 546.

[64] T. Liu, Y. Liang, Q. Liu, X. Sun, Y. He, A.M. Asiri, Electrodeposition of cobalt-sulfide nanosheets film as an efficient electrocatalyst for oxygen evolution reaction, *Electrochem. Commun*, 60 (2015) 92-96.

[65] A. Han, H. Chen, Z. Sun, J. Xu, P. Du, High catalytic activity for water oxidation based on nanostructured nickel phosphide precursors, *Chem. Commun*, 51 (2015) 11626-11629.

[66] W. Zhou, X.-J. Wu, X. Cao, X. Huang, C. Tan, J. Tian, H. Liu, J. Wang, H. Zhang, Ni_3S_2 nanorods/Ni foam composite electrode with low overpotential for electrocatalytic oxygen evolution, *Energ. Environ. Sci*, 6 (2013) 2921-2924.

[67] A.T. Swesi, J. Masud, M. Nath, Nickel selenide as a high-efficiency catalyst for oxygen evolution reaction, *Energ. Environ Sci*, 9 (2016) 1771-1782.

[68] N-T. Suen, S-F. Hung, Q. Quan, N. Zhang, Y.-J. Xu, H.M. Chen, Electrocatalysis for the oxygen evolution reaction: recent development and future perspectives, *Chem. Soc. Rev*, 46 (2017) 337-365.

[69] B.E. Conway, L. Bai, Determination of the adsorption behaviour of ‘overpotential-deposited’hydrogen-atom species in the cathodic hydrogen-evolution reaction by analysis of potential-relaxation transients, *J. Chem. Soc*,

Faraday Transactions 1: Physical Chemistry in Condensed Phases, 81 (1985) 1841-1862.

[70] B.N. Grgur, N.V. Krstajić, N.R. Elezović, V.D. Jović, Electrodeposition and characterization of Fe–Mo alloys as cathodes for hydrogen evolution in the process of chlorate production, *J. Serb. Chem. So*, 70 (2005) 879-889.

Chapter # 02

Instrumentation

This chapter describes the theory of techniques used for characterization of the synthesized tetra metallic catalyst. The details of UV-Vis spectroscopy, cyclic voltammetry, X-ray diffraction, scanning and tunneling electron microscopy, linear sweep voltammetry are given in the forthcoming sections.

2.1 UV-Visible spectroscopy

Light properties can be explained in term of electromagnetic radiation. The electric component of light is linked with stationary and well moving charge particle while magnetic component of light is related with stationary charge particle. The characteristics properties of light are elaborated in shadow of speed of light (c), wavelength (λ) and frequency (ν). UV-Visible spectroscopy also called electronic spectroscopy and electronic spectra range from 100-800 nm. Out of this wavelength, visible region range from 420 nm to 700 nm, near ultra violet 200-400 nm and far ultra violet is below 200 nm. UV-Visible (Schimadzu 1601) spectrophotometer is used to characterize dispersed, transparent/colored and diluted solution.

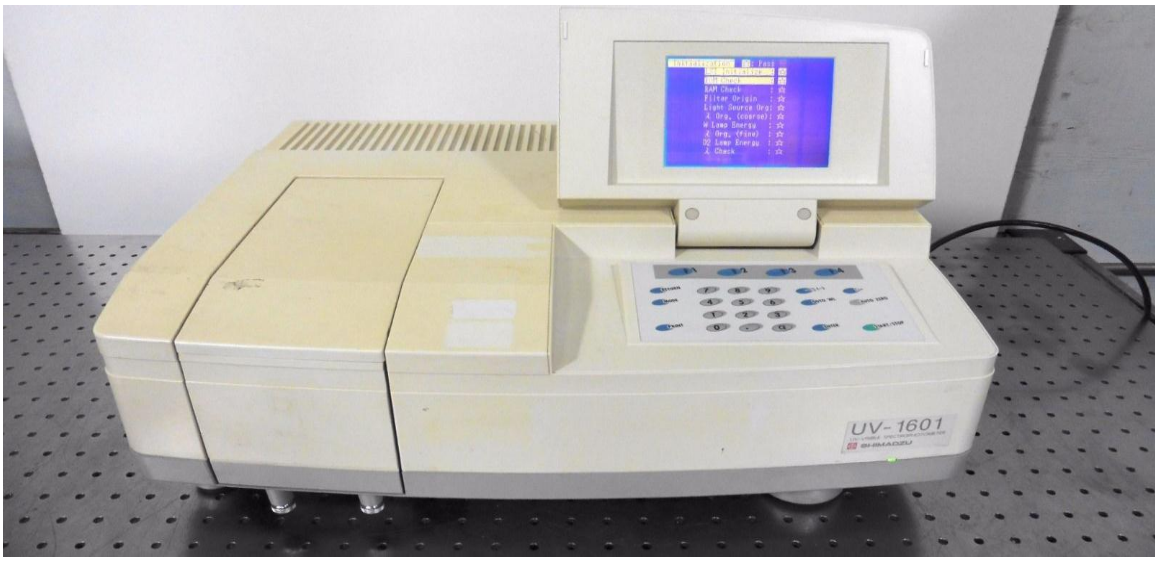

.

Figure 2.1 UV-Visible Spectrophotometer (Schimadzu 1601)

Peak intensity of the absorbed light is a function of the analyte concentration according to Beer-Lambert Law, when a radiation having specific wavelength and frequency pass through a medium, the light being transmitted or absorbed is proportional of the concentration of analyte and also proportional of the path length of the cell through which the radiations pass [1].

Mathematically,

$$A = \text{Log}\ I_o / I = \varepsilon\ c\ l \qquad (2.1)$$

Where *A* is the measured absorbance (Absorbance Units (AU)), I_o is the incident light intensity at a given wavelength, I intensity of transmitted light, *l* is for the path length of cell, and *c* the concentration of the species which absorb light. For each species and wavelength, ε represents the molar absorptivity and also expressed as extinction coefficient and it is constant for each wavelength and specie. This constant is a fundamental molecular property in a given solvent.

$$- \text{Log}\ I/I_o = - \log T = \varepsilon\ c\ l\ \text{or} \text{Log}\ I_o/I = A = \varepsilon\ c\ l \qquad (2.2)$$

2.2 Cyclic voltammetry

Cyclic voltammetry is a powerful electrical technique that deals to find the Oxidation and reduction potential of molecular species. Cyclic voltammetry also used to investigate the chemical reactions initiated via electron transfer which includes catalysis. Specie after losing elecron is consider as oxidized specie and reverse process occur when a specie gets reduced. In heterogeneous electron transfer process electron is either from HOMO of electrode to the LUMO level of specie (reduction) or from HOMO level of specie to LUMO level of electrode. External driving force (Potentiostate) is required to applied the voltage to working electrode, by varying the value of applied potential we can tune the energy level of electrons of working electrode. Homogeneous electron transfer proceeds through reductant specie that donates the electron to the analyte which is getting reduced. In typical voltammogram x-axis represents the parameter that is imposed on the system here is applied potential (V) and at y-axis here current is taken that is produced in the response of applied voltage as represented in **Figure 2.2.**

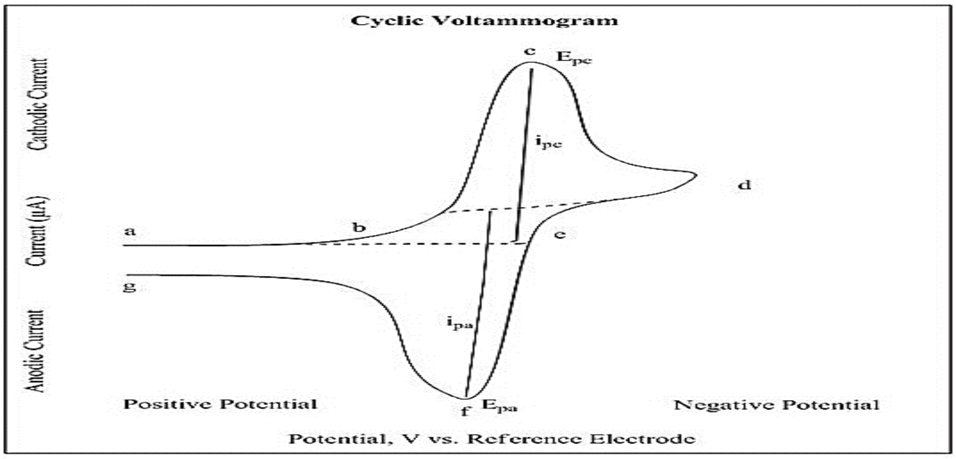

Figure 2.2 General representation of Cyclic Voltammetry.

Two conventions are commonly used to report the CV data, US and IUPAC conventions. The only difference between these two conventions is that these will appear to be reported by 180 ^{0}. Nernst Equation links the cell potential (*E*) to standard potential of specie (E). In equation

$$E = E^o + \frac{(RT)}{(nF)} ln \frac{(Ox)}{(Red)} \quad = \quad E = E^o + 2.303 \frac{(RT)}{(nF)} log_{10} \frac{(Ox)}{(Red)} \qquad (2.3)$$

F represents faraday constant, *R* is universal Gas constant, *T* is temperature and *n* reprents number of electrones. Nernst Equation provides a meaningful way to elaborate the response of system to the change of concentration of analyte in bulk or change of applied voltage.

According to the Nernst Equation availability of analyte varies near the working electrode sufrace as potential scans during CV experiment. Concentration of analyte relative to the distance from electrode interface is strongly linked with applied potential and how species travel between electrode sufarce and bulk of elecctrolyte solution. The potential of working electrode is measured in comparison with reference eleclrode which establish a constant potential. As potential scan negatively (Reduction), the concentration of specie A^+ which is getting reduced is depleted near the electrode surface and accumulation of reduced specie A occurs at electrode surface indicated as diffusion layer. Thickness of difussion layer goes on increasing throughout potential scan. With the increase in thickness of difussion layer the mass transport of A^+ towards electrode surface decreases. Consequently, as potential becomes more and more negative rate of difussion of A^+ from bulk to electrode surface bocomes slower resulting in decrease in current value as scane proceeds from a to d. At point d potential is reversed , this point is denoted as switching potential point. Now, potential scans in positive direction. The concentration of A specie starts depleted due to back conversion of A to A^+. Point r represents the $E_{½}$ called half wave potential, at this point the concentration of A becomes equal to the concentration of A^+. Diffussion of specie to and from electrode surface causes the separation of two peaks . For the electrochemically or chemically reversible reduction process peak to peak separation is 57 mV at 25° C (2.2 *RT/F*) and during forward scan the width of half maxima of the peak is 59 mV. The electrochemical reversibilty explains that specie is stable on reduction and can be sunsequently reoxidized. Reversibility factor provides the straight forward information about kinetics of electron transfer between analyte and electrode. When there is low kinteic barrier (electrochemical reversibilty) for electron transfer the system will attains equilibrium immediately upon a minor change in applied potential. By contrast, electrochemical irreversibilty offers the high kinetic barrier demanding more negative potential for species to be reduced and giving rise to the lager value of ΔE_p. Scan rate is rate which applied potential is scaned with respect to time. At high scane rate the thickness of diffussion layer decreases resulting high current value. Randles – Sevcik equation showes the relationship between scane rate and peak current [2].

$$i_p = 0.446nFAC^o[\frac{nF_vD_o}{RT}]^{1/2} \quad (2.4)$$

Randles-Savcik equation gives an indication that whether an analyte is freely diffusing in bulk solution or adsord on electrode surface. Above equation describes that graph between i_p and $v^{1/2}$ should be linear for adsorbed specie. Current response for an adsorbed specie on electrode surface is denoted as,

$$i_p = \frac{n^2F^2}{4RT}\Gamma^* \quad (2.5)$$

Γ^* is surface access concentration of asorbed specie with units of mole/cm^{-2}. The responce of i_p vs $v^{1/2}$ deviates form linearity for the species wich are thought to be diffuse freely in bulk solution. Deviation from linearity shows that either there is qausi-reversibilty or electron-transfer is occuring via adsobed specie. Peak to peak separation decides the reason behind the deviation. Peak to peak separation shift is observed for qausi-reversible process while for surface-adsorbed specie there is no peak to peak separation.

2.3 Linear sweep voltametry

LSV is an experimental technique utilizes the potentipstate consist of three electrodes system. The three electroode system comprises of working electrode, counter electrode and third one is reference electrode (RE). Linear sweep voltammetry shows the linear relationshiop of potential change with respect to time and scane rate. In LSV just the first half cycle of a linear sweep voltammetry plot is recorded and examining begins at a potential where no electrochemical process happens. The estimation of current can be seen at the potential where the charge exchange starts, which causes the increments in the potential. Be that as it may, after a most highest value it begins to decrease because of the consumption of diffusion layer at the interface of working electrode. Usually a rotaing disk electrode can be utilized in LSV experiment. Rotaing disk like electrode occurs during experiment and resulting enhancement in current depends opon the rotation of electrode [3]. Now the resulting currnet will be controlled by the rat at which solution flows across the disk electrode in contrast to the CV and LSV where resulting current modulations are totally difussion controlled. Speed of rotating disk electrode decides the rate of mass transport to and from the electrode surface. It can be tuned by changing its speed. Position of rotating disk electrode is verticle and set on rotaation with a constant angular velocity. Fluid viscosity factors depends uopn the angular velocity of rotating disk electrode. General representation of LSV is expressed in **Figure 2.3**

$$\omega = 2\pi f$$

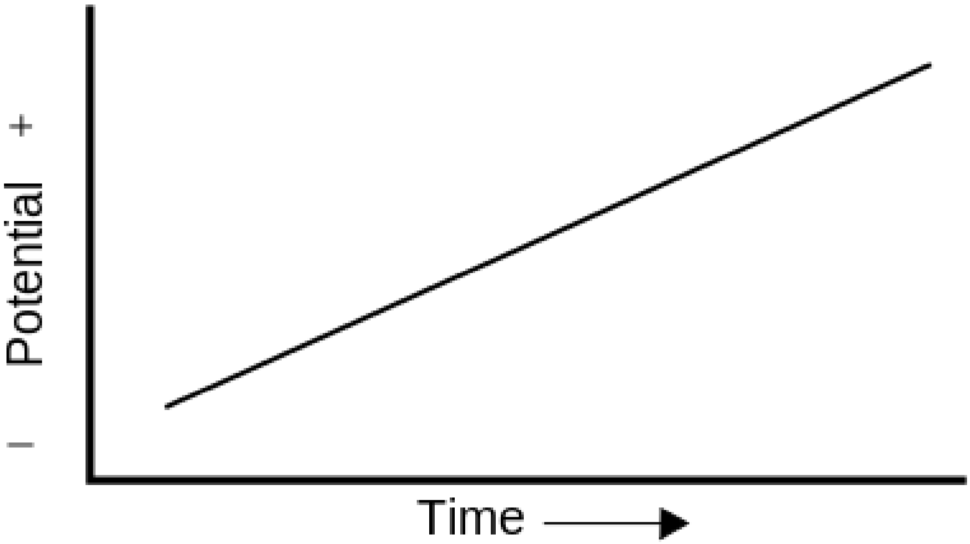

Figure 2.3 General representation of a linear potential sweep.

Where f has the meaning of rotational frequency with the units of revolution per minuts (rpm) or hertz. Rotational frequency also relys on many other factors like radial distance from the center of the disk (r), the coefficient of kinematic viscosity of the fluid (γ) and on the axial distance from the surface of the disk [4]. The Koutečky-Levich equation, considering both electron transport kinetics and mass transport can be written as [5].

$$\frac{1}{j} = \frac{1}{j_k} + \frac{1}{j_{lim}} \qquad (2.6)$$

J represents observed value of curent density, the disk current density in the absence of diffusion control current. The equation explaining the electron transfer process can be written as,

$$J_k = Fk\,(E)\,C \qquad (2.7)$$

Under the mass-transport limited conditions we can get the diffusion-limited current by the Levich equation. j_{lim} is given by equation [6].

$$j_{lim} = 0.21nFCD^{2/3}\gamma^{1/2}\omega^{1/6} \qquad (2.8)$$

Where, ω is the rate of rotation in rpm, and γ is the kinematic viscosity of the solution in which electrodes are rotating and the rest of the symbols stand for their usual notations. LSV can identify unknown species and can also determine the concentration of solutions. The unknown specie scan be identify with the help of $E_{1/2}$whiletheconcentration of analyte in solution can be determined using height of the limiting current. The sensitivity of current changes vs. voltage is directly related with the scan rate. Higher the value of potential per second result in more oxidation/reduction of analyte at the surface of the working electrode (FTO).While CV is applicable to most cases where LSV is used, there are some instances where linear sweep voltammetry is more useful. For example when the reaction is irreversible CV will not give any additional data that LSV would give us [7]. In one example, LSV was used to examine direct methane production via a bio-cathode. Since the production of methane from CO_2 is an irreversible reaction, CV did not present any distinct advantage over LSV.

2.4 Chronoamperometry (CA)

Chronoamperometry is an electrochemical system in which the potential of the working anode is ventured and the subsequent current from faradic process happening at the cathode surface (caused by the potential advance) is checked as a component of time. Constrained data about the identification of the electrolyzed species can be gotten from the proportion of the oxidation peak current versus the decrease in peak current. Be that as it may, similarly as with all pulsed strategies, CA produces higher benefits of charging current, which rot exponentially with time like any Randles circuit (RC). The Faradaic current which is because of electron exchange occasions and is frequently the current segment of interest decays as depicted in the Cottrell condition (eq. 2.15). CA is ordinarily used to explore with three cathodes framework. Since the current is incorporated over generally longer time interims, CA gives a superior signal to noise proportion in contrast with other amperometric techniques.

In CA the current is estimated as a component of time after use of a potential step perturbation. For instance, in **Figure 2.4 (a),** the potential is ventured from E_1 when there is zero current stream, i.e., where the reduction or oxidation of the electrochemically dynamic species does not occur, to E_2 which alludes to the redox response of analyte at the surface of cathode. The present time bend mirrors the adjustment in the fixation angle close to the interface of FTO working electrode. This includes a steady extension of the diffusion layer related with the consumption of the analyte with time. Subsequently, the current decays with time (at a planar terminal) as shown in **Figure 2.4 (b)** [8-10]**.** The Faradic current streams at any time after utilization of the potential step will comply with the Cottrell eq (2.9) [11].

$$I_{(t)} = nFaCD^{1/2}/\pi^{1/2}t^{1/2} = kt^{-1/2} \qquad (2.9)$$

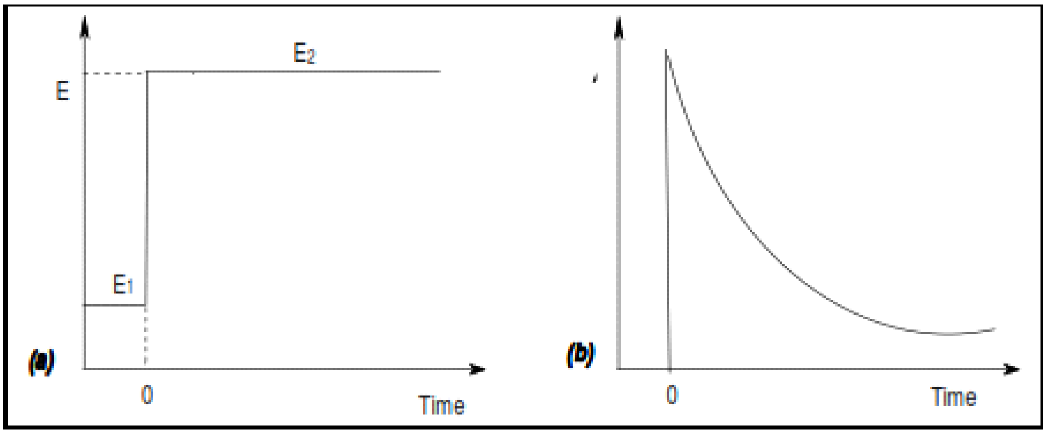

Figure 2.4 Potential Step Chronoamperometry (**a**) schematics application of potential steps (**b**) Chronoamperometry response.

Where *n*, n, F, A, c, D, and t are the number of electrons, Faradays constant, the surface area, the concentration, the diffusion coefficient, and time respectively. This equation demonstrates that $I_{(t)}$ differs with $t^{1/2}$. CA is regularly utilized for estimating the dispersion coefficient of electroactive species or the surface area of the working electrode. It can likewise be connected to explore the components of electrode processes [12].

2.5 X-ray Diffraction (XRD)

XRD is basically utilized for the recognizable proof of the phases of a crystalline material. This strategy can likewise be utilized for the recognizable proof of coated materials on electrodes, for example, FTO or ITO covered films. XRD depends on useful impedance of monochromatic X-beams and a crystalline sample. These X-beams are generated with the assistance of cathode beam tube then filtered to deliver monochromatic rays, followed by collimation to concentrate, and subjected to the target sample. The interaction of the beams generated with the target sample at that point an impedance is produced when conditions hold Bragg's Law ($n\lambda = 2d \sin \theta$) [13]. This law represents a relationship between the wavelength λ of electromagnetic radiation (EMR) to the diffraction edge θ and the crystal layer spacing d in a crystalline sample. These X-rays after diffraction are then recognized, prepared and analyzed by filtering the target material via a scope of 2θ angles (**Figure 2.5**). All possible diffraction bearings of the cross segments should be refined as a result of the unpredictable course of the target substance.

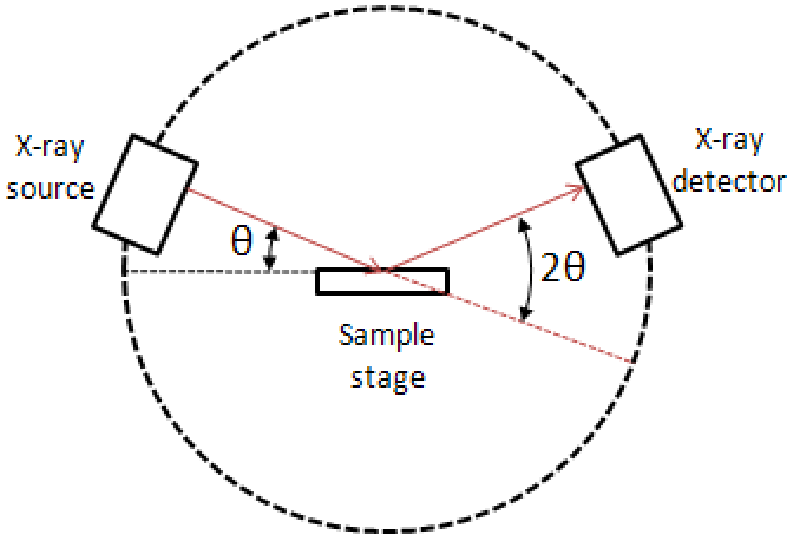

Figure 2.5 Schematics of the fundamental principle of XRD

Change of the diffraction peaks to line-spacing grants the recognizing evidence of the because of each material has a course of lattice with one of kind line-spacing [14]. Ordinarily, this can be expert by standing out the line-separating from some standard reference plans. X-ray beam diffractometer contains three basic parts:

(i) Cathode rays beam tube (ii) sample holder and (iii) an X-ray identifier as shown in **Figure 2.6.**

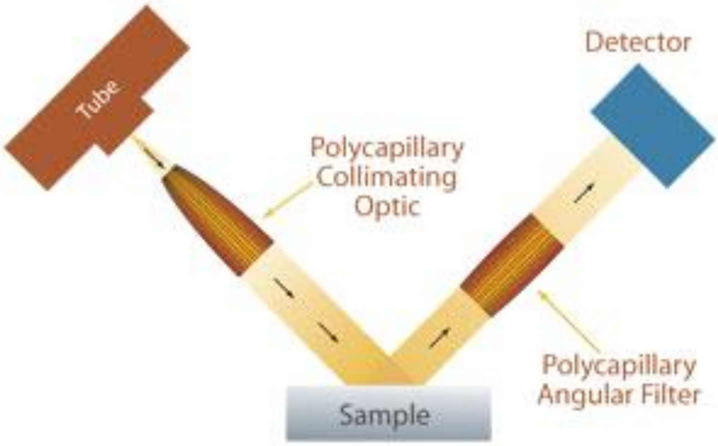

Figure 2.6 Instrumental setup of XRD.

X-Rays are generated in a cathode beam tube by warming filament to generate electrons, stimulating the electrons toward the target specie by applying a voltage, and blasting the target substance with these electrons. Exactly when electrons have satisfactory energy to clear inner shell electrons of the goal material, by then X-beam spectra are conveyed. These spectra include a couple of parts, the most generally perceived are $K\alpha$ and $K\beta$. $K\alpha$ involves $K\alpha1$ and $K\alpha2$. $K\alpha1$ has a barely shorter wavelength and two fold the intensity as $K\alpha2$ (**Figure 2.7**). Every objective material has its own characteristic wavelength (Cu, Fe, Mo, and Cr). Filtration using monochromaters of crystals or foils is obligatory to make monochromatic X-rays required for diffraction. Copper is the most broadly perceived target material for single-gem diffraction with Cu $K\alpha$ rays = 1.5418å [91, 92]. These X-rays radiations are then collimated and thereafter organized onto the target material. As the target material and detector are turned, the intensity of the X-beams which is reflected is analyzed and recorded. Exactly when the geometry of the striking X-rays impinging the example satisfies the Braggs Equation, accommodating check happens. A marker by then records and analyses this X-rays peaks and changes over the flag to a check rate which is then the yield to a gadget, for instance, a printer or PC screen.

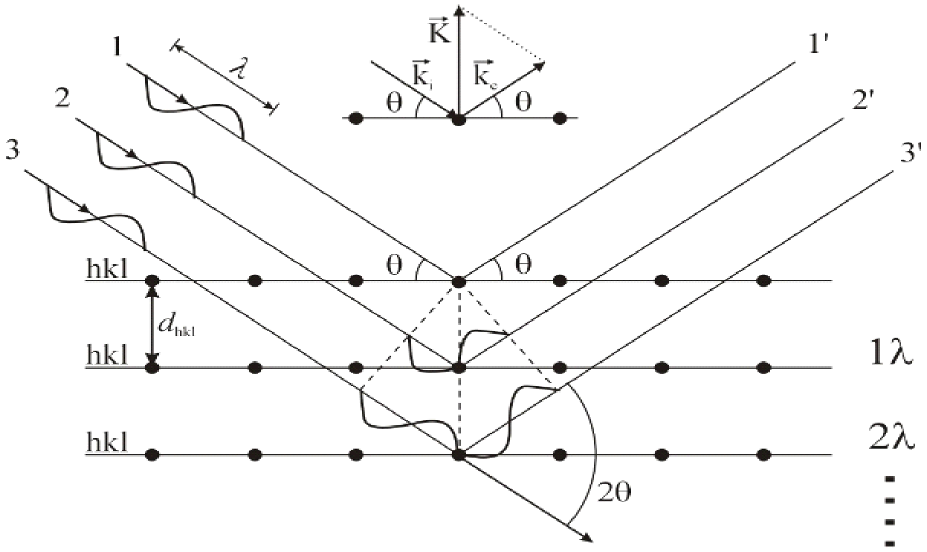

Figure 2.7 X-ray diffraction pathways in a sample of interest.

XRD analysis is most commonly done for the quantification and qualification of unclear crystalline species (e.g. minerals, inorganic mixtures and FTO/ITO covered films of variety of the substances). Declaration of doubtful solid materials is basic to consider in geology, natural science, material science, and biology. Further uses of XRD include:

- The assurance of unit cell measurements
- Analysis of sample purity
- Finding the crystal structures of target materials
- Quantitative investigation of materials like minerals)

Fabricated thin films characterized by:

- Determining lattice confuse amongst film and substrate
- Determining disengagement thickness and nature of the film by rocking curve measurement
- Determining the roughness, thickness and density of the film by making focus on frequency of reflective X-rays.

The force of diffracted X-beams is particularly related to the rotation of detector and sample tested, recorded as the target sample and detector turns through their separate degrees. A peak in intensity occurs when the mineral contains cross segment planes having line-separating appropriate to diffracted X-beams at that estimation of θ [15-17]. In spite of the fact that each peak involves two separate reflections (Kα1 and Kα2), at little estimations of 2θ the peak areas cover. More critical separation occurs at higher estimations of θ. These closely spaced peaks are managed as one. Results are commonly exhibited as peak positions at 2θ and X-ray intensity in tabulated form or a x-y plot as showed up in (**Figure 2.8**). Either peak height or area under the peak in case of incorporated intensity reveals the intensity of peak, which is the power above base line. The relative intensity is discovered as the extent of the peak height to that of the most intense sharp peak (relative force = I/I1 x 100).

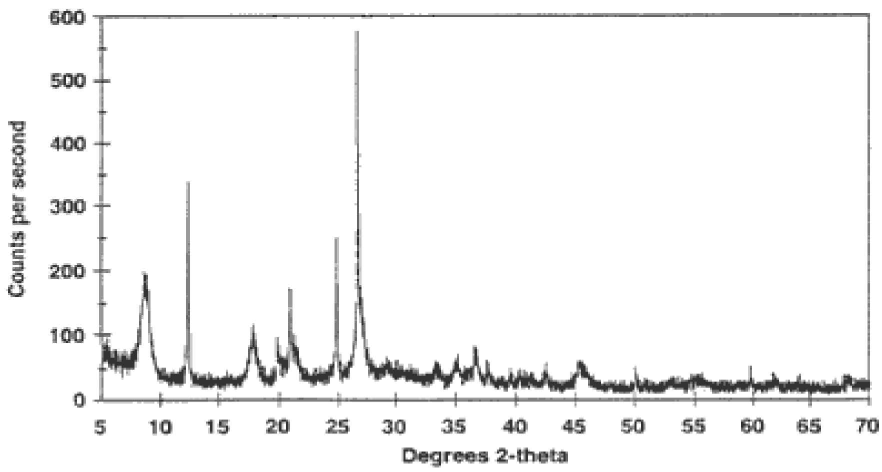

Figure 2.8 X-Y plots of intensity *vs.* 2θ.

2.6 Scanning electron microscopy (SEM)

SEM characterization is a kind of electron microscopy that involves the use of high energy electrons that interact with atom in materials and create the image corresponding to the surface morphology of that material. The signals that originate as a result of interaction of high energy beam with materials containing a lot of information about that material including material compositions, morphology and crystallinity of materials. Different types of signals originate including secondary electrons images (SEI), back scattered electron images (BSEI) and Characteristics X-ray and light (CL). SE images are produced as a result emission of electrons from very close to the specimen surface.

Figure 2.9 A commonly used SEM instrument, with the sample chamber, EDX detector, electron column, electronics console and display monitors.

It provides the information about surface morphology with high resolution. BSEI images originates when electrons are emitted from deeper surface of material. BSEI images clarify the distribution of elements, not identify in specimen material. The inner shell electron is removed by X-ray beam of high energy electrons [18-21]. When excited electrons come to ground energy level (to fill these shells) causing the release of energy. The intensity of peak can be measure by energy dispersive X-ray spectroscopy (EDX).

2.7 References

[1] A. Primer, Fundamentals of UV-visible spectroscopy, Copyright Hewlett-Packard Company, Hewlett-Packard publication, (1996).

[2] F.J. Holler, D.A. Skoog, S.R. Crouch, Chapter 1, Principles of instrumental analysis (6th ed.). Cengage Learning, (2007) 9.

[3] E.I. Rogers, D.S. Silvester, D.L. Poole, L. Aldous, C. Hardacre, R.G. Compton, Voltammetric characterization of the ferrocene| ferrocenium and cobaltocenium| cobaltocene redox couples in RTILs, *J. Phys. Chem C*, 112 (2008) 2729-2735.

[4] J-A. Ni, H-X. Ju, H-Y. Chen, D. Leech, Amperometric determination of epinephrine with an osmium complex and nafion double-layer membrane modified electrode, *Anal. Chim. Acta*, 378 (1999) 151-157.

[5] R.D. Rocklin, R.W. Murray, Kinetics of electrocatalysis of dibromoalkyl reductions using electrodes with covalently immobilized metallotetraphenylporphyrins, *J. Phys. Chem A*, 85 (1981) 2104-2112.

[6] A.J. Bard, G. Inzelt, F. Scholz, Electrochemical dictionary, Springer Science & Business Media 2008.

[7] S. Cheng, D. Xing, D.F. Call, B.E. Logan, Direct biological conversion of electrical current into methane by electromethanogenesis, *Environ. Sci. Technol*, 43 (2009) 3953-3958.

[8] A.J. Bard, L.R. Faulkner, J. Leddy, C.G. Zoski, Electrochemical methods: fundamentals and applications, Wiley Vol, 2, New York (1980).

[9] P. Kissinger, W.R. Heineman, Laboratory Techniques in Electroanalytical Chemistry, revised and expanded, CRC press 1996.

[10] S.N. GUPTA, Some theoretical aspects of polarography.

[11] A.J. Bard, L.R. Faulkner, Fundamentals and applications, Electrochemical Methods, 2 (2001) 482.

[12] A.M. Bond, S. Fletcher, F. Marken, S.J. Shaw, P.G. symons, electrochemical and x-ray diffraction study of the redox cycling of nanocrystals of 7, 7, 8, 8-tetracyanoquinodimethane. observation of a solid–solid phase transformation controlled by nucleation and growth, *J. Chem. Soc*, Faraday Transactions, 92 (1996) 3925-3933.

[13] L. McCusker, R. Von Dreele, D. Cox, D. Louër, P. Scardi, Rietveld refinement guidelines, *J. Appl. Crystallogr*, 32 (1999) 36-50.

[14] J.B. Brady, S.J. Boardman, Introducing mineralogy students to x-ray diffraction through optical diffraction experiments using lasers, *J. Geol. Ed*, 43 (1995) 471-476.

[15] B. Dutrow, Better living through minerals: X-ray diffraction of household products, Teaching Mineralogy, Mineralogical Society of America, Washington, DC, (1997) 349-359.

[16] J.B. Brady, R.M. Newton, S.J. Boardman, New uses for powder X-ray diffraction experiments in the undergraduate curriculum, *J. Geol. Ed*, 43 (1995) 466-470.

[17] J.B. Brady, Making solid solutions with alkali halides (and breaking them), Teaching Mineralogy. Mineralogical Society of America Monograph, 3 (1997) 91-96.

[18] A. Clarke, C.N. Eberhardt, C. Eberhardt, Microscopy techniques for materials science, Woodhead Publishing2002.

[19] R.F. Egerton, Electron Optics, Physical Principles of Electron Microscopy, Springer2016, pp. 27-54.

[20] Z.K. Heiba, N. Imam, M.B. Mohamed, Coexistence of cubic and hexagonal phases of Cd doped ZnS at different annealing temperatures, *Mater. Sci. Semicond. Process*, 34 (2015) 39-44.

[21] L. Reimer, Scanning electron microscopy: physics of image formation and microanalysis, Springer2013.

Chapter # 03

Experimental methodology

This chapter offers the details of chemicals, research methodology adopted, and scheme for the preparation of tetra metallic electrocatalyst for water electrolysis.

3.1 Chemicals used

In the development of electrocatalyst, analytical grade salts and solvents were used without further purification. Glass ware used during experimental section was rinsed with ethanol, acetone and finely with de-ionized water and dried for further use. All chemicals used were provided by sigma Aldrich with 98 percent purity. All salt solution required for alloy formation were prepared in de-ionized water. FTO were used as conducting substrate. Before use FTO were cleaned carefully. FTO were rinsed tab water and followed by ultrasonication with ethanol for 20 mints, acetone for 20 mints and distilled water for 20 mints. In-situ electrodeposition method was utilized for development of thin film on FTO substrate. All chemicals and solvents consumed during research work were listed below with their chemical formula, molar mass and Supplier Company.

General scheme comprises of three steps [1].

Step (1) Preparation of aqueous solution of metal salts of Co, Ni, Fe & Zn.

Step (2) Ultrasonication of FTO surfaces with Acetone and distilled water to remove contaminations.

Step (3) Fashioning of tetrametallic films on FTO using different electrolyte media.

Step (4) Optimization of electrolyte media both for CPE and LSV by comparing the results of CPE and LSV of FTO coated films deposited in different media.

Step (5) Modified FTO thin films examined via XRD, SEM and EDX.

Step (6) Differentiating the performances of catalytic activity in Acidic, Basic and Neutral medium.

Step (7) Comparison of catalytic results of Bi-metallic, tri-metallic and tetrametallic electrocatalyst in previously optimized electrolyte medium. **Table 3.1** expresses the list of chemicals used in present work.

Table 3.1 List of chemical used with their chemical formula, molar mass and Supplier Company.

Sr. No	Names of Salts/Chemicals	Chemical Formula	Molar Mass (g/mole)	Supplier
1	Cobalt (II) Sulfate Heptahydrate	$CoSO_4.7H_2O$	281.10	Sigma Aldrich
2	Nickel (II) Sulfate Pentahydrate	$NiSO_4.5H_2O$	249.69	Sigma Aldrich
3	Zinc Sulfate Heptahydrate	$ZnSO_4.7H_2O$	287.56	Sigma Aldrich
4	Iron (II) Sulfate Heptahydrate	$FeSO_4.7H_2O$	278.01	Sigma Aldrich
5	Potassium Hydroxide	KOH	56.11	Sigma Aldrich
6	Boric Acid	H_3BO_3	61.83	Sigma Aldrich
7	Lithium Sulfate	Li_2SO_4	109.94	Sigma Aldrich
8	Potassium Chloride	KCl	74.55	Sigma Aldrich
9	Citric Acid	$C_6H_8O_7$	192.12	Sigma Aldrich
10	Sodium Sulphate	Na_2SO_4	142.04	Sigma Aldrich

3.2 Detail note on scheme followed during experimental work

3.2.1 Preparation of aqueous solution of Co, Ni, Fe and Zn.

Initially 0.002 M solution of zinc sulphate 0.002 M Nickel Sulphate, 0.003 M solution of Cobalt Sulphate and 0.004 M Iron Sulphate was prepared in 100 mL of distilled water by dissolving calculated amount of respective salts. All the selected metals salts were highly soluble in acidic medium confirmed via UV Visible. Metals salts when dissolved in basic medium precipitates were formed.

3.2.2 Sonication of FTO surfaces for 15 minutes with Acetone and water to remove contamination.

Since FTO surfaces being highly conductive were used as substrate material. FTO surfaces having surface area $1cm^{-2}$ were initially washed with tab water to remove small grains of glass. After that FTO surfaces were sonicated for 15 mints first with acetone then with distilled water for their preparation for modification. Modification of transparent conducting substance is reported rarely. FTO (fluorine doped tin oxide) and ITO (Indium doped tin oxide) are widely used TCO (transparent conductive oxides). However potential barrier between TCO and other conducting layers limits the manufacturing of energy devices. In contrast to the other conducting devices work function of FTO is tunable [2, 3].

FTO (Fluorine doped Tin Oxide) glass substrate is highly conductive and widely used in variety of energy devices consisting applications like energy saving windows, thin film photovoltaic, touch screen displays, opto-electronics and insulating applications. FTO acts as promising substance because it mechanically hard, chemically inert, it offers the relative stability under atmospheric conditions, tolerance to mechanically abrasion, cost effective than Indium Tin Oxide, increasing light transmittance, thermal and heated glass performance, optimizing electrical conductivity and high heat resistance. TEC glass substances from Pilkington are considered as superior material with respect to performance and cost. However FTO substances avoid problems with indium diffusion into N-type TiO_2 and ZnO nanostructured thin Films.

3.2.2.1 Peculiar features of FTO coated glass substrate.

1. Electrically conductive. FTO glass sheets are highly conductive for thermal and heat control, reduced transmittance and electrostatic dissipation of electromagnetic radiation.
2. Color neutral glass. FTO shows reflector color, enhance light transmittance and reduces haze for clear visibility
3. Easily fabricated. Durable pyrolytic surface of FTO can be easily cut, handled, heat-strengthened, laminated, tempered and insulated using standard methods.
4. Bendable TEC Glass™. FTO sheets are moldable after production and can be heat processed, unlike soft or sputter-coated glass products.
5. Durable Pyrolytic Surface. FTO surface offers unlimited shelf life minimizes scratches and rubs. It will not change color or oxidize over time.
6. Available in a variety of glass thicknesses and surface resistivity ranging from 7 Ω/sq. up to 13 Ω/sq.

3.2.3 Fashioning of tetrametallic films on FTO using different electrolyte media.

3.2.3.1 Electrochemical Deposition.

The field of electrochemistry provides with comprehensive note on different processes (e.g. corrosion and electrophoresis), devices (electrochemical and electrobiological sensors, electrochromical displays, fuel cells and batteries), and various methodologies (the electrodeposition of metals and the production of aluminum and chlorine at large-scale) The technology of electrochemical deposition of metals and alloys involves the reduction of ions from aqueous, organic, and fused salt electrolysis. The deposition of material species involves reduction of ions in the solution as, MZ+ Sol + Ze → M lattice. The seemingly simple single reaction needs pre and post-complex steps before contributing to the whole deposition process as shown in **Figure 3.1**. This is a response of charged particles at the interface between bulk solution and solid electrode surface. The two kinds of charged species, an electron and an ion can cross the electrode-solution interface [4]. Hence, four types of fundamental areas associated in the deposition process:

(1) electrode-solution interface as the locus of deposition process,

(2) Kinetics and mechanism of the deposition process,

(3) Nucleation and growth processes of the deposits, and

(4) Structure and properties of the deposits.

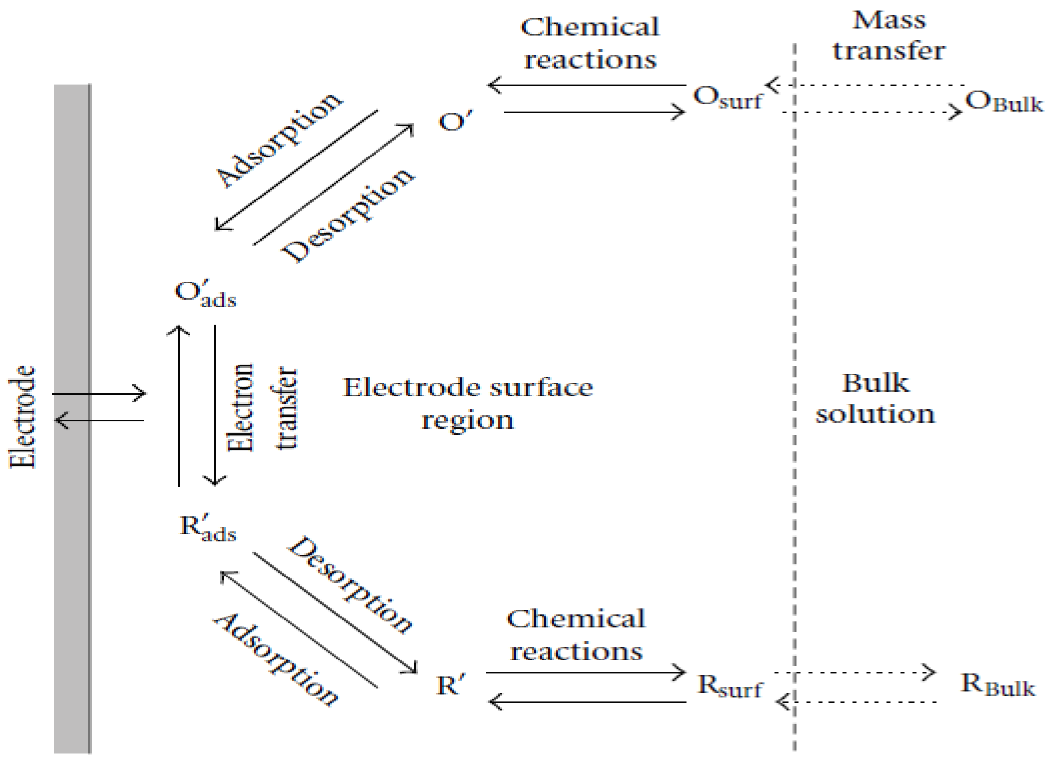

Figure 3.1: Pathway of a general electrode reaction.

Small is not only beautiful but also eminently useful. The increasing interest in this field is justified by the various unique characteristics of electrodeposited materials and these electrodeposited systems have shown components of properties like catalytic sensors, optical, magnetic, electrical, magneto-optical and opt-electrical devices. The fabrication of electrodeposited materials for industry has fruited in a tremendous development in innovative stable thin film processing schemes. Various technologies have been carried out to design thin films. While each fabrication scheme results in materials having unique features depending upon the scheme applied and material is used. Electrochemistry has reached sufficient maturity and sophistication to be used for the deposition of fine-structured films. Fundamentally, electrodeposition can yield grain sizes in the nano-crystalline range when the electrodeposition variables (e.g., bath composition, pH, temperature, current density) are chosen such that nucleation of new grains is favorably improved as compared to the growth of existing grains. Size reduction of the crystals based upon low temperature of formation is getting to be prominent due to "clean" fabrication. At low temperature, the population of critical clusters, that is, nucleation increases whereas the rate at which further atoms get close (growth of nuclei) to the cluster decreases because of expanded dissemination hindrance. Similar to the Cryoelectrochemistry many developments was made in low temperature aspects of electrochemistry. Cryoelectrochemistry (at around −70◦C) has certain limitations for electrochemical analysis in nonpolar medium is has rarely been studies for electro study in aqueous medium. Studies have been limited to synthesis of insoluble products to as low as 10◦C. The reports have primarily enrolled the impacts of the parameter either on the morphological and property varieties or the electrochemical investigation. Linkage of the morphological development and structural with the nucleation growth mechanism isn't unmistakably comprehended and, accordingly, should be investigated.

Despite the fact that during nucleation will be favored at low temperatures of electrodeposition, the film progression may get blocked because of poor consistency of the electroplating. Joined connections of low temperature and ultrasound can be obvious in this shortage regarding good appearance, adherence, great surface Coverage, and solidness of films. Ultrasound has been observed to be valuable by (I) causing greatly quick mass transport, (ii) influencing the development of solid film at the anode surface and (iii) upgrading the kinetics of dissolution and mixing at low temperature. A few authors have additionally announced the electro study at that low temperature, yet their work was mostly centered on electrochemical synthesis and study of soluble products. Be that as it may, to the best of our insight, no particular earlier work has been completed on testimony arrangement at low temperature; however the sufficient writing is accessible on the impacts of this parameter on structure and properties of stores at room and high temperatures. The pace and advancement of improvements is expanding a space being used of low temperature and ultrasound towards thin film fabrication. Precise finely examination of nucleation and growth mechanism, structural variation, solid state process, phase boundaries and the warm and mechanical and thermal stability of thin film frameworks are expected to enhance the fundamental comprehension of the procedure [5]. Before fashioning of metal ions at FTO cyclic voltammetry characterization was conducted in acidic solution containing 0.5 M Boric acid and 0.1 M Lithium sulphate surface to find the reduction potential of metals ions. Cyclic voltammetry was performed using three electrodes assembly in which FTO as working electrode, Pt wire as counter electrode and Ag/AgCl was used as reference electrode. Purging of N_2 gas was carried out for

8-10 mints before every CV scan to remove the dissolve Oxygen. After determination reduction potential selected metals Chronoamperometry was conducted in order to electroplate metal on electrode surface. To electrochemically deposit these metals at electrode surface we have to provide more negative potential then the reduction potential of respective metal. So, for the purpose to get thin, stable and porous surface catalyst film on FTO surface, metals were deposited electrochemically instead of mechanically. Electroplating was carried out in both acidic and alkaline medium. **Figures 3.2** shows the images of FTO films modified under alkaline conditions while the **Figure 3.3** expresses FTO coating under acidic conditions. On the basis of electrodeposition pattern, thickness and porosity of film developed influence of acidic and alkaline solution was investigated.

-1.30 V -1.40 V -1.50 V

Figure 3.2 FTO modified surfaces under acidic conditions.

-1.30 V -1.40 V -1.50 V

Figure 3.3 FTO modified surfaces under alkaline conditions.

To find most suitable electrolyte solution to carry out electroplating of single and tetrametallic catalyst film various medium were electrochemically tested. In first step Chronoamperometry for single metal deposition at FTO surface was conducted in acidic and alkaline solution followed by the electroplating of tetrametallic film deposition in acidic and basic conditions. 5 ml from each salt solution ($ZnSO_4$+$CoSO_4$+$NiSO_4$+$FeSO_4$) and 20 ml of electrolyte solution was taken in electrochemical assembly cell containing three electrodes. It was ensured that all three electrodes were dipped in solution. After that Chronoamperometry was conducted at three potential ranges -1.3 V, -1.4 V and -1.5 V for 900 seconds. Once FTO surfaces were modified in different electrolyte solution then LSV was conducted at 10 mv/ sec in alkaline solution of pH = 13.

3.2.4 Optimization of electrolyte media both for CPE and LSV by comparing the results of CPE and LSV of FTO coated films deposited in different media.

CPE and LSV results of FTO films were compared and finely medium was optimized and further all deposition was conducted in optimized medium.

3.2.5 Modified FTO thin films examined via XRD, SEM and EDX.

As from CPE and LSV results we have conclude that a thin and stable film was formed in acidic medium containing 0.5 M H_3BO_3 coupled with 0.1 M Li_2SO_4. SEM images of usually provide information about surface morphology of various materials.

So different FTO surfaces were modified with mono and tetrametallic catalyst films and in order to examine these films various characterization techniques i.e. XRD, SEM and EDX were carried out.

3.2.6 Differentiating the performances of catalytic activity in Acidic, Basic and Neutral medium.

Electrocatalysis can be carried out in wide range of pH from acidic to neutral and basic medium. OER kinetic vary in acidic and basic conditions depending upon the materials utilized for catalysis. Usually catalyst driven from 3d transition metals does OER catalysis in alkaline solution more favorably as compared to in acidic solution while catalysts like Ir and Ru and their derivatives drive OER more easily in acidic condition. It usually depends upon the mechanism followed during catalysis.

Many scientists published various review to summarize various reported OER mechanism. In present work behavior of developed electrocatalyst was also investigated in acidic, neutral and basic solution. For this purpose three FTO surfaces were separately modified with tetrametallic electrocatalyst under optimized conditions after that linear sweep voltammogram was conducted for each modified FTO to check their response in acidic, neutral and basic conditions.

The behavior of developed electrocatalyst was also investigated in acidic, neutral and basic solution. For this purpose three FTO surfaces were separately modified with tetrametallic electrocatalyst under optimized conditions after that linear sweep voltammogram was conducted for each modified FTO to check their response in acidic, neutral and basic conditions.

3.2.7 Effect of binder and concentration of metals salts on catalytic activity.

To monitor the effect of binder on catalytic activity of tetrametallic electrocatalyst different FTO surface was modified with tetrametallic electrocatalyst in acidic medium followed by drop wise addition of SDS on catalyst film. After drying the film LSV was carried out at 10 mV /sec in alkaline medium.

3.2.8 Comparison of catalytic results of Bi-metallic, tri-metallic and tetrametallic electrocatalyst in previously optimized electrolyte medium.

All possible combinatorial screening of bimetallic and Trimetallic combinations of selected four transition metals (Fe, Zn, Ni & Co) was deposited on FTO under acidic conditions and their LSV scans was carried out at scan rate of 10 mV/sec.

3.3 Instrument used

All the electrochemical experiments were performed by means of computer controlled potentiostat Metrohm Autolab PGSTAT-302N running with NOVA 1.11 software and FRA32M module specially designed for electrochemical impedance spectroscopy (see **Figure 3.4**). The PGSTAT302N is the successor of the popular PGSTAT30. It has a maximum current of 2 A. Its current range can be extended to 20 A with the BOOSTER20A, the current resolution is 30 fA at a current range of 10 nA.

Figure 3.4 PGSTAT 302N Metrohm-Autolab.

3.4 References

[1] J. Wang, L. Ji, Z. Chen, In situ rapid formation of a nickel–iron-based electrocatalyst for water oxidation, *ACS. Catal*, 6 (2016) 6987-6992.

[2] M. Abellán, R. Schrebler, H. Gómez, Electrodeposition of Bi_2Te_3 thin films onto FTO substrates from DMSO solution, *Int. J. Electrochem. Soc*, 10 (2015) 7409-7422.

[3] D. Han, C. Wu, Y. Zhao, Y. Chen, L. Xiao, Z. Zhao, Ion implantation-modified fluorine-doped tin oxide by zirconium with continuously tunable work function and its application in perovskite solar cells, *ACS. Appl. Mater. Interfaces*, 9 (2017) 42029-42034.

[4] A.J. Bard, Chemical modification of electrodes, *ACS. Publications*, 1983.

[5] M. Khelladi, L. Mentar, M. Boubatra, A. Azizi, Study of nucleation and growth process of electrochemically synthesized ZnO nanostructures, *Mater. Lett*, 67 (2012) 331-333.

Chapter 04

Results and Discussion

This chapter deals with the all experimental results that ensure the synthesis of tetrametallic electrocatalyst via Chronoamperometry technique. The chapter under discussion also includes the characterization results (XRD, EDX SEM) of tetrametallic catalyst film developed at FTO surface confirming formation of catalyst film. Electrochemical OER catalytic performance of the designed catalyst is presented in the subsequent sections.

4.1 Cyclic voltammetry of metal ions in 0.5 M H_3BO_3 + 0.1 M Li_2SO_4

In order to find the reduction potential of metals ions, cyclic voltammetry characterization was conducted in acidic solution containing 0.5 M Boric acid and 0.1 M Lithium sulphate [1].

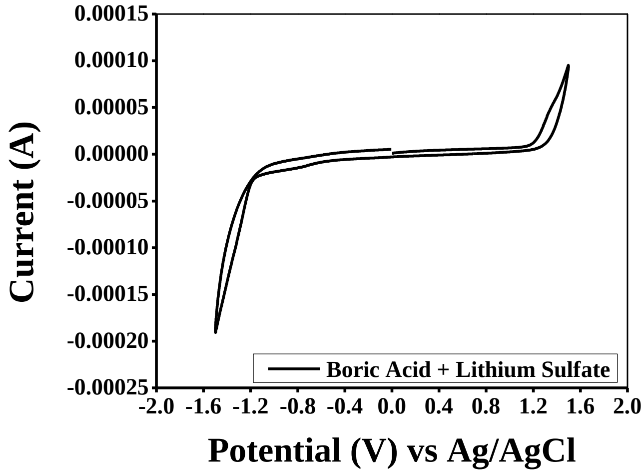

Figure 4.1 Cyclic voltammogram profile of pure electrolyte solution (0.5 M H_3BO_3 + 0.1 M Li_2SO_4).

Cyclic voltammetry was performed using FTO as working electrode. Bubbling N_2 gas into the solution was carried out for 8-10 minutes before each CV scan to remove the dissolve oxygen. At first cyclic voltammogram was run in pure electrolyte (0.5 M H_3BO_3 + 0.1 M $LiSO_4$) containing no analyte. An observation of **Figure 4.1** reveals that the voltammogram is dead i.e. no redox signal is observable in both the forward scan and reverse scan After setting the base line in electrolyte solution, cyclic voltammetry was performed for Cobalt solution containing 10 mL of $CoSO_4$ and 10 mL supporting electrolyte solution. The corresponding CV graph is presented in

Figure 4.2. In the forward scan two peaks at 1.12 V and 1.21 V corresponding to the oxidation of Co to Co^{+2} and Co^{+2} to Co^{+3} were noticed, while in the reverse scan a signal appeared at -1.12 V showing the reduction of Co ion at the electrode surface. Cross over of current profile was also seen in the reverse cycle demonstrating the progressive nucleation growth of Cobalt atoms at the FTO surface. The recorded redox potential value of Cobalt is comparable with its reported redox signals in acidic medium.

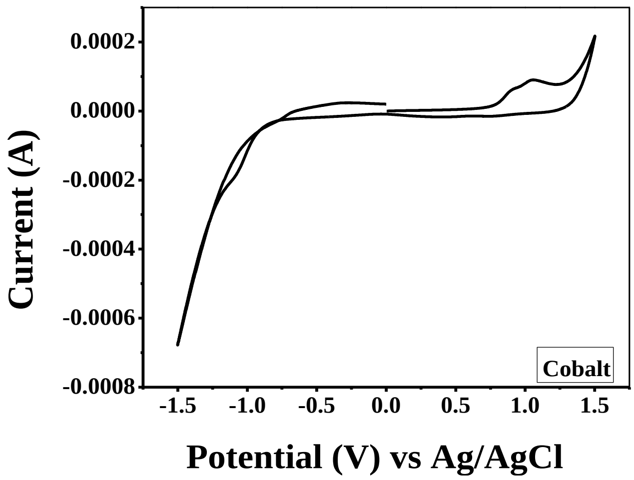

Figure 4.2 Cyclic voltammetry profile of 3mM $CoSO_4$ in 0.5 M H_3BO_3 + 0.1 M Li_2SO_4.

Following the same procedure as stated above cyclic voltammetry was performed to find the reduction potential of Nickel in the same electrolyte as discussed above [2, 3].

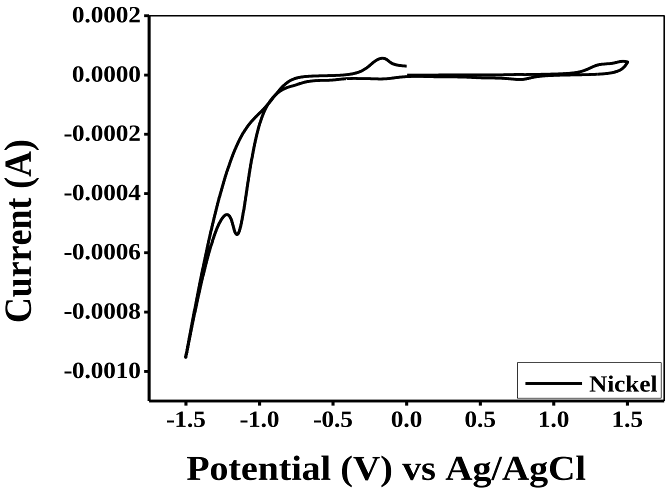

Figure 4.3 Cyclic voltammetry profile of 2 mM $NiSO_4$ in 0.5 M H_3BO_3 + 0.1 M Li_2SO_4.

The cathodic peak at -1.15 V as shown in **Figure 4.3** showed the reduction of Ni ions**.** The crossover of forward and reverse scan suggested the progressive nucleation of Ni at the electrode surface. Stripping of electroreduced Ni ions was ensured from the appearance of an anodic signal around 0.2 V.

Cyclic voltammetry was also employed to check the potential at which Fe ions get reduced [4, 5]. In the cyclic voltammetry profile reduction peak at -1.19 V demonstrated the reduction of Fe ions at electrode surface as shown in **Figure 4.4**. The signal around 0.5 V confirms stripping of electroreduced ions.

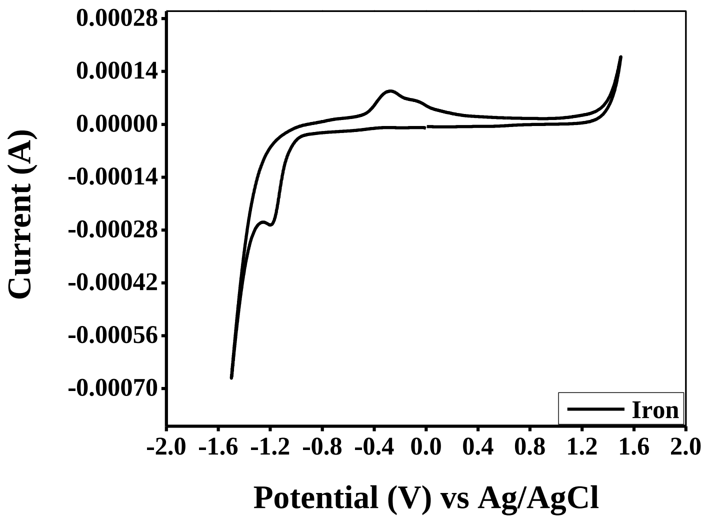

Figure 4.4 Cyclic voltammetry profile of 4 mM $FeSO_4$ in 0.5 M H_3BO_3 + 0.1 M Li_2SO_4.

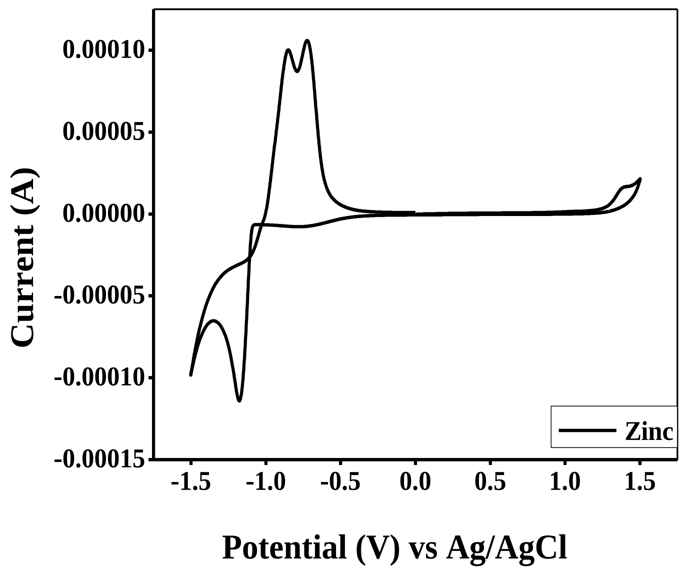

Figure 4.5 Cyclic voltammetry profile of 2mM $ZnSO_4$ in 0.5 M H_3BO_3 + Li_2SO_4.

Similarly cyclic voltammetry was performed for probing the redox response of Zinc. A signal at -1.18 V suggested reduction of Zn ions at the electrode surface in accordance with the data reported in literature [6, 7]. In reverse scan a peak at -0.6 V offered clues about the oxidation/stripping away of Zn ions into the bulk solution. Like the previously discussed metal ions, crossover of the forward and backward current profiles also occurred in case of Zn ion that can be related to the onset of progressive nucleation growth at the FTO surface. **Table 4.1** shows the reduction potential values of Fe, Co, Ni and Zn under optimized conditions.

Table 4.1 Reduction potential of Co, Ni, Zn and Fe **at** 100 mv/sec scan rate.

Metal	V vs Ag/AgCl
$CoSO_4$	**-1.12**
$NiSO_4$	**-1.15**
$ZnSO_4$	**-1.18**
$FeSO_4$	**-1.19**

4.2 Electroplating metallic electrocatalyst at the FTO surface via CPE

Chronoamperometry was conducted in order to electroplate metal ions on the electrode surface. On the basis of reduction potential of Fe, Co, Ni and Zn ions (as discussed in **section 4.1**) more negative reduction potentials were selected to electrochemically deposit these metal ions at the working electrode surface. For achieving a thin, stable and porous catalyst film over the FTO surface, metals were deposited electrochemically rather than mechanical approach. In bulk solution metals were present in the form of ions and when potential greater than their reduction potential was applied, metals ions moved towards respective electrode and deposited in the form of metal atoms. In the electrochemical fabrication approach, films are affected by various factors like deposition potential, deposition temperature, agitation of solution, pH and ionic species concentration. Film shape can be tuned by varying the deposition potential value because elemental concentration in film varies linearly with applied potential.

4.2.1 Electroplating of Fe metal at FTO surface in H_3BO_3+ Li_2SO_4

Control Potential Electrolysis (CPE) at constant voltage was performed for *in-situ* electroplating of Fe^{2+} ions from bulk solution at the electrode surface [8-12]. 0.5 M boric acid coupled with 0.1 M lithium sulphate was used as supporting medium. **Figure 4.6** depicts the deposition pattern of Iron on the surface of FTO at three potential values -1.3, -1.4 and -1.5 V vs. Ag/Ag/Cl. Electrodeposition was carried out for 900 seconds. An increase in cathodic current value was observed with the increase in deposition potential value. At -1.5 V more negative current was obtained as compared to at -1.4 and -1.3 V as shown in **Figure 4.6.** The high value of current at -1.5 V indicates that -1.5 V is a more suitable potential for electroplating Iron at FTO. Electrodeposition of Iron ions at FTO surface followed progressive nucleation mechanism at-1.3 V, -1.4 V, and -1.5 V.

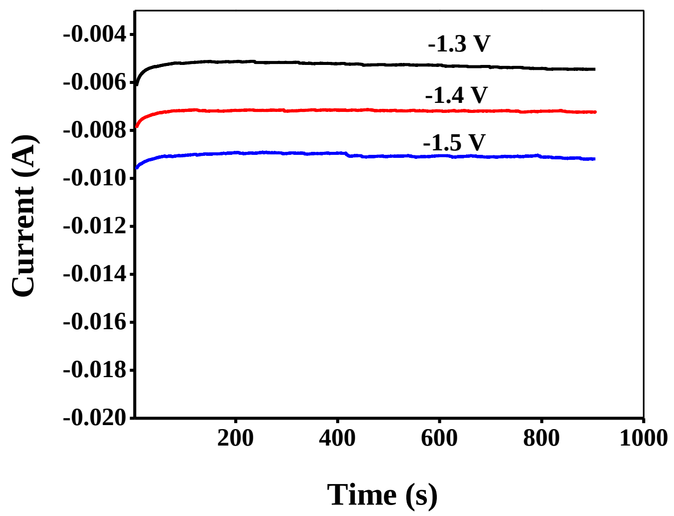

Figure 4.6 Electrodeposition of Fe at FTO surface using 0.5 M H_3BO_3 + 0.1 M Li_2SO_4 at different values of deposition potential for 900 sec.

4.2.2 Electroplating of Fe metal at FTO surface in 1 M KOH

CPE was conducted for the purpose to electroplate the Fe^{2+} ions from bulk solution at FTO surface via Chronoamperometry. 1 M KOH was used as electrolytic medium. **Figure 4.7** explains the electroplating of Iron over FTO surface at different values of applied potential i.e. at -1.3 V, -1.4 V and -1.5 V according to the method reported in literature [11, 12]. CPE was carried out for 900 seconds. Evidently it can be observed that low value of cathodic current is obtained at -1.5 V in KOH as compared to the current value obtained under similar conditions of deposition potential and time using H_3BO_3 + Li_2SO_4. This behavior suggests that metals successfully deposited at the electrode surface in acidic medium. It will not diffuse towards the electrode surface in basic medium because in basic medium metals salt precipitate out in the form of hydroxides. Precipitates of metal ions in alkaline solution are sluggish one to move towards the FTO surface; hence a lower cathodic current is generated at -1.5 V.

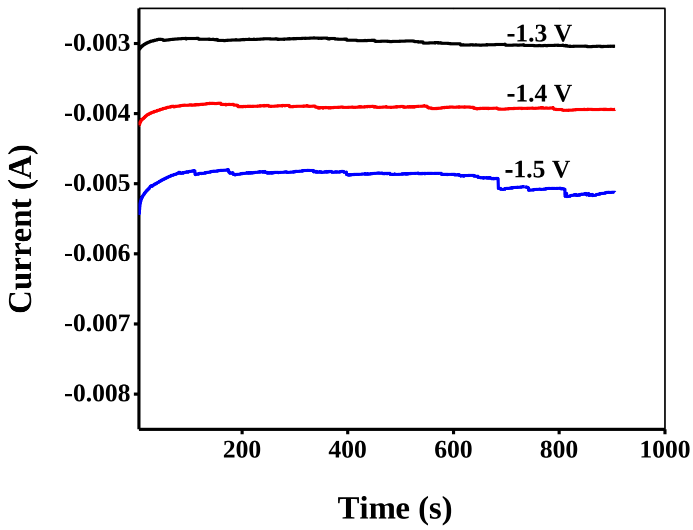

Figure 4.7 Electrodeposition of Fe at the FTO surface using 0.1 M KOH as an electrolytic medium at different value of deposition potential for 900 sec.

4.2.3 Electroplating of Co metal at FTO surface H_3BO_3+ Li_2SO_4

Chronoamperometry was conducted for in-situ deposition of Co^{+2} ions from bulk solution at the electrode surface. A 0.5 M H_3BO_3 along with 0.1 M Li_2SO_4 was used as supporting medium. Acidic medium was preferred for electrodeposition of metal at electrode surface because of high solubility of metals salts in acidic medium. Boric acid was preferably used as an electrolyte for electrodeposition to develop electrocatalyst. Boric acid was coupled with Lithium Sulphate to increase conductance of metals ions towards electrode surface **Figure 4.8** represents the electrodeposition pattern obtained during the electroplating of Co ions at the FTO surface. It can be easily concluded that a successful deposition occurs in acidic medium [9]. As potential value increases from -1.3 V to -1.5 V an increase in cathodic current occurs. Electrodeposition was carried out for 900 seconds. At -1.3 V instantaneous nucleation growth mechanism was observed possibly because initially a large number of active sites were vacant which led to instantaneous rise in current response, while for remaining two potential ranges progressive nucleation growth mechanism was investigated during electrodeposition.

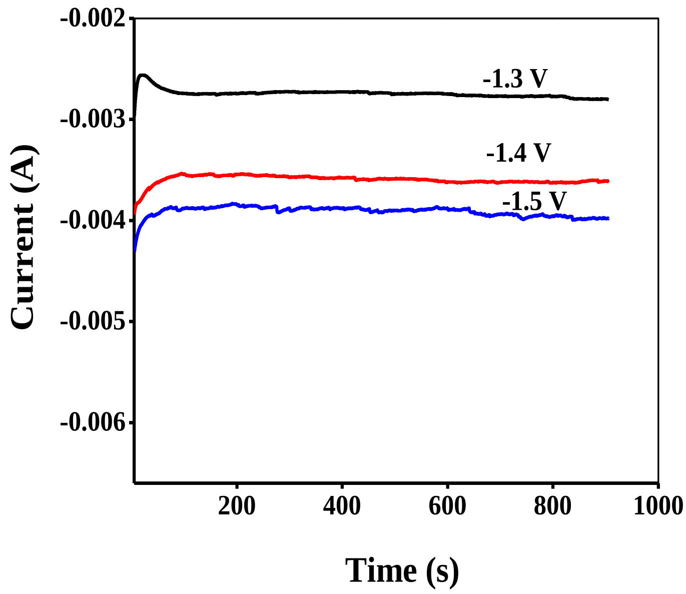

Figure 4.8 Electrodeposition of Co at the FTO surface in a solution containing 0.5 M H_3BO_3 and 0.1 M Li_2SO_4 at different values of deposition potential for 900 sec.

4.2.4 Electroplating of Co metal at FTO surface in 1 M KOH

Electrodeposition of Cobalt ions in alkaline solution was carried out at negative potential values. **Figure 4.9** shows the electrodeposition behavior of Co at the FTO surface according to the literature reported method [9].

It can be observed from this figure that for each potential value deposition curve ends with decreasing value of cathodic current as compared to current value obtained as starting point of deposition curve. This type of behavior confirms low diffusion ability of Cobalt ions towards FTO surface in basic solution because it forms precipitates in basic medium. However, a higher value of current was observed at -1.5 V ensuring that this value of potential is the most suitable to carry out electrodeposition of Cobalt in alkaline solution.

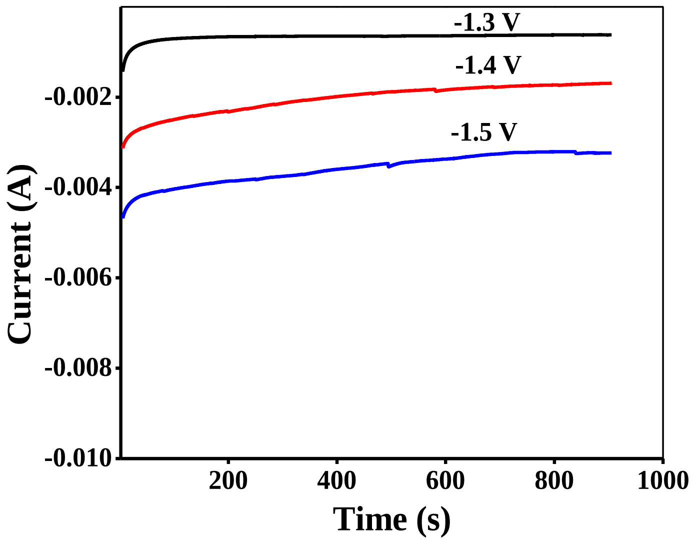

Figure 4.9 Electrodeposition of Co at FTO surface in 0.1 M KOH at different values of deposition potential for 900 sec.

4.2.5 Electroplating of Zn metal at FTO surface H_3BO_3+ Li_2SO_4

Electroplating of Zinc at the electrode surface from bulk solution was also carried out. **Figure 4.10** shows the electrodeposition behavior of Zinc in acidic solution.

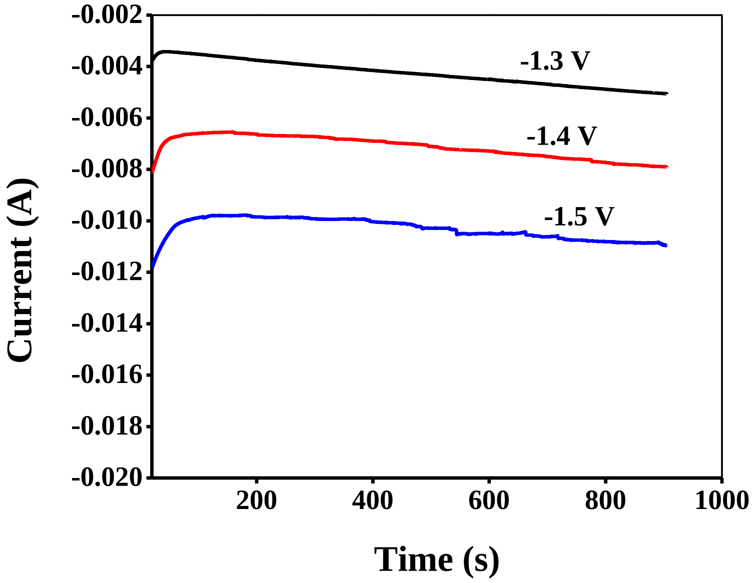

Figure 4.10 Electrodeposition of Zn at the FTO surface in a solution containing 0.5 M H_3BO_3 and 0.1 M Li_2SO_4 at different values of deposition potential for 900 sec.

Similar electrolyte medium was also used for fashioning of Zinc metal at electrode surface. Due to high solubility factor of Zinc salt in acidic condition, metal ions transfer with greater rate from bulk solution to the electrode surface. A stable and thin film of Zn metal at FTO surface was established under acidic environment.

Zinc has shown a successful deposition at electrode surface in acidic medium because progressive nucleation growth mechanism occurred at -1.3 V, -1.4 V and -1.5 V as explained by Cottrell equation $\left(i = \frac{nFAC^{o}j\sqrt{Dj}}{\sqrt{\pi t}}\right)$. In addition to that as potential value increased from -1.3 V to -1.5 V a high value of cathodic current was generated. Electrodeposition was carried out for 900 sec [7, 8, 10].

4.2.6 Electroplating of Zn metal at FTO surface in 1 M KOH

Chronoamperometry was performed for the electroplating of Zn^{+2} ions from bulk solution to electrode surface.

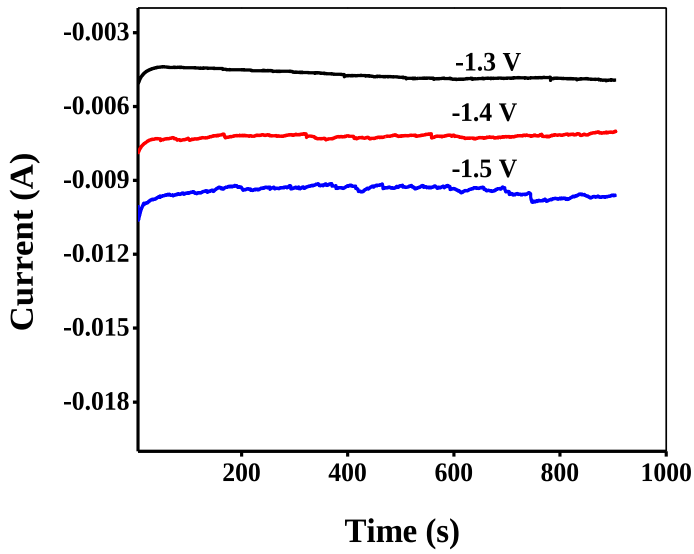

Figure 4.11 Electrodeposition of Zn at FTO surface using 0.1 M KOH at different values of deposition potential for 900 sec.

I M KOH was used as conducting medium. **Figure 4.11** offers evidence about the electrodeposition behavior of Zinc in alkaline solution. Electroplating was carried out at three potential ranges -1.3 V, -1.4 V and -1.5 V for 900 seconds. From **Fig 4.11** it can be seen that with the increase in deposition potential value from -1.3 V to -1.5 V an increase in cathodic current was observed. At -1.3 V deposition curve ended with increase in cathodic current value while at -1.4 V and -1.5 V deposition curve ended with decrease in negative current value showing that at diffusion of Zinc ions towards electrode surface became more difficult in basic medium.

4.2.7 Electroplating of Ni metal at FTO surface H_3BO_3+ Li_2SO_4

Figure 4.12 explains the electrodeposition behavior of Nickel from bulk to electrode surface in acidic medium. The current transient was seen at -1.3 V, -1.4 V and -1.5 V.

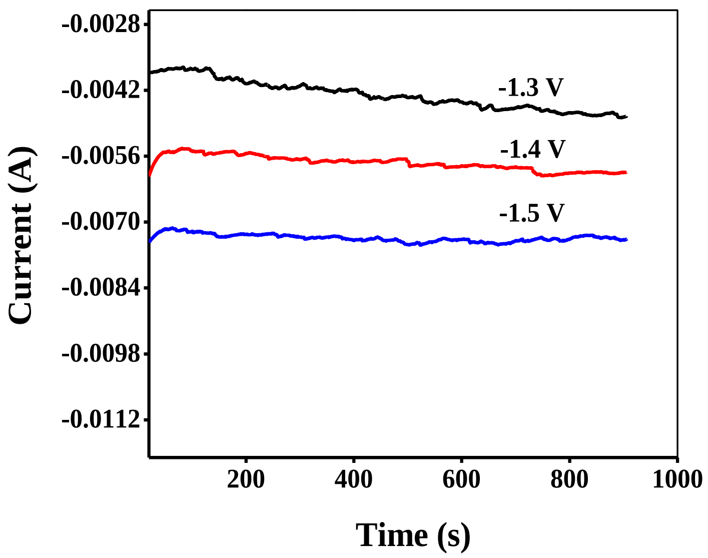

Figure 4.12 Electrodeposition of Ni at FTO surface using 0.5 M H_3BO_3 + 0.1 M Li_2SO_4 at different value of deposition potential for 900 sec.

As deposition time started current generated was decreased slightly after that a progressive increase in negative current was observed up to the end point of deposition curve. Electrodeposition was carried out for 900 sec [9, 11]. The progressive nucleation growth mechanism was observed at -1.3 V, -1.4 V and 1.5 V ensuring that successful deposition of Nickel on electrode surface occurred in acidic medium.

4.2.8 Electroplating of Ni metal at FTO surface in 1 M KOH

Chronoamperometry was carried out to electroplate Nickel at the FTO surface in alkaline solution**. Figure 3.13** explains the deposition behavior of Nickel from bulk to electrode surface at -1.3 V, -1.4 V and -1.5 V. similar to other metals ions Ni ions also show the good conductance and solubility under acidic conditions and precipitated out in basic medium. A successful deposition was not occur in 1 M KOH due to the reasons discussed above and a low value of cathodic current was obtain at all three value of potential applied.

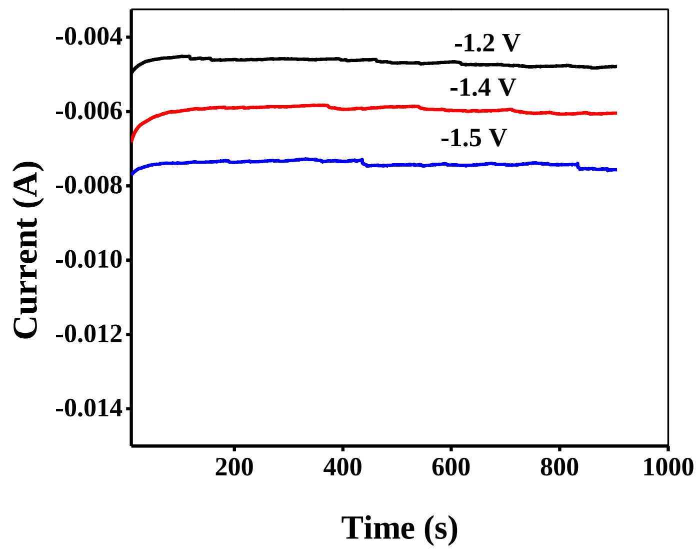

Figure 4.13 Electrodeposition of Ni at FTO surface in 1 M KOH at different values of deposition potential for 900 sec.

The above given figure shows that as applied potential value is increased from -1.3 V to -1.5 V cathodic current increase but for each fixed value of potential the generated cathodic current remained constant during electroplating [9, 11].

4.2.9 In-situ electrodeposition of Fe-Zn-Ni-Co at FTO surface in H_3BO_3+ Li_2SO_4

Following the same procedure as above CPE was run for Fe-Zn-Ni-Co system. A 0.5 M boric acid and 1M lithium sulphate was used as supporting electrolyte. Controlled potential electrolysis was operated at different reduction potential values. Deposition time was set as 900 sec. As discussed in the previous section that single metal was successfully deposited at electrode surface under acidic condition. It was expected that tetrametallic system would show good electrodeposition under this condition. Solubility and conductance are the primary factors that decide the nature of film developed at substrate surface. In acidic medium due to high conduction and solubility a thin and stable film of tetrametallic catalyst was fabricated at electrode surface. The **Figure 4.14** demonstrates that as deposition potential become more negative more and more ions are being deposited on FTO surface with consequent successive increase in cathodic current [8-12].

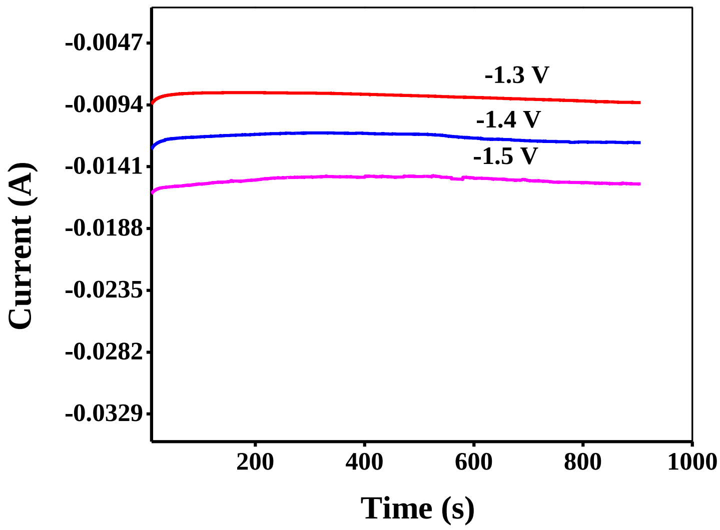

Figure 4.14 In-situ electrodeposition of Fe-Zn-Ni-Co at FTO surface in 0.5 M H_3BO_3 coupled with 0.1 M Li_2SO_4 as supporting electrolyte for 900 sec.

On comparison with other supporting electrolyte, 0.5 M Boric acid coupled with 1M Lithium Sulphate was suggested to be the best for deposition of the selected metal ions. It can also be observed that a good electrolytic nucleation growth occurs in this case. Moreover increase in cathodic current with respect to increase in deposition potential is seen to be more in this case.

4.2.10 In-situ electrodeposition of Fe-Zn-Ni-Co at FTO surface in 1 M KOH

The deposition of tetrametallic films at FTO surface was also carried out in 1 M KOH. In basic medium all four metals ions were precipitated out in the form of hydroxides. It can be seen from **Figure 4.15** that a very low value of current generates at -1.5 V. As stated above that single metal ions have shown poor film formation under alkaline medium so, similar results were expected in the electroplating of tetrametallic film at FTO surface under same conditions.

In comparison with the acidic medium electrodeposition of selected four metals was investigated. Many of research groups working on synthesis and application of electrocatalysis in basic conditions because OER catalysis occurs more favorably in basic conditions as compared to acidic and neutral conditions. Formation of precipitates is sluggish one when electroplating of metals ion were carried to form an

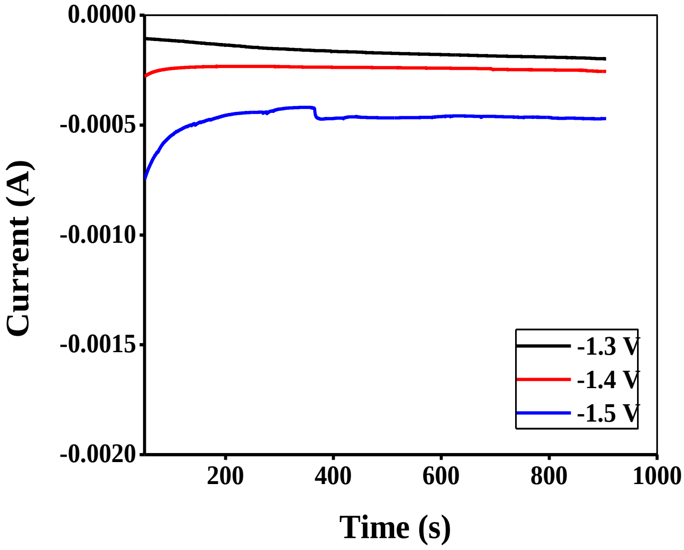

Figure 4.15 In-situ electrodeposition of Fe-Zn-Ni-Co at FTO surface in 1 M KOH as supporting electrolyte for 900 sec.

Alloy film at conducting substrate i.e. FTO and this serious issue leads to an unstable film formation at electrode surface. Nucleation growth of metals particles at electrode surface does not occur under alkaline conditions and provided low value of cathodic current during electrodeposition.

4.2.11 In-situ electrodeposition of Fe-Zn-Ni-Co at FTO surface in 0.5 M H_3BO_3

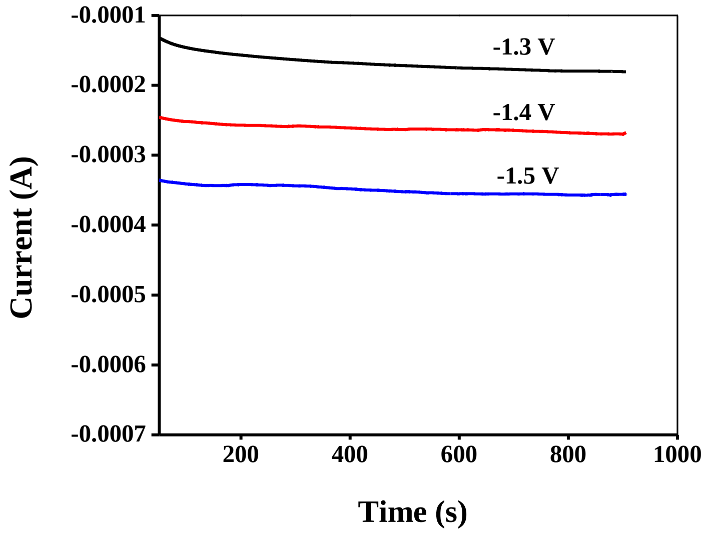

Figure 4.16 In-situ electrodeposition of Fe-Zn-Ni-Co at FTO surface in 0.5 M H_3BO_3 as supporting electrolyte for 900 sec.

Chronoamperometry was carried out for in-situ deposition of tetra metals from solution at FTO substrate. 0.5 M Boric acid was used as supporting electrolyte. **Figure 4.16** shows the electrodeposition of selected four metal ions at the FTO at various cathodic potentials (-1.3, -1.4 & -1.5) V respectively. CPE was carried out for 900 sec. It can be seen from graph that with the passage of time cathodic current increases that's reflects the good nucleation growth of metals on FTO surface [8-12]. It can also be seen that as value of deposition potential increases, negative current generated also increases showing that more and more metals are going to be settled on FTO substrate.

4.2.12 In-situ electrodeposition of Fe-Zn-Ni-Co at FTO surface in $H_3BO_3 + Na_2SO_4$

To make the thin layer of the selected metal alloy on FTO substrate, CPE was carried out at different cathodic potential values depending upon the reduction potentials observed in cyclic voltammogram. Deposition time was kept 900 sec. CPE was carried out for -1.3, -1.4 & -1.5 V respectively. 0.5 M Boric acid coupled with 1 M Sodium Sulphate was used as supporting media.

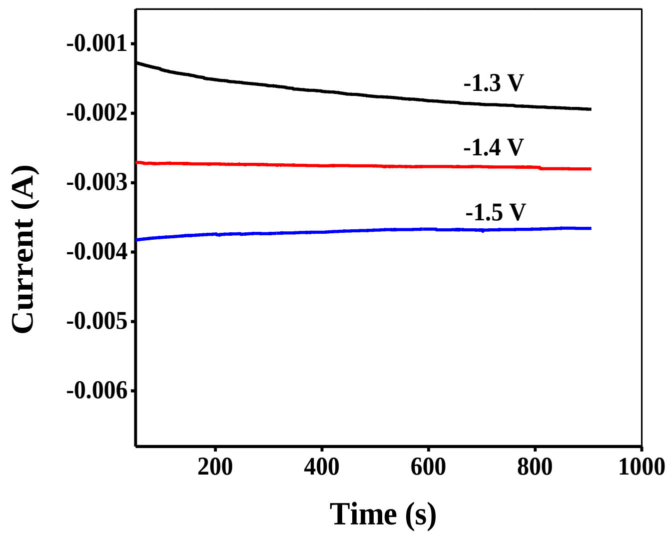

Figure 4.17 In-situ electrodeposition of Fe-Zn-Ni-Co at FTO surface in 0.5 M H_3BO_3 coupled with 0.1 M Na_2SO_4 as supporting electrolyte.

It can be seen from graph pattern that as deposition potential increases, current generated by electrode also increases reflecting that at high value of deposition potential more and more metals ion get occupied on FTO surface.

4.2.13 In-situ electrodeposition of Fe-Zn-Ni-Co at FTO surface 0.5 M $C_6H_8O_7$

Like Boric acid, Citric acid was also tested for electrodeposition of the selected four metals on FTO surface. CPE was operated at a potential of -1.2 V, -1.3 V, & -1.5 V. In acidic medium all salts were highly soluble. When potential greater than the reduction potential, metals ions migrate from bulk phase to the electrode surface where they get reduced in the form of metal. During electrodeposition in acidic medium there is completion among hydrogen ions and metals ions. Hydrogen ions get reduced and liberate H_2 molecules.

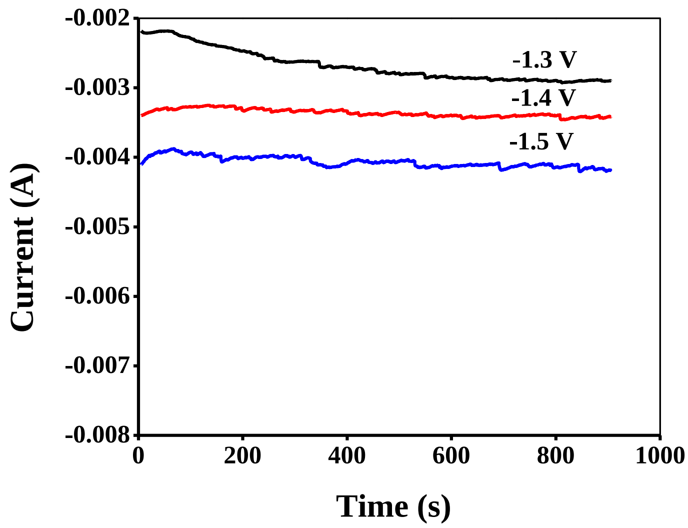

Figure 4.18 In-situ electrodeposition of Fe-Zn-Ni-Co at FTO surface in $C_6H_8O_7$ of pH = 4 as supporting electrolyte.

It can be investigated from **Figure 4.18** that as deposition potential increases, current gets a gradual increase suggesting deposition of more and more ions on FTO substrate surface [13, 14]. Moreover, nucleation growth of selected metals on FTO surface increases as a function of deposition time. It can be concluded that that electrically stimulated nucleation growth occurs more feasibly in acid media as compared to neutral and alkaline medium

4.2.14 In-situ electrodeposition of Fe-Zn-Ni-Co at FTO surface in KOH (pH = 9.3)

Controlled potential electrodeposition of the selected four metals was also carried out in KOH. Different constant reduction potentials were selected for electrodeposition at the FTO surface. CPE was run for -1.3 V, -1.4 V, & -1.5 V respectively. The pH of the supporting electrolyte solution was adjusted as 4.13 to create acidic environment.

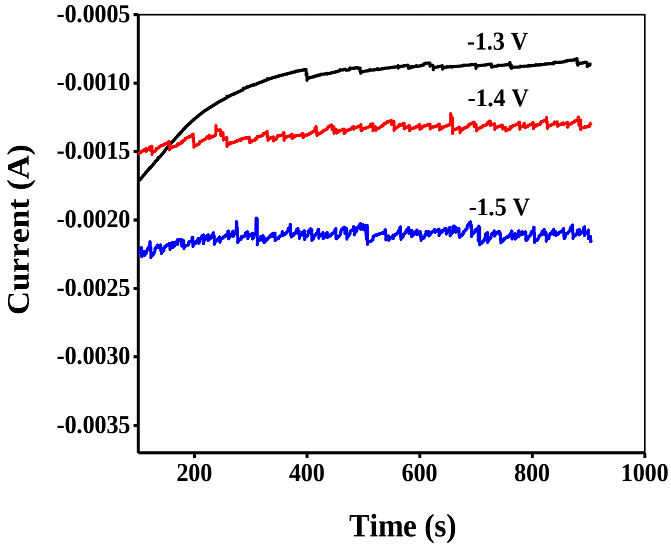

Figure 4.19 In-situ electrodeposition of Fe-Zn-Ni-Co at FTO in 1 M KOH of pH = 9.3

It can be concluded from **Figure 4.19** that increase in current value with an increase in deposition potential value is very low that shows that deposition of selected metals is not favorable in KOH of pH = 9.3. It can also be observed from graph that with the passage of time nucleation growth does not occur here because lines of graph for each deposition value rises upward slightly along time axis.

4.3 LSV of tetrametallic catalyst films developed in various electrolyte media

A thin film of tetrametallic alloy was deposited on FTO in various electrolyte media i.e. Boric acid, Boric acid coupled with Sodium Sulphate, Boric Acid coupled with Lithium Sulphate, Citric Acid, 1 M KOH (pH = 14.3) and 1M KOH (pH = 9.13) at various values of deposition potential. Modified FTO electrodes after drying were used to check the activity of films towards water electrolysis in order to get H_2 and O_2 which further cab be used as fuel cell and many other energy purposes. KOH (pH = 13) was used as supporting electrolyte in LSV analysis. All LSV scans were taken at

10 mV/sec scan rate. Before running LSC scan purging with N_2 gas was done for 8 minutes to remove dissolved oxygen.

4.3.1 LSV of the tetrametallic catalyst film design in H_3BO_3 + Li_2SO_4 and 1 M KOH

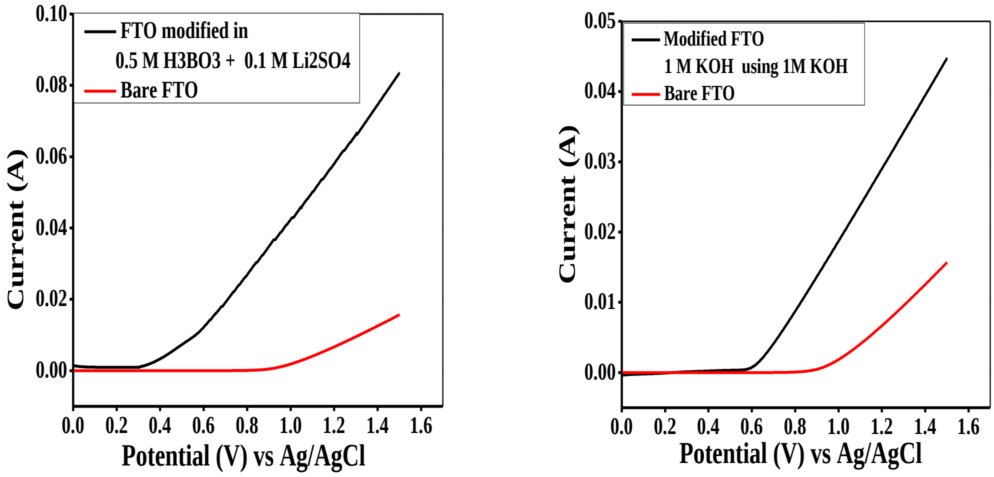

Figure 4.20 (a) LSV of tetrametallic catalyst film (designed in 0.5 M H_3BO_3 + 0.1 M Li_2SO_4) at 10 mV/sec. **(b)** LSV of tetrametallic catalyst film (designed in 1 M KOH) at 10 mV/sec.

Figure 4.20 (a) shows the catalytic behavior of tetrametallic catalyst film which was fabricated in 0.5 M H_3BO_3 + 0.1 Li_2SO_4. Red solid curve in voltammogram explains response of bare FTO while black solid curve shows output of modified FTO catalyst film. From linear sweep voltammogram it can be seen that catalyst film which was designed in 0.5 M H_3BO_3 + 0.1 Li_2SO_4 has shown excellent catalytic performance in the context of high current value of about 85 (mA) at very low value of onset potential (0.31 V vs. Ag/AgCl). **Figure 4.20 (b)** shows the catalytic performance of tetrametallic catalyst film designed in 1 M KOH. Linear sweep voltammogram shows that film which was deposited in alkaline solution has shown low value of current (44 mA) with high value of onset potential (0.59 V vs. Ag/AgCl). Thus catalyst deposited over the electrode surface under acidic medium shows figures of merit compared to that prepared under alkaline conditions.

4.3.2 LSV of the tetrametallic catalyst film design in H_3BO_3 and H_3BO_3 + 0.1 M Na_2SO_4

Figure 4.21 (a) shows the catalytic performance of tetrametallic catalyst film fabricated in 0.5 M Boric Acid. It can be observed form voltammogram that in this case a current value of 53 mA with 0.50 V vs. Ag/AgCl onset value of potential was observed. However, **Figure 4.21 (b)** shows the catalytic activity of tetrametallic catalyst film formed in 0.5 M Boric acid coupled with 0.1 M Sodium sulphate. Voltammogram expresses the current value of 59 mA with High value of onset potential 0.56 V vs. Ag/AgCl.

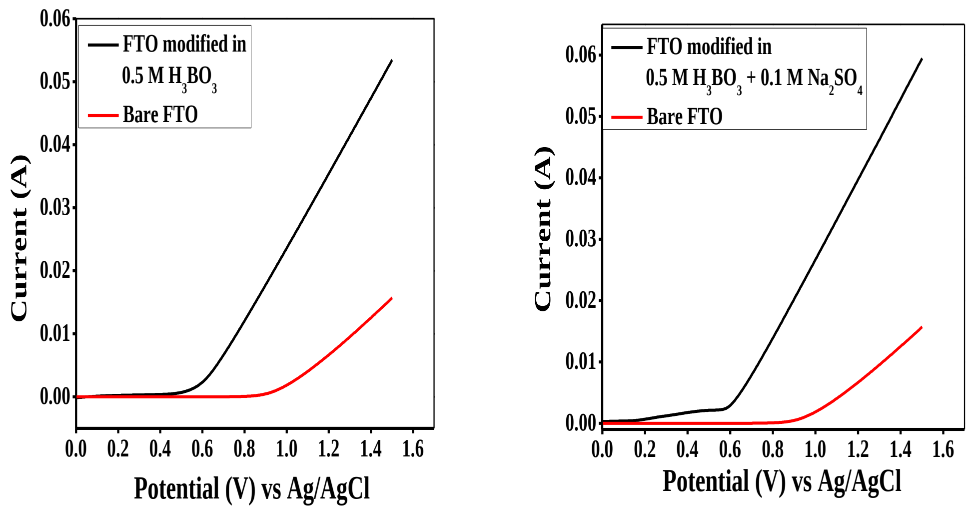

Figure 4.21 (a) LSV of tetrametallic catalyst film designed in 0.5 M H_3BO_3) at 10 mV/sec, **(b)** LSV of tetrametallic catalyst film designed in 0.5 M H_3BO_3 + 0.1 M Na_2SO_4) at 10 mV/sec.

4.3.3 LSV of the tetrametallic catalyst design in $C_6H_8O_7$ and 1 M KOH (pH = 9.3)

Fig 4.22 (a) expresses the linear sweep voltammogram of tetrametallic catalyst film which was fabricated in 0.5 M Citric Acid. Voltammogram obtained has shown that a current value of 34 mA with 0.67 V vs. Ag/AgCl value of onset potential was observed. While **Fig 4.22 (b)** explains the catalytic performance of tetrametallic film modified in 1 M KOH of pH = 9. The current value of 48 mA at 0.55 V vs. Ag/AgCl onset value of potential was obtained.

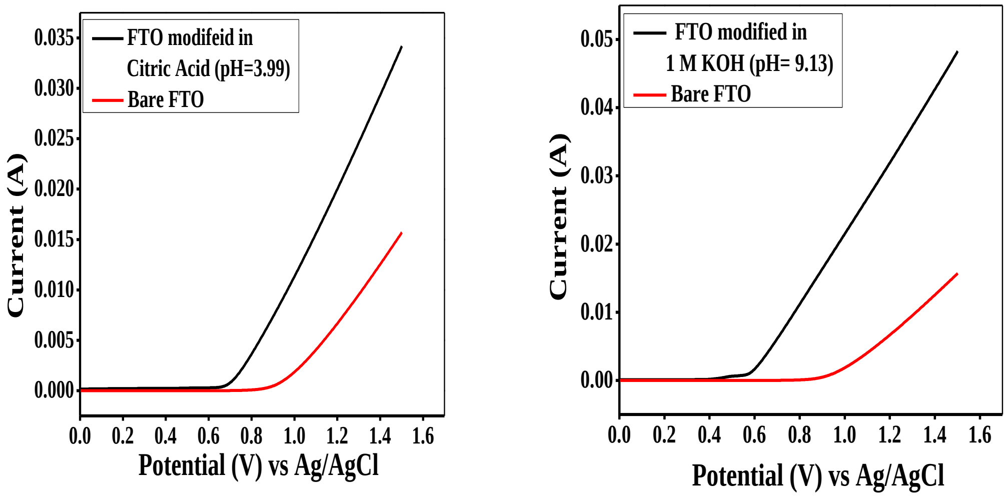

Figure 4.22 (a) LSV of tetrametallic catalyst film designed in 0.5 M $C_6H_8O_7$) at 10 mV/sec. **(b)** LSV of tetrametallic catalyst film (designed in 1 M KOH pH = 9.3) at 10 mV/sec.

The performance of the designed tetrametallic catalyst in different supporting electrolytes can be seen from the values of current and onset potentials as listed in **Table 4.2**

Table 4.2 Comparison of CPE and LSV results of tetrametallic catalyst film designed in various electrolytic solutions.

Medium for electrodeposition	**Current (A) value in CPE at -1.5 V**	**Current (A) value in LSV**	**Onset potential (V) vs. Ag/AgCl**	**Onset potential (V) vs. NHE**
Boric Acid + Lithium Sulphate	-0.0153	0.0836	0.31	1.283
KOH PH = 14.3	-0.000469	0.0446	0.59	1.563
Boric Acid	-0.000356	0.053	0.50	1.473
Boric Acid + Sodium sulphate	-0.0036	0.059	0.56	1.533
Citric acid	-0.0041	0.0341	0.67	1.643
KOH pH = 9.13	-0.0021	0.0482	0.55	1.523

.

4.3.4 Media optimization to fashion tetrametallic catalyst film at FTO

Table 4.2 summarizes the CPE and LSV results of tetrametallic catalyst films fabricated in various medium. An observation of the tabulated values reveals that catalyst film which was deposited in H_3BO_3 + Li_2SO_4 has the best water splitting catalytic performance.

In addition to that if we make comparison of catalytic performance of catalyst films developed in Boric acid + Lithium with Boric acid + Lithium sulphate then we can conclude that addition of Lithium sulphate increases the solubility, hence conduction of metal ions towards electrode surface increases. Addition of Lithium sulphate to Boric acid is more effective than sodium sulphate because Lithium has smaller size and high charge density. Similarly those films which were designed in basic medium have shown low catalytic performance because in alkaline solution instead of progressive nucleation growth at FTO agglomeration of precipitates occurs at FTO which results in the formation of thick and unstable film at FTO surface. So, finely on the basis of CPE and LSV results medium for electrodeposition was optimized and further all the electrodeposition were carried out in 0.5 M H_3BO_3 coupled with 0.1 M Li_2SO_4.

4.4 Characterization of tetrametallic catalyst film designed at FTO

From CPE and LSV results we conclude that a thin and stable film is formed in acidic medium containing 0.5 M H_3BO_3 coupled with 0.1 M Li_2SO_4. So different FTO surfaces were modified with mono and tetrametallic catalyst films and in order to examine these films various characterization techniques i.e. XRD, SEM and EDX were carried out. XRD analysis was carried out to determine the physical characteristics, composition and structure of tetrametallic electrocatalyst film.

Deposition of four metals was confirmed by comparing the XRD peaks appear in single and tetrametallic catalyst film SEM analysis provided way to analyze the surface structure of catalyst film developed at FTO surface. Surface porosity of catalyst film was studied via SEM analysis that decides the performance of catalyst OER. Elemental analysis of developed catalyst film was performed via EDX.

4.4.1 X-ray diffraction pattern of catalyst films fashioned at FTO surface

To investigate the crystalline nature of thin film deposited on FTO at different potentials, XRD analysis was performed. XRD pattern of nanostructure coated films on FTO vs Ag/AgCl in acidic medium are shown in **Figure 4.23.**

XRD pattern explain the confirmation of all four metals deposited on FTO. In addition to peaks appear in case of bare FTO some other peaks also appear ensuring the presence of selected four metals. Peak appear at 33^0 that confirms the Fe metal oxide deposited on FTO because a similar peaks appear at 33^0 in case of single metal and tetrametallic XRD pattern. A peak for Zn confirmation also appears in the same region as that of characteristic peaks of bare FTO at near 38^0. Similarly, at 42.5^0 and 76^0 peaks corresponds to Cobalt and Nickel deposition on FTO substrate. When XRD pattern of individual metal was compared XRD pattern of tetrametallic film coinciding peaks were found confirming the deposition of all four metals at FTO surface [1, 7-10, 15, 16].

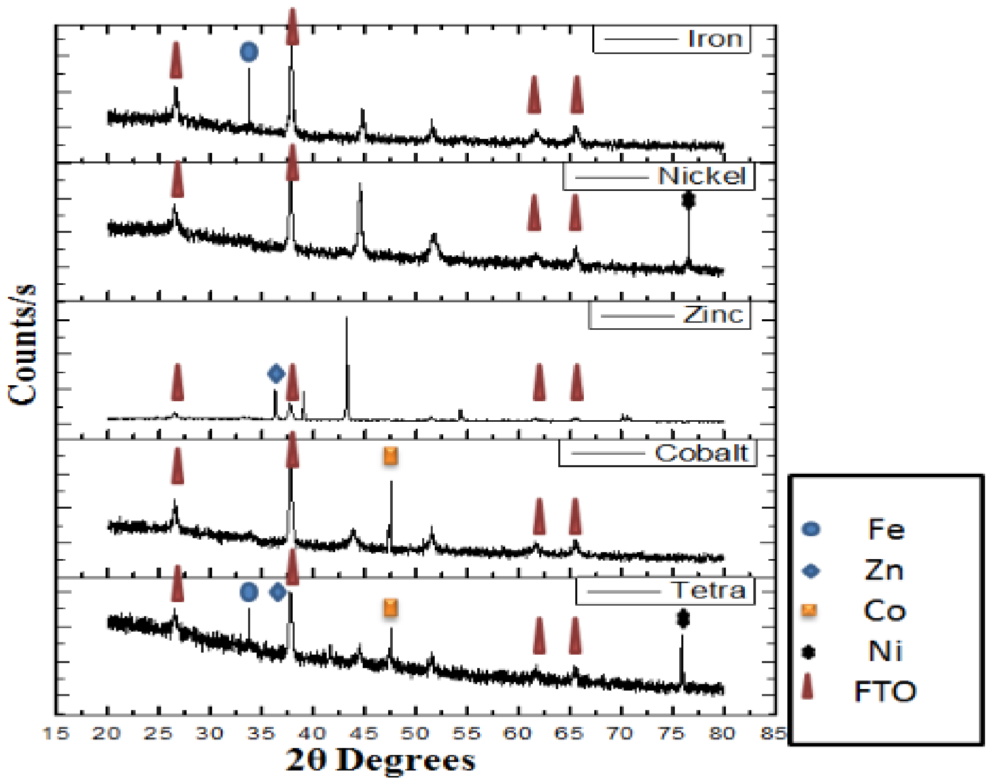

Figure 4.23 XRD pattern of tetrametallic (Fe-Ni-Zn-Co) electrocatalyst film coated on FTO in acidic medium (0.5 M H_3BO_3 + 0.1 M Li_2SO_4, pH = 4.5) at -1.5 V

4.4.2 SEM micrographs of catalyst films developed at FTO surfaces

4.4.2.1 SEM images of catalyst film consisting of single metal

SEM images of usually provide information about surface morphology of various materials. Different FTO surfaces were modified with single metal film. When SEM images of modified FTO were compared with bar FTO surface have shown the surface roughness, porosity, inter-metallic distribution, material homogeneity. It can be observed form each images that material is uniformly distributed over FTO surfaces. It can also be seen that SEM images of FTO surface containing Iron, Cobalt, Zinc [17] and Nickel have shown the best porosity and roughness while FTO surface containing Cobalt metal showed compactness of material when compared in against to bare FTO [18].

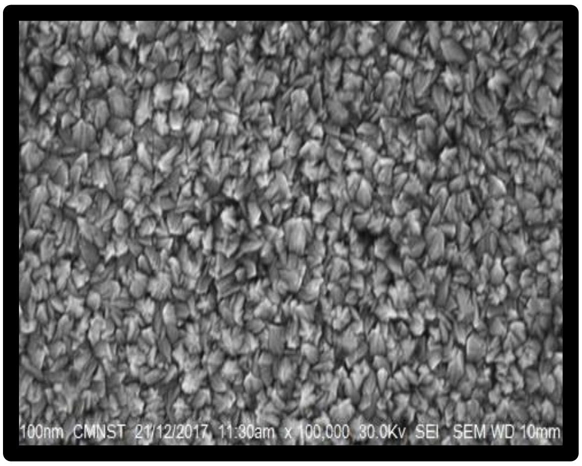

Figure 4.24 SEM micrograph of bare FTO

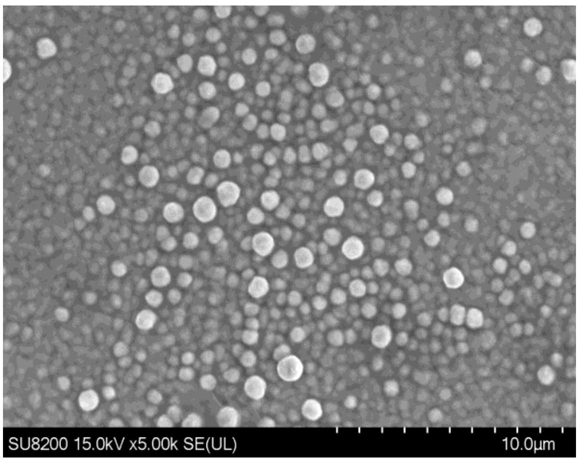

Figure 4.25 SEM micrograph of FTO surface modified with Zn metal.

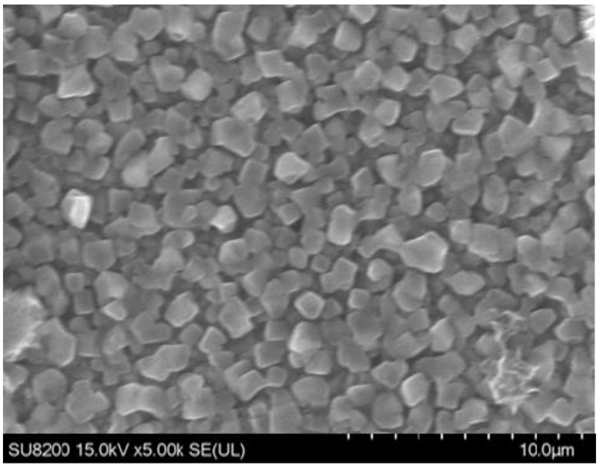

Figure 4.26 SEM micrograph of FTO surface modified with Fe metal.

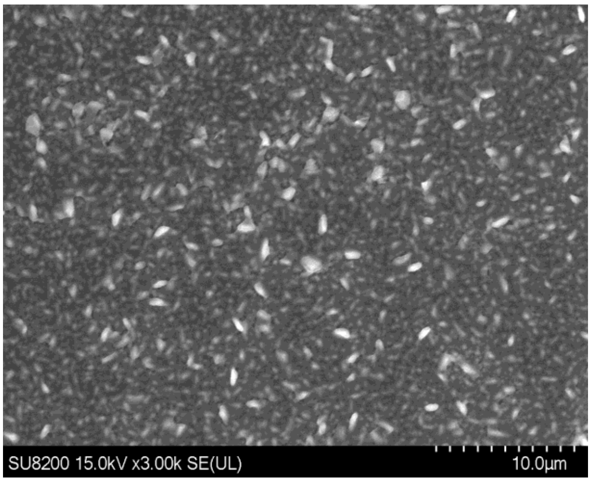

Figure 4.27 SEM micrograph of FTO surface modified with Co metal.

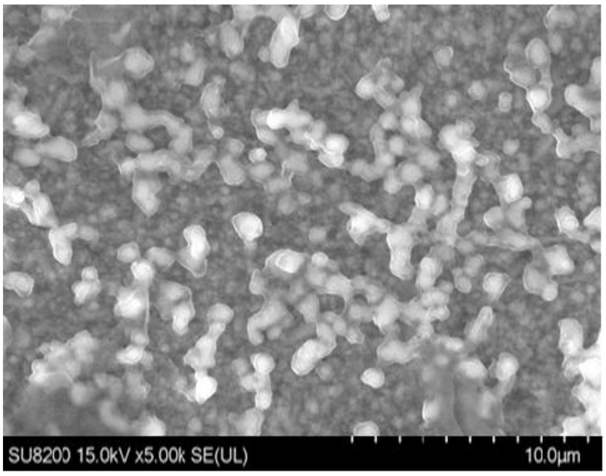

Figure 4.28 SEM micrograph of FTO surface modified with Ni metal.

4.4.2.2 SEM analysis of tetrametallic catalyst film

In order to study and analyze the surface morphology of tetrametallic catalyst film SEM analysis was applied. **Figures 4.29-4.31** show the surface anatomy of catalyst film at 5.00, 3.00 and 2.00 µm of resolution.

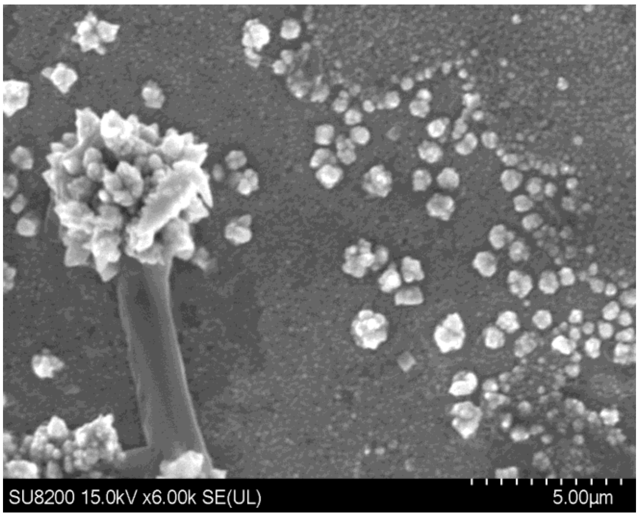

Figure 4.29 SEM micrograph of FTO surface modified with Fe-Co-Ni-Zn at 5.00 µm.

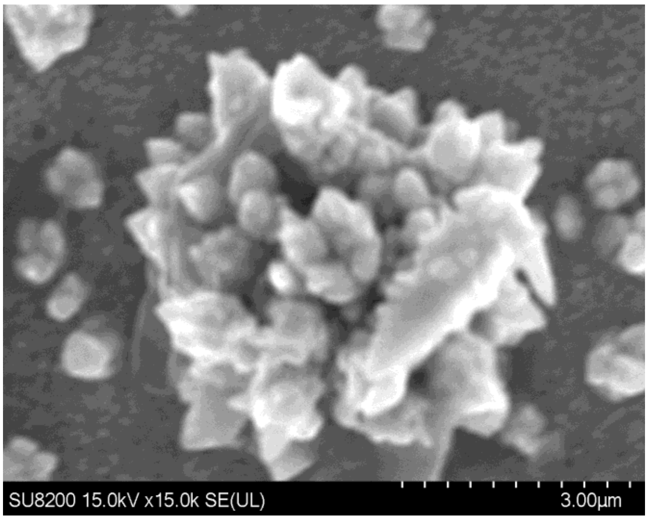

Figure 4.30 SEM micrograph of FTO surface modified with Fe-Co-Ni-Zn at 3.00 µm.

It was very interesting to see the formation of flower like structures. Surface roughness is the critical factor that decides the catalyst performance of catalyst material. Flower like morphology is very helpful to trap O_2 produced [19].

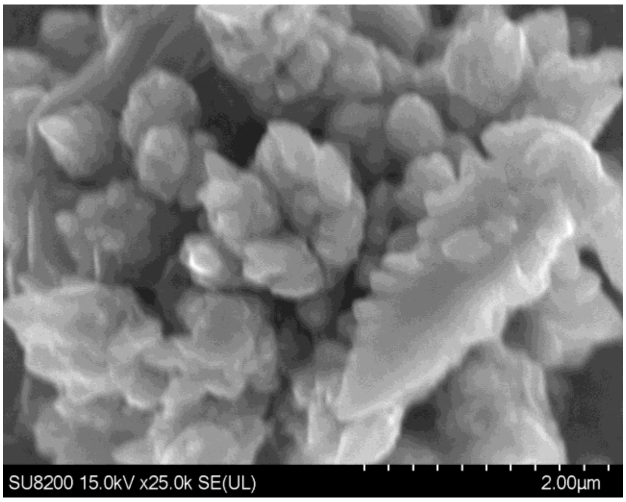

Figure 4.31 SEM micrograph of FTO surface modified with Fe-Co-Ni-Zn at 2.00 μm.

4.2.3 EDX characterization of tetrametallic catalyst film designed at FTO

EDX analysis was performed to analyze the presence of all metals that were deposited over FTO surface. **Figure 4.32** explains the EDX results of tetrametallic catalyst film developed in acidic solution at -1.5 V depositions potential. It becomes clear that all the metals were successfully at FTO surfaces.

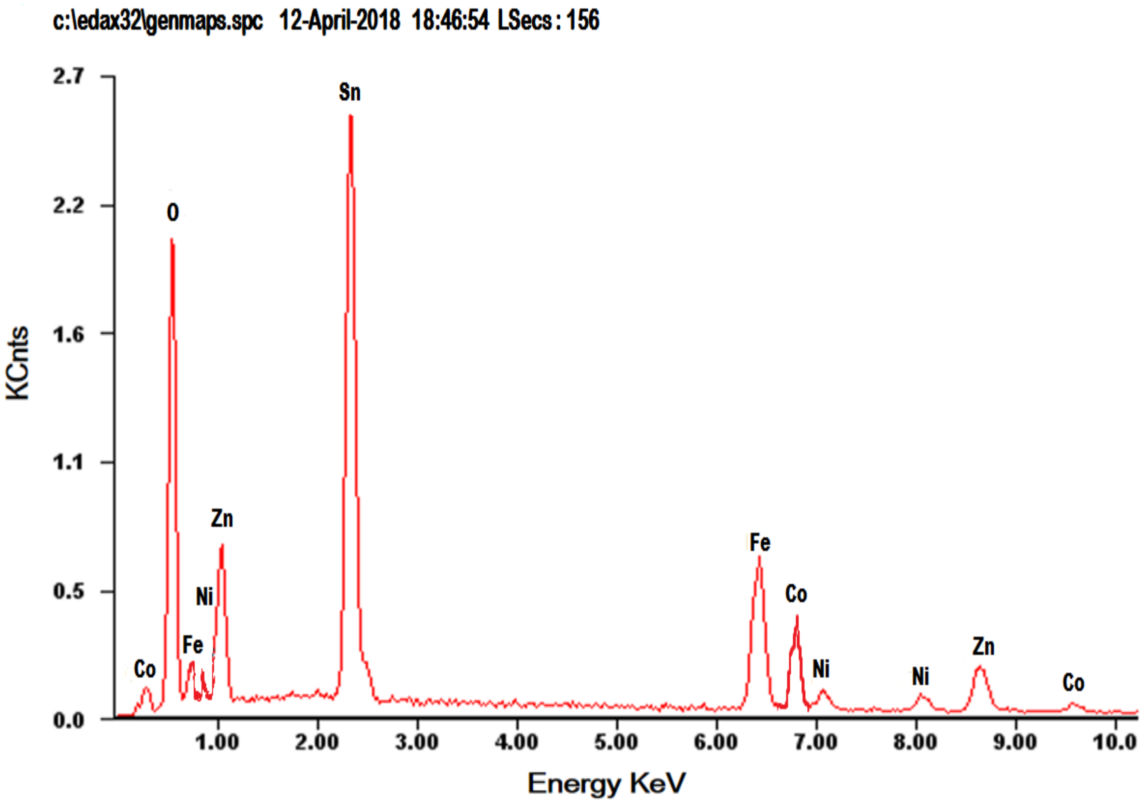

Figure 4.32 EDX of FTO modified with tetrametallic electrocatalyst film.

4.5 OER catalysis in acidic, neutral an alkaline solution

Electrocatalysis can be carried out in wide range of pH from acidic to neutral and basic medium. OER kinetic vary in acidic and basic conditions depending upon the materials utilized for catalysis. Usually catalyst driven from 3d transition metals does OER catalysis in alkaline solution more favorably as compared to in acidic solution [20-22]. While catalysts like Ir and Ru and their derivatives drive OER more easily in acidic condition. It usually depends upon the mechanism followed during catalysis. Many scientists published various review to summarize various reported OER mechanism. In present work behavior of developed electrocatalyst was also investigated in acidic, neutral and alkaline solution. For this purpose three FTO surfaces were separately modified with tetrametallic electrocatalyst under optimized conditions after that linear sweep voltammogram was taken for each modified FTO to check their response in acidic, neutral and basic conditions [23]. Accordingly to the reaction mechanism of OER catalysis in alkaline conditions hydroxyl ions generate the molecular oxygen by step wise electron transfer. While on other side under acidic conditions Hydroxyl ions are liberated with resulted in hydrogen production and pH of solution due to hydroxyl ions production becomes more acidic. Moreover, under acidic conditions hydrogen gas is brusted out at surface of electrode making the catalyst film unstable.

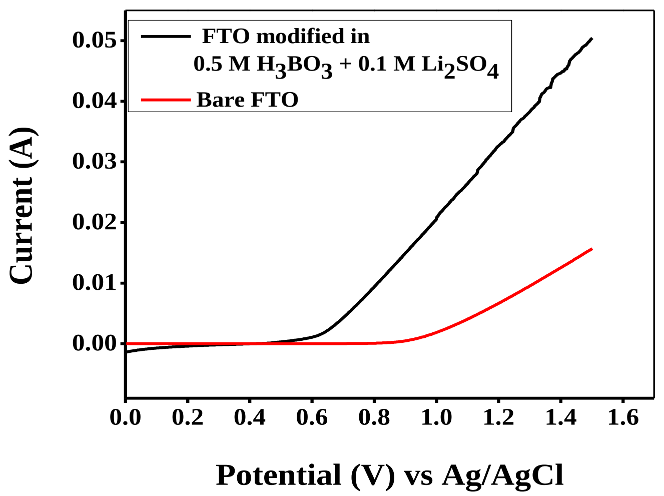

Figure 4.33 LSV response of tetrametallic electrocatalyst in acidic medium (Boric Acid).

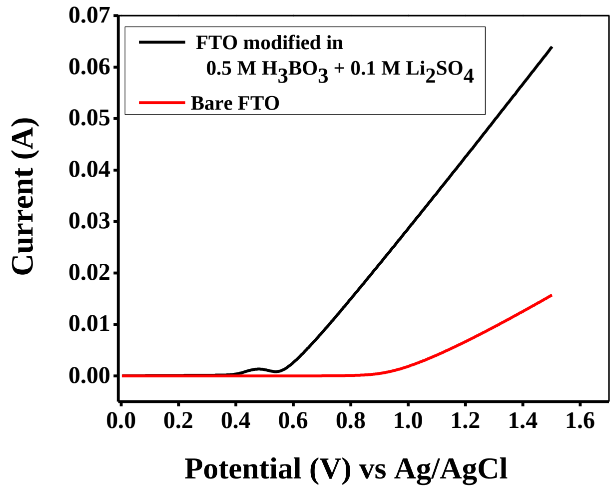

Figure 4.34 LSV response of tetrametallic electrocatalyst in neutral solution (Na_2CO_3).

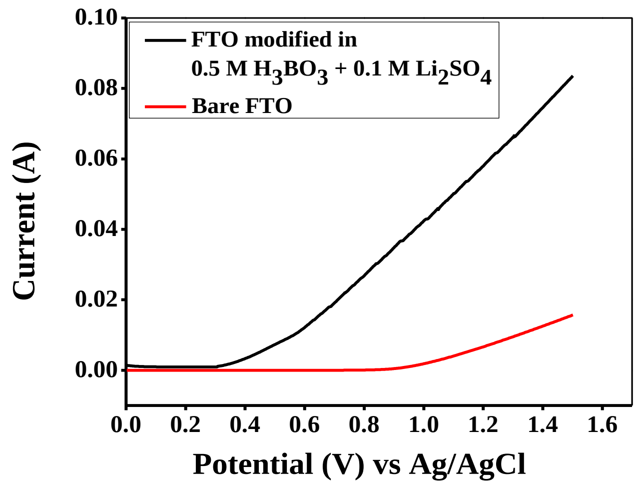

Figure 4.35 LSV response of tetrametallic electrocatalyst in alkaline solution (KOH).

Table 4.3 Summary of OER catalysis in acidic, neutral and alkaline conditions.

Supporting electrolyte	Current (A) in LSV	Onset potential value (V) vs Ag/AgCl	Onset potential value (V) vs NHE
Boric Acid	0.502	0.56	1.533
Sodium Carbonate	0.064	0.41	1.383
KOH pH = 13	0.084	0.31	1.288

Table 4.3 summarizes the OER catalysis results of developed catalyst under acidic, neutral and basic environment. It be realized that electrocatalytic performance of tetrametallic electrocatalyst was better under basic conditions as compared to under acidic medium in context of high current density and low onset potential.

4.6 Effect of Binder on catalytic performance of tetrametallic catalyst

Figure 4.36 shows the effect of binder on catalytic activity of tetrametallic electrocatalyst. FTO surface was modified with tetrametallic electrocatalyst in acidic medium followed by drop wise addition of Triton X-100 on catalyst film. After drying the film LSV was carried out at 10 mV /sec in alkaline medium. Blue solid curve shows the response of bare FTO and red curve shows the response of modified FTO film along with binder while black solid curve stands for modified FTO without binder. It can be realized that Triton X-100 used as was found to compromise that catalytic activity in term of low current value and high onset potential value while catalyst film without binder was found to high value of catalytic performance in context of high current value and low onset value of potential. Binder was applied to catalyst film in order to get stable film. In addition to that binder also increases the surface area of design electrocatalyst. One of primary reason behind the low catalytic performance of design catalyst along with binder is that binder blocks the active sites of catalyst film, that's why research groups working on OER catalysis preferred to design a catalyst without binder support.

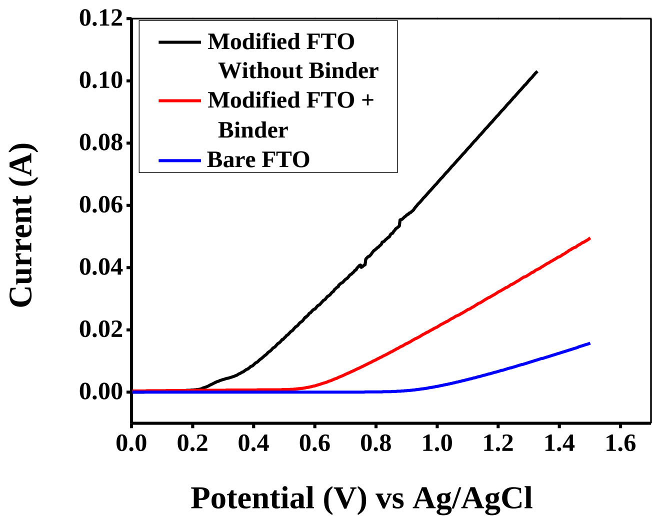

Figure 4.36 Effect of binder (Triton X-100) on catalytic activity of tetrametallic electrocatalyst.

4.7 Effect of metals ion concentration on catalytic performance

In order to optimize the concentration to get maximum current value at low onset value of potential metals concentration was tuned. **Figure 4.37** shows the variation in current value and onset potential value as a function of concentration of metals ions. By increasing the concentration of metals ion up to a limit current value increased and after the limit a decrease in current value was observed. So concentrations of metals salts were optimized at which high current value was obtained for further study.

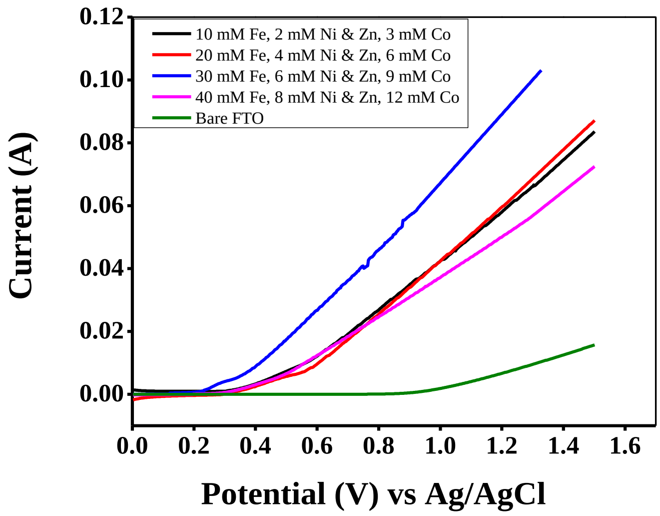

Figure 4.37 Effect of metals ions concentrations on catalytic response of tetrametallic electrocatalyst.

Table 4.4 Effect of concentration on LSV.

$FeSO_4$ Concentration (Mole dm^{-3})	**$NiSO_4$ Concentration (Mole dm^{-3})**	**$ZnSO_4$ Concentration (Mole dm^{-3})**	**$CoSO_4$ Concentration (Mole dm^{-3})**	**Effect on LSV Current value (A)**
0.01M	0.002 M	0.002 M	0.003 M	0.0836
0.02 M	0.004 M	0.004 M	0.006 M	0.0874
0.03 M	0.006 M	0.006 M	0.009 M	0.1025
0.04 M	0.008 M	0.008 M	0.012 M	0.0720

Table 4.4 shows the effect of metals ion concentration at catalysis behavior of developed catalyst. Concentration of catalyst increases the rate of reaction by lowering the kinetic energy barrier without changing the reaction equilibrium. Electrocatalyst go a step further as compared to other catalyst and also lower the kinetic energy barrier of elementary steps.in redox mechanism during water splitting. Increase in rate of reaction means faster will be the electron transfer rate at high concentration of metal ions. Higher is the concentration of metals ions higher value of current obtained. That's why higher concentration resulted high current value.

4.8 Bimetallic and Trimetallic electrocatalysts of Fe, Zn, Ni and Co

All possible combinatorial screening of bimetallic combinations of selected four transition metals (Fe, Zn, Ni & Co) was deposited on FTO under acidic conditions and their LSV was conducted at 10 mV/sec scan rate. It was investigated that catalytic performance towards water splitting of all bimetallic combinations was less than tetrametallic combination of selected four metals. CPE and LSV for bimetallic catalysts were carried out under similar conditions as for tetrametallic catalysts. Similarly all possible Trimetallic combinations of selected four transition metals (Fe, Zn, Ni & Co) was deposited on FTO under acidic conditions and their LSV scans was carried out at scan rate of 10 mV/sec.

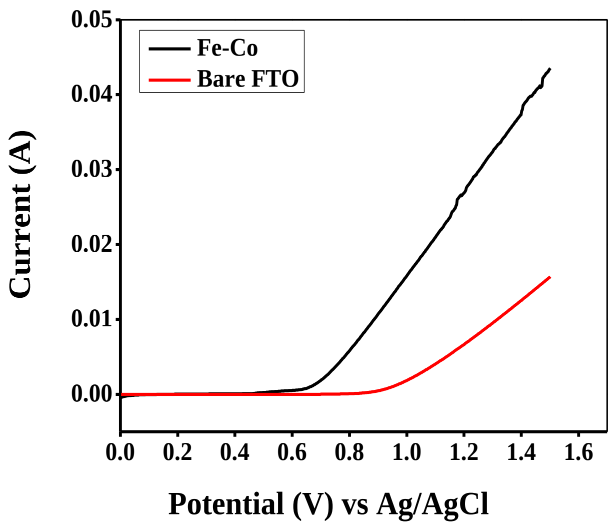

Figure 4.38 LSV response of FTO modified with Fe-Co catalyst film in basic medium.

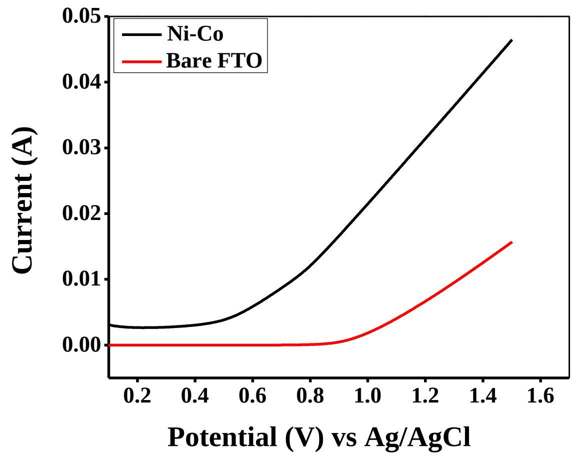

Figure 4.39 LSV response of FTO modified with Ni-Co catalyst film in basic medium.

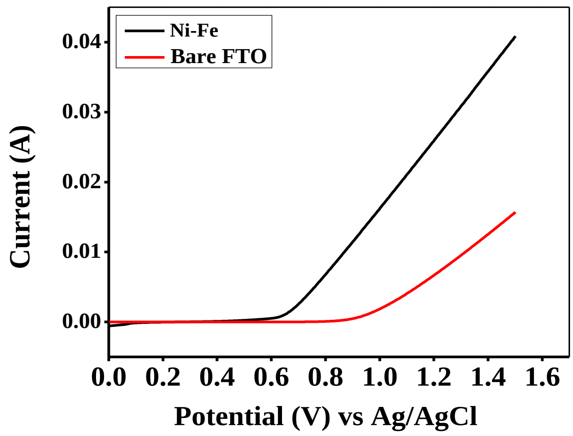

Figure 4.40 LSV response of FTO modified with Ni-Fe catalyst film in basic medium.

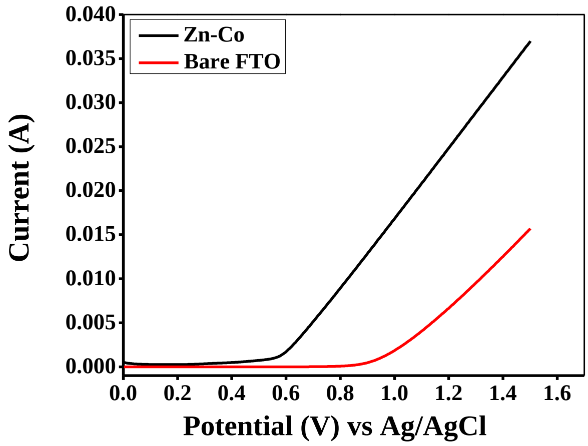

Figure 4.41 LSV response of FTO modified with Zn-Co catalyst film in basic medium.

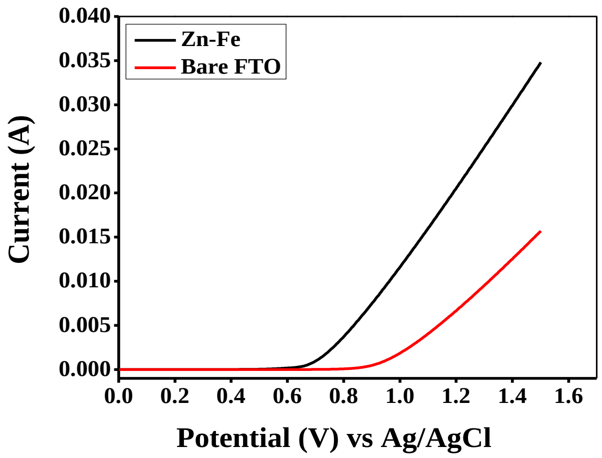

Figure 4.42 LSV response of FTO modified with Zn-Fe catalyst film in basic medium.

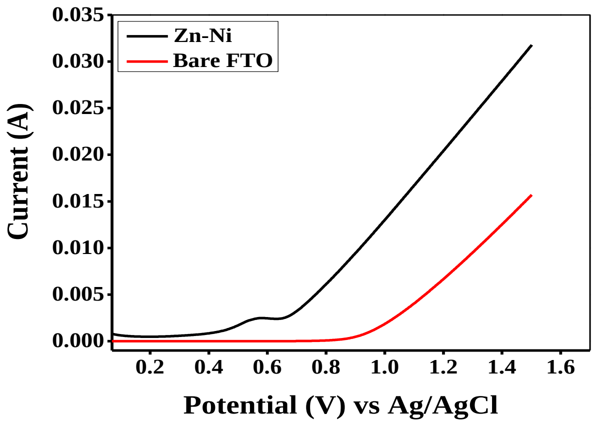

Figure 4.43 LSV response of FTO modified with Zn-Ni catalyst film in basic medium.

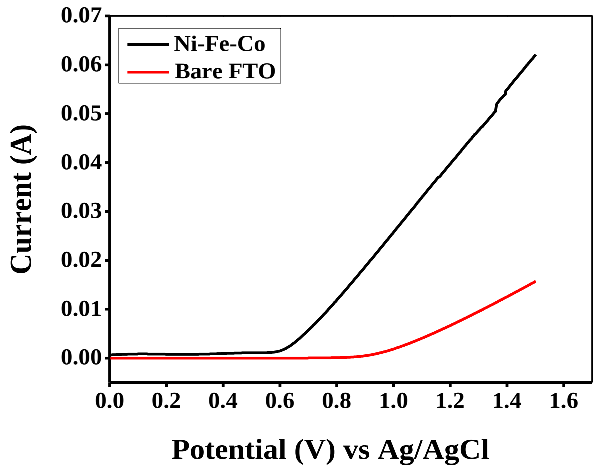

Figure 4.44 LSV response of FTO modified with Ni-Fe-Co catalyst film in basic medium.

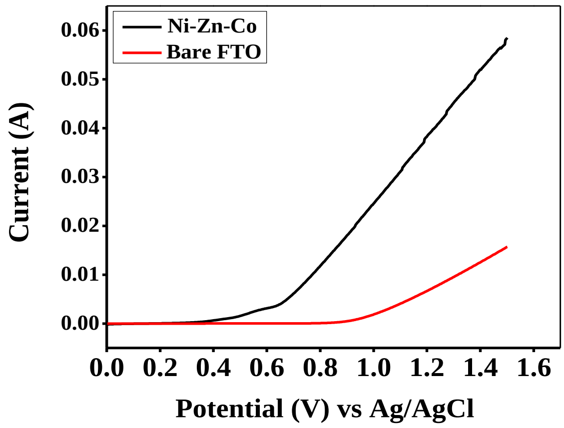

Figure 4.45 LSV response of FTO modified with Ni-Zn-Co catalyst film in basic medium.

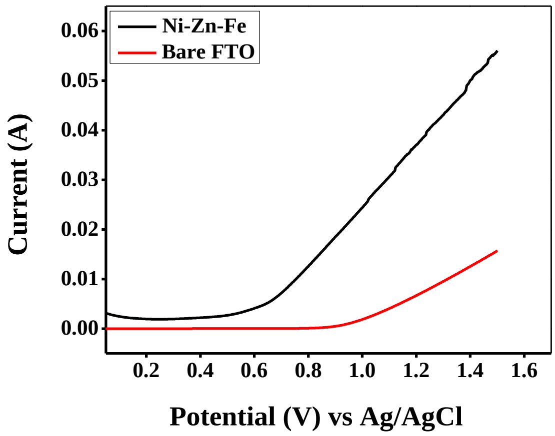

Figure 4.46 LSV response of FTO modified with Ni-Zn-Fe catalyst film in basic medium.

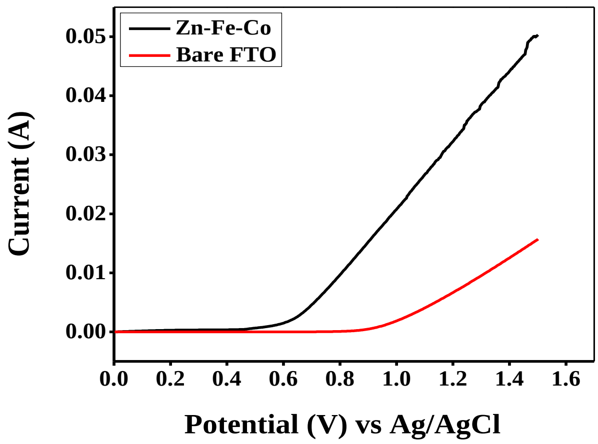

Figure 4.47 LSV response of FTO modified with Zn-Fe-Co catalyst film in basic medium.

It was observed that catalytic performance towards water splitting of all bimetallic combinations was less than tetrametallic combination of selected four metals. CPE and LSV for Trimetallic catalysts were carried out under similar conditions as for tetrametallic catalysts [24-26]. **Table 4.5** compares the catalysis behavior bi, tri and tetrametallic electrocatalyst toward OER.

Table 4.5 Summary of catalytic performances of bi, tri and tetrametallic catalysts.

Metals Combinations	Onset (V) vs Ag/AgCl	Onset (V) vs NHE	Over potential η(V)	Current (A) in LSV
Fe-Co	0.65	1.623	0.393	0.0435
Ni-Co	0.48	1.453	0.223	0.0464
Ni-Fe	0.62	1.593	0.363	0.0407
Zn-Co	0.56	1.533	0.303	0.0369
Zn-Fe	0.67	1.643	0.413	0.0348
Zn-Ni	0.45	1.423	0.193	0.0318
Ni-Fe-Co	0.60	1.537	0.307	0.0621
Ni-Zn-Co	0.43	1.403	0.173	0.0583
Ni-Zn-Fe	0.49	1.463	0.233	0.0596
Zn-Fe-Co	0.56	1.533	0.303	0.0503
Fe-Zn-Ni-Co	0.315	1.288	0.058	0.0906

4.9 Tafel slope

In order to compare the electrocatalytic activity and to justify the reaction mechanism of the synthesized electrocatalyst, tafel plot analysis is generally utilized. Tafel slopes are useful to obtain information about the reaction mechanism of electrocatalyst, the From tafel slope calculations it was concluded that tetrametallic electrocatalyst fashioned at FTO surface in acidic medium have shown very high catalytic performance in context of very low value of overpotential 52.6 mV at 1.0 mA/cm^2. **Table 4.6** summarizes the catalytic performance of various heterogeneous electrocatalysts for OER catalysis. On the basis of these points tafel plots **Figure 4.48** was determined by measuring the output of reaction that is the stable current density (j) which is a function of overpotential in 1M KOH as a solvent. By definition, overpotential is expressed as $\eta = Vapp - 1.23\,V$, where $Vapp$ is the applied potential vs. NHE and 1.23 V is the thermodynamic potential for the oxidation of water at the pH of the solution of our own interest V vs. NHE = V vs. Ag/AgCl (0.059* pH) + 0.206.role of inhibitor of reaction, coatings and activation energy of the reaction.

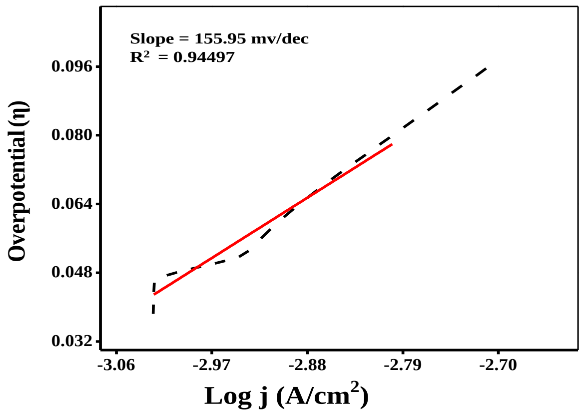

Figure 4.48 Tafel slope of tetrametallic electrocatalyst fashioned at FTO surface.

Table 4.6 Comparison of various heterogeneous electrocatalyst for OER catalysis.

Catalyst	**Ƞ (mV at 1.0 mA/cm^2)**	**Refs**
Annealed CuO	430 mV at 0.1 mA/ cm^2	[27]
CuO from Cu-TPA	600 mV at 0.1 mA/ cm^2	[28]
Cu bi-functional	749 mV at 0.1 mA/cm^2	[29]
CuO nanowires	550 mV at 0.1 mA/cm^2	[30]
Cu-Bi	530 mV at 0.1 mA/cm^2	[31]
Cu-TEOA	780 mV at 0.1 mA/cm^2	[32]
CuO-Cu hybrid	485 mV at 0.1 mA/cm^2	[33]

$(Ni\text{-}Fe\text{-}Co\text{-})_3Se_4$	230 mV at 10 mA/cm^2	[18]
$FeNi_2Se_4$ Reduced Graphene Oxide	170 mV at 10 mA/cm^2	[34]
$CoNi_2Se_4$ bifunctional	160 mV at 10 mA/cm^2	[35]
Porous microparticles of Nickel Cobalt Perselenide	320 mV at 10 mA/cm^2	[36]
Ni(Fe)OOH	760-330 mV at 0.1 mA/cm^2	[37]
Fe-Co-Ni-Zn in KOH	**52.6 mV at 1 mA/ cm^2**	**This work**

4.10 Conclusion

The development of cost affordable, efficient and environmental friendly water splitting techniques can contribute in addressing the key challenges for energy production. An efficient novel tetrametallic electrocatalyst for water electrolysis was designed via a facile and cost affordable method in contrast to catalysts from precious metals (Au, Pt, Ru and Ir). The findings of this work elaborate efficient catalytic performance of the designed binder-free tetrametallic electrocatalyst to catalyze OER. The solution containing boric acid and lithium sulphate was found as the best medium for the electrodeposition of a film of tetrametallic catalyst on FTO surface. Successful deposition of metals on FTO surface was ensured from the results of XRD, SEM & EDX. Modified FTO was found to demonstrate the best water splitting response in basic medium of pH = 13. The results of linear sweep voltammetry revealed that a current density of 1 mA/cm^2 demands overpotential of just 52.6 mV, thus suggesting promising candidature of the designed electrocatalyst for efficiently catalyzing OER. The binder was found to compromise the conductivity and performance of the catalyst. So the electrocatalyst without binder was found to enhance current density at lower onset potential. These desired water splitting features of the electrochemically grown catalyst over the surface of electrode point to its suitability for use in the development of industrial alkaline water electrolysers.

4.11 References

[1] A. Aldalbahi, E. Mkawi, K. Ibrahim, M. Farrukh, Effect of sulfurization time on the properties of copper zinc tin sulfide thin films grown by electrochemical deposition, *Sci Rep,* 6 (2016) 32431.

[2] A. Irshad, N. Munichandraiah, electrodeposited nickel–cobalt–sulfide catalyst for the hydrogen evolution reaction, *ACS Appl Mater Interfaces*, 9 (2017) 19746-19755.

[3] G. Nemţoi, H. Chiriac, O. Dragoş, M.-O. Apostu, D. Lutic, The voltammetric characterization of the electrodeposition of cobalt, nickel and iron on gold disk electrode, *Acta Chemica Ia*, 17 (2009) 151-168.

[4] L.J. Brogan, Electrochemistry of $FeSO_4$-$Na_2S_2O_3$ and $CuSO_4$-$Na_2S_2O_3$ systems for template-assisted nanowire synthesis, UC Berkeley, 2011.

[5] R.A. Santana, S. Prasad, E.S. Moura, A.R. Campos, G.P. Silva, P. Lima-Neto, Studies on electrodeposition of corrosion resistant Ni–Fe–Mo alloy, *J. Mater. Sci*, 42 (2007) 2290-2296.

[6] M. Khelladi, L. Mentar, M. Boubatra, A. Azizi, Study of nucleation and growth process of electrochemically synthesized ZnO nanostructures, *Mater. Lett*, 67 (2012) 331-333.

[7] M. Blanco, J. Barragan, N. Barelli, R. Noce, C.S. Fugivara, J. Fernández, A.V. Benedetti, On the electrochemical behavior of Cu–16% Zn–6.5% Al alloy containing the β′-phase (martensite) in borate buffer, *Electrochim. Acta*, 107 (2013) 238-247.

[8] J. Ballesteros, C. Gomez-Solis, L. Torres-Martinez, I. Juárez-Ramírez, Electrodeposition of Cu-Zn intermetallic compounds for its application as electrocatalyst in the hydrogen evolution reaction, *Int. J. Electrochem. Sci*, 10 (2015) 2892-2903.

[9] L. Mentar, A study of the electrodeposition of Co–Cu alloys thin films on FTO substrate, *Ionics*, 18 (2012) 223-229.

[10] N.I.S. kopeli, electrodeposition and characterization of cu-zn alloy films obtained from a sulfate bath, *Mater. Tehnol*, 48 (2014) 221-226.

[11] V. Torabinejad, M. Aliofkhazraei, S. Assareh, M. Allahyarzadeh, A.S. Rouhaghdam, Electrodeposition of Ni-Fe alloys, composites, and nano coatings–A review, *J. Alloy. Compd*, 691 (2017) 841-859.

[12] S. Silkin, A. Gotelyak, N. Tsyntsaru, A. Dikusar, Electrodeposition of alloys of the iron group metals with tungsten from citrate and gluconate solutions: Size effect of microhardness, *J. Appl. Electrochem*, 53 (2017) 7-14.

[13] X. Geng, E. Navarrete, W. Liang, E.J. Podlaha, Electrodeposited Fe-Mo-Ni nanowires and Cu-Mo-Fe-Ni alloy nanowire segments, *Mater. Lett*, 211 (2018) 9-12.

[14] V. Kublanovsky, Y.S. Yapontseva, Electrocatalytic properties of co-mo alloys electrodeposited from a citrate-pyrophosphate electrolyte, *Electrocatalysis-Us*, 5 (2014) 372-378.

[15] P.Y. Chen, M.C. Lin, I.W. Sun, Electrodeposition of Cu-Zn alloy from a lewis acidic $ZnCl_2$-EMIC molten salt, *J. Electrochem. Soc*, 147 (2000) 3350-3355.

[16] X. Xu, P. Du, Z. Chen, M. Huang, An electrodeposited cobalt–selenide-based film as an efficient bifunctional electrocatalyst for full water splitting, *J. Mater. Chem. A*, 4 (2016) 10933-10939.

[17] E.J. Popczun, J.R. McKone, C.G. Read, A.J. Biacchi, A.M. Wiltrout, N.S. Lewis, R.E. Schaak, Nanostructured nickel phosphide as an electrocatalyst for the hydrogen evolution reaction, *J. Am. Chem. Soc*, 135 (2013) 9267-9270.

[18] X. Cao, Y. Hong, N. Zhang, Q. Chen, J. Masud, M. Asle Zaeem, M. Nath, Phase exploration and identification of multinary transition metal selenides as high-efficiency oxygen evolution electrocatalysts through combinatorial electrodeposition, *ACS. Catal*, (2018).

[19] J. Yao, K. Zhang, W. Wang, X. Zuo, Q. Yang, H. Tang, M. Wu, G. Li, Remarkable enhancement in the photoelectric performance of uniform flower-like mesoporous Fe_3O_4 wrapped in nitrogen-doped graphene networks, *ACS. Appl. Mater. Interfaces*, (2018).

[20] J.O. Bockris, T. Otagawa, Mechanism of oxygen evolution on perovskites, *J. Phys. Chem. A*, 87 (1983) 2960-2971.

[21] W.H. Wade, N. Hackerman, Anodic phenomena at an iron electrode, *Trans. Faraday. Soc*, 53 (1957) 1636-1647.

[22] S. Anantharaj, S.R. Ede, K. Sakthikumar, K. Karthick, S. Mishra, S. Kundu, Recent trends and perspectives in electrochemical water splitting with an

emphasis on sulfide, selenide, and phosphide catalysts of Fe, Co, and Ni: a review, *ACS. Catal*, 6 (2016) 8069-8097.

[23] T. Lim, M. Sung, J. Kim, oxygen evolution reaction at microporous pt layers: differentiated electrochemical activity between acidic and basic media, *Sci. Rep*, 7 (2017) 15382.

[24] S.M. Bawaked, I.H. Abd El Maksod, A. Alshehri, A simulation study for trimetallic nanosized alloy (Ni, Cu and Ag) in hydrogenation of organic compounds: a case study of "nitrophenols", *J. nanomater*, 2017 (2017).

[25] J. Lan, C. Li, T. Liu, Q. Yuan, One-step synthesis of porous PtNiCu trimetallic nanoalloy with enhanced electrocatalytic performance toward methanol oxidation, *J. Saudi. Chem. Soc*, (2018).

[26] J. Xu, J. Li, D. Xiong, B. Zhang, Y. Liu, K.-H. Wu, I. Amorim, W. Li, L. Liu, Trends in activity for the oxygen evolution reaction on transition metal (M = Fe, Co, Ni) phosphide pre-catalysts, *Chem. Sci*, 9 (2018) 3470-3476.

[27] M. Jafarian, O. Azizi, F. Gobal, M. Mahjani, Kinetics and electrocatalytic behavior of nanocrystalline CoNiFe alloy in hydrogen evolution reaction, *Int. J. Hydrogen Energy*, 32 (2007) 1686-1693.

[28] X. Liu, H. Jia, Z. Sun, H. Chen, P. Xu, P. Du, Nanostructured copper oxide electrodeposited from copper (II) complexes as an active catalyst for electrocatalytic oxygen evolution reaction, *Electrochem. Commun*, 46 (2014) 1-4.

[29] X. Liu, H. Zheng, Z. Sun, A. Han, P. Du, Earth-abundant copper-based bifunctional electrocatalyst for both catalytic hydrogen production and water oxidation, *ACS. Catal*, 5 (2015) 1530-1538.

[30] X. Liu, S. Cui, Z. Sun, P. Du, Copper oxide nanomaterials synthesized from simple copper salts as active catalysts for electrocatalytic water oxidation, *Electrochim. Acta*, 160 (2015) 202-208.

[31] F. Yu, F. Li, B. Zhang, H. Li, L. Sun, Efficient electrocatalytic water oxidation by a copper oxide thin film in borate buffer, *ACS. Catal*, 5 (2014) 627-630.

[32] T-T. Li, S. Cao, C. Yang, Y. Chen, X.-J. Lv, W.-F. Fu, Electrochemical water oxidation by in situ-generated copper oxide film from [Cu (TEOA)($H_2O)_2$][SO_4] complex, *Inorg. Chem*, 54 (2015) 3061-3067.

[33] J. Du, Z. Chen, S. Ye, B.J. Wiley, T.J. Meyer, Copper as a robust and transparent electrocatalyst for water oxidation, *Angew. Chem. Int. Ed*, 54 (2015) 2073-2078.

[34] S. Umapathi, J. Masud, A.T. Swesi, M. Nath, $FeNi_2Se_4$–reduced graphene oxide nanocomposite: enhancing bifunctional electrocatalytic activity for oxygen evolution and reduction through synergistic effects, *Adv. Sustainable. Syst*, 1 (2017) 1700086.

[35] B. GolrokháAmin, $CoNi_2Se_4$ as an efficient bifunctional electrocatalyst for overall water splitting, *Chem. Commun*, 53 (2017) 5412-5415.

[36] D.V. Shinde, L.D. Trizio, Z. Dang, M. Prato, R. Gaspari, L. Manna, Hollow and porous nickel cobalt perselenide nanostructured microparticles for enhanced electrocatalytic oxygen evolution, *Chem. Mater*, 29 (2017) 7032-7041.

[37] J. Zaffran, M.B. Stevens, C.D. Trang, M. Nagli, M. Shehadeh, S.W. Boettcher, M. Caspary Toroker, Influence of electrolyte cations on Ni(Fe)OOH catalyzed oxygen evolution reaction, *Chem. Mater*, 29 (2017) 4761-4767.